THE UNIVERSITY OF MICHIGAN

INDUSTRY PROGRAM OF THE COLLEGE OF ENGINEERING

SIMULATION AND CONTROL OF TRANSIENT FLOW IN THE DIESEL INJECTION SYSTEM

Mohamed Fathy El-Erian

A dissertation submitted in partial fulfillment
of the requirements for the degree of
Doctor of Philosophy in the
University of Michigan
Department of Mechanical Engineering
1972

April, 1972

IP-842

To my wife and parents

ACKNOWLEDGMENT

I would like to express my sincere appreciation to Professors Jay A. Bolt and Benjamin E. Wylie, Co-Chairmen of my doctoral committee, for suggesting this area of research. In particular, thanks are extended to Professor Bolt for his inspiration, guidance and valuable advice throughout my graduate studies, to Professor Wylie for his inspiration, guidance and valuable suggestions provided in numerous discussions of the mathematical simulation and control techniques; to Professor Victor L. Streeter for developing my initial interest in studying transient flow problems and for his interest and cooperation throughout the course of the study; and to Professors Milton A. Chace and Robert B. Keller for their participation and cooperation.

I am also indebted to Professor N. Abdou Henein for his sincere counsel during my undergraduate and graduate studies and for developing my interest in the area of diesel engines.

The financial support of the U. S. Public Health Service, and later the Environmental Protection Agency, is gratefully acknowledged. Without this support, this project could not have been completed. The financial assistance of the Chevron Research Company in making possible purchase of needed equipment is also acknowledged. I would like also to express my gratitude to the Mechanical Engineering Department and the International Center of the University of Michigan for their support in the form of tuition scholarships during my graduate studies.

I would further like to extend my thanks to Mr. Bela Petry, Mr. Arthur Bauer and Mr. Sam Onyegegbu, graduate students at the University of Michigan for their able assistance during the course

of this study. The help of technicians and machinists in the Automotive Laboratory is also gratefully acknowledged.

For assistance in the preparation of the manuscript, I gratefully acknowledge the help of Dr. Ismail Eldumiati and Mr. Richard Winsor for their valuable comments while editing the manuscript. Thanks are also due to Miss Ruth Howard for typing the original manuscript, and to the staff of the Industry Program and the Office of Research Administration of the University of Michigan for final preparation and publication of the manuscript.

Particular thanks are also due to my wife Magda for her patience and understanding.

TABLE OF CONTENTS

LIST OF FIGURES

LIST OF FIGURES (CONT'D)

LIST OF FIGURES (CONT'D)

LIST OF FIGURES (CONT'D)

LIST OF FIGURES (CONT'D)

LIST OF TABLES

NOMENCLATURE

Symbol	Meaning
A	Pipe cross-sectional area, or area of opening at orifice
a	Wave propagation velocity
C_d	Discharge coefficient
C_t	Time averaged flow resistance coefficient, defined in Equation 2.1
C_{vf}	Viscous friction coefficient for fuel leakage past the needle
c	As a subscript, refers to cylinder pressure into which injection occurs
c.v.	As a subscript, refers to control valve
D	Pipe diameter
d	As a subscript, refers to pump delivery chamber
E	Injection system average elastic energy
F	Force acting on needle or delivery valve
f	Friction coefficient at valve or needle
f	Darcy-Weisbach friction factor
f	As a subscript, refers to pump feed chamber
g	Acceleration of gravity
h	As a subscript, refers to the nozzle injection holes
i	As a subscript, refers to nozzle injection chamber
INJ	As a subscript, refers to equivalent pipe length of injector volumes
J	a ratio; $J=f\Delta t/2DA$
K	Bulk modulus of elasticity
k	Spring static force
L	Delivery pipe length
l	As a subscript, refers to nozzle lower chamber

Symbol	Meaning
M	A ratio; $M=gA/\gamma a$
m	Mass of valve or needle
N	Pump cam shaft speed
n	As a subscript, refers to injector needle
p	Pressure
p_t	Time averaged pressure over the injection period
p	As a subscript, refers to pumping chamber
PUMP	As a subscript, refers to equivalent pipe length of the pump delivery chamber volume
Q	Volumetric flow rate
r	Spring stiffness
Re	Reynolds number
S	Valve, needle or pump plunger displacement
t	Time
TOT	As a subscript, refers to total pipe length including equivalent lengths of volumes at pump and injector
u	As a subscript, refers to upper nozzle and delivery chambers combined
V	Velocity
~~V~~	volume of fluid enclosures in pump and injector
v	As a subscript, refers to pump delivery valve
W	Mass flow rate
w	Weight of delivery valve or needle
W,Ws,Wd, $W_1..W_6$	As subscripts, refer to positions in the x-t plane
x	Distance

Symbol	Meaning
X, X_4, X_5	As subscripts, refer to positions in the x-t plane
$Y, Yd, Y_1..Y_5$	As subscripts, refer to positions in the x-t plane
$Z, Z_1..Z_6$	As subscripts, refer to positions in the x-t plane
Zd	As a subscript, refers to the instantaneous flow in the delivery pipe line at the pump delivery chamber
Zs	As a subscript, refers to the instantaneous flow in the supply pipe at the pump feed chamber
Zu	As a subscript, refers to the instantaneous flow in the delivery pipe at the injector
γ	Specific weight of fluid
Δp	Frictional pressure drop
ΔV	Volume change
Δt	Characteristic method time step
$\Delta\theta$	Injection period in degrees
θ	Pump cam angle in degrees
τ_o	Pipe wall shear stress
φ	A time function representing the time rate of change of pressure in the concentrated volumes at the pump and injector

I. INTRODUCTION

1.1 Purpose and Background

The injection system of a diesel engine is of critical importance since it has a major influence on the combustion of the engine. This is especially true today in view of the air pollution problem, and the fact that combustion characteristics limit the present uses of the diesel engine.

The diesel fuel injection system is an assembly of many complex and intricate mechanical components, each with specific functions. In addition to the behavior of individual components, the interaction of these components has an important influence on the ultimate operation of the system. However, the fundamentals of the operating characteristics of some of the components and the interactions between these components are not fully understood. Consequently, much experimental trial-and-error development of injection systems occurs among the diesel engine and equipment manufacturers.

The response of the fuel injection system is primarily dependent upon the action of the pump and the pressure wave propagation phenomena in the delivery pipe line. The pump action with its delivery chamber and valve is not independent of the injector and delivery pipe line, since a complete system interaction takes place.

One of the most persistent injection system problems is related to wave phenomena in the high pressure line between the pump

and nozzle assembly of the most popular type of injection system. These pressure waves commonly result in a secondary opening of the fuel injection nozzle following the normal injection, which is referred to as after-injection. This contributes to smoking of the engine. This problem has been attacked in the past using experimental cut-and-try procedures with limited success. However, within the past decade, procedures have been developed which permit a design or synthesis approach to transient flow problems.

This study is divided into two major phases. The first phase deals with the formulation and solution of the transient flow problem in the diesel injection system. It includes a comparison of the analytical results with experimental data taken on actual test equipment. The second phase is concerned with the investigation of an analytical method to define means for control of the after-injection phenomenon.

1.2 Literature Review

The common textbook approach,[17,22] employed to simulate this problem is based on the use of a simplified form of the equation describing the wave mechanism in the supply and delivery lines. These simple approximations bear little resemblence to the performance of the true hardware in either theory or operation since it neglects many factors, including:

1. The change in geometry of fixed and moving parts.

2. The change in fluid properties.

3. The dynamics of moving parts.

4. The coefficient of flow variations through different passages in the system.

5. The flow friction in the supply and delivery lines.

6. The possible opening of vapor cavities.

In the existing research work, a great variety of both theoretical and experimental procedures have been used to study the diesel injection system. Prior to 1960, injection simulation studies were limited by lengthy mathematical computations and graphical techniques. They were only possible under many simplifying assumptions. This made it impractical to apply theoretical simulation in the design stage and led to experimental trial-and-error procedures.

One of the earliest significant contributions to fuel injection systems is due to Davis and Giffen,[9] 1931. Their discussion includes many of the significant variables involved in the system, namely: fluid compressibility, elastic deformation, pressure wave propagation, fluid friction, and pump and nozzle characteristics, including secondary injection. De Juhasz,[10] 1937, used graphical water hammer concepts to provide an analysis of a linear model of typical simplified injection systems, including the elements of the pipeline, pump, nozzle, and a fluid volume. On the other hand, Giffen and Row,[13] 1939, theoretically solved the equations representing the injection system, taking into account the effect of pressure

waves in the delivery pipe and the capacity effects of the volumes located in the pump and nozzle system. They placed the differential equations in finite difference form and found an algebraic expression for the solution. This method of solution was limited to simple injection models because of the time required for mathematical solutions.

Knight,[18] 1960, introduced a model for viscous friction and cavitation in the delivery pipe and used the same model for the pump and nozzle system described by Giffen and Row.[13] His calculations were performed using a digital computer.

Becchi,[4] 1962, used a model which comprised a detailed representation of the injector and the pump, but he neglected friction in the delivery pipe and had no provision for possible occurrence of vapor cavities. He solved the system of differential equations by an iterative method after writing them in finite difference form.

Brown and McCallion,[8] 1967, combined Becchi's detailed representation of the pump and injector with a model that included viscous friction and possible cavitation in the delivery pipe. They also considered a detailed modeling of the delivery valve as described by Stone[27] and solved the system of equations by another iterative method.

The work of Walwijk, Van der Graaf, and Jansen,[30] 1969, is also to be noted. Their experimental apparatus enabled them to actually measure the motion of the delivery valve and injector

needle as well as the pressure in various locations in the system. Particular attention was devoted to the motion of the delivery valve in their simulation on a digital computer. A good correlation was achieved between experimental and computed results.

Recently Becchi,[5] 1971, extended his model to allow for variations in piping cross-sectional areas and possible opening of vapor cavities. He also included the possibility of using a single plunger distributor pump. Yamaoka, Saito and Okazaki,[33] 1971, simulated an injection system of the by-pass type where the fuel spill is controlled by a by-pass valve located in the pump delivery chamber, and not by the commonly used spill port.

Many factors are likely to affect the accuracy of the injection model and have been discussed by many investigators. The value of the residual pressure in the delivery pipeline is important for a meaningful comparison between the model and experimental results. In addition, a treatment of vapor pressure in the delivery pipeline is also needed for a complete model. Kreith and Eisentadt,[20] 1956, and Lichtarowicz, Duggins and Markland,[21] 1965, presented experimental results of the variation of the coefficient of discharge over a wide range of Reynolds number and length to diameter ratio. Giffen and Row,[13] 1939, cautioned of the danger of using coefficients of discharge from the literature. They preferred to use experimentally determined values for the particular nozzle under consideration. The data of Gelalles,[12] 1931, in which he tested different nozzle

configurations, showed that the coefficient of discharge, besides depending on length to diameter ratio and Reynold's Number, is also greatly dependent on the configuration of the reservoir leading to the nozzle holes.

The stability and convergence of the analytical solutions are of prime importance. Henrici,[15] 1964, discussed three different methods of numerical solution of a system of differential equations: 1) the iterative solution of simultaneous algebraic equations, 2) the expansion methods (Taylor's method or Runge Kutta method), and 3) the numerical integration methods. The first and second methods require the use of very small time steps and a prior knowledge of the size of the time step. The third method includes the predictor-corrector method which offers the advantage of an adjustable time increment, dependent upon a given error bound. This particular advantage is of great value for reducing computation time.

Experimental measurements of transient pressures, valve movements, and transient discharges are of great importance in describing the injection system performance. The measurement of pressure is possible by using piezo-quartz pressure transducers. For the movement of valves, Bassi,[3] 1963, used a capacitive type distance detector in measuring needle lift and a light source and a photo cell to measure the relief valve movement.

The instantaneous flow measurement is the most challenging one. Ibrahim,[16] 1964, used two methods of high-speed, mechanically operated collectors. In a third method he measured the pressure due to the injection in a filled volume with fuel, and deduced the instantaneous flow by relating the pressure to the discharge using the compressibility relation. He concluded that the third method is the best provided that a high frequency pressure pick up is used and enough damping of the secondary oscillations in the measuring volume is ensured. Komarof, Iwan, and Kurt,[19] 1966, measured the distance travelled by a piston in a cylinder full of fuel due to the introduction of injected fuel. This method has the advantage of discharging in a constant pressure while the previous method is discharging in a highly varying pressure. Bosch,[16] 1966, used a specially designed long tube to isolate one pressure pulse and then related the intensity of the pulse to the instantaneous flow.

Considerable theoretical work has been conducted to control the performance of hydraulic systems. Streeter and Wylie[29] used the valve stroking technique for some large scale complex systems and obtained good confirmation with experimental results. However, little theoretical work has been done in the area of diesel injection control. Most of the work has been experimentally oriented to obtain a desirable performance over a required range. Most often, the system performance has been satisfactory for only a part of the range.

A study by Bradbury,[7] 1950, showed that after-injection invariably occurred at conditions of simultaneous high engine speed and load. In addition, his studies on the relation between the specific fuel consumption and break-mean-effective-pressure indicated the need for large injector holes to achieve large output, and that small holes were more adequate for part-loads. He concluded that small holes are preferred over the whole range if it is possible to eliminate after-injection at high outputs. Furthermore, Mansfield,[24] 1965, stated that it is difficult if not impossible, for a pump to perform satisfactorily on a heavy-duty engine under all conditions of speed and load, and that the high rates of pressure change, which must occur in all injection systems, lead to secondary injection.

Recently, Dolenc and Lees,[11] 1968, and Lustgarten and Dolenc,[23] 1969, used a pump plunger with a stepped helix which provided a throttling effect during the early part of the fuel spill period. Their experimental results showed that the modified system had a better performance than the original one. This was evidenced by less after-injection and reduced cavitational damage. Anders,[1] 1971, used a variety of shapes of the pump plunger helix and pump spill port. He recommended the decrease of the dynamic flow delivery during the spill period through a better design of the plunger helix and the pump spill port, by using aerodynamically contoured ducts and helices.

1.3 Scope of Investigation

The objective of this thesis is to conduct the following investigations:

1. A theoretical analysis on an actual Bosch type injection system analyzing each component in terms of the basic equations, and combining the analysis into a comprehensive digital computer simulation.
2. Measurement of the transient pressures and flow data taken on an actual injection system, and comparing these data with the computer simulation results.
3. Studying an analytical method to define means for control of the after-injection phenomenon.

The experimental apparatus is described in Chapter II. This includes a description of the construction details, instrumentation and experimental procedures. Factors affecting the accuracy of the theoretical model are emphasized. These factors include the pipe residual line pressure and the coefficient of discharge through the nozzle holes. The results of an experimental survey of the after-injection phenomenon are presented toward the end of Chapter II.

In Chapter III a theoretical model of the fuel injection system is developed. A list of the assumptions used in the model is presented, and the importance of an adequate model is discussed. The solution of the model is presented in Chapter IV. Experimental data is

compared with results from the analytical model, and the important factors affecting the accuracy of the comparisons are discussed.

A theoretical investigation of a design parameter to control the after-injection phenomenon is given in Chapter V. This includes the formulation of a design program which utilizes the average elastic energy in the injection system as a controlling parameter. Two examples are introduced to illustrate the usefulness of the design program. The first deals with the elimination of after-injection by adding a control valve in the pump delivery chamber. In the second example, the same goal is achieved by redesigning the pump spill port. Results of both examples are presented in Chapter VI. In this chapter the simulation program is used to check the results obtained from the design program.

II. TEST EQUIPMENT, INSTRUMENTATION AND EXPERIMENTAL RESULTS

2.1 Purpose of the Experiment

There were several reasons for conducting experimental tests. First, knowledge of some experimentally measured parameters is essential for an accurate determination of the theoretical system response. Examples of these parameters are the system residual line pressure and the flow coefficient of discharge through the nozzle holes. Secondly, the computer simulation model results should be compared with experimental data to check the validity of the assumptions and techniques used in the study. A third reason is the need to study the system performance, especially the undesirable phenomena of after-injection and cavitation. The above reasons require a quantitative determination of the time variant response of the predominant variables in the apparatus during a normal operating cycle.

The analytical simulation treats each component part in great detail. It is not practical to measure all the variables, therefore, a satisfactory confirmation between the theory and experiment is believed to be demonstrated if the theoretical results agree with the experimental data using pre-selected variables. It should be noted that these variables must be chosen to represent the performance of the system adequately. In this study the experimentally determined system response was identified by the transient

pressures, measured at specific locations, and by an overall measurement of the fuel input to the pump, the injected fuel and the fuel leakages.

2.2 General Description of the System

A general view of the diesel injection test bench is shown in Figure 1. This shows the injection pump mounted on a stand. The pump was an American Bosch APE1B type and had a plunger diameter of 10 mm. It was connected to the injector by a high pressure pipe line 0.067 in. inside diameter, 0.25 in. outside diameter, and 36.4 in. long. The injector was an American Bosch ADB-150S type. The pump drive system included a substantial flywheel to provide uniform rotation and was driven by a variable speed dc motor. The pump cam shaft speed was variable within the range of 100 rpm to 1000 rpm. The fuel rack was positioned by a micrometer that had a travel of 0 to 1 inch, corresponding to maximum and minimum fuel delivery, respectively, with a minimum graduation of 0.001 inch. References (2) and (3) were very helpful in the design and construction of the test equipment.

A detailed view of the pump, pipe and injector system is illustrated in Figure 2, while Figure 3 shows the pump and construction details of the drive system. Figure 4 displays the injector with modifications to allow for its instrumentation. Figure 5 is a schematic representation of the diesel injection system with the

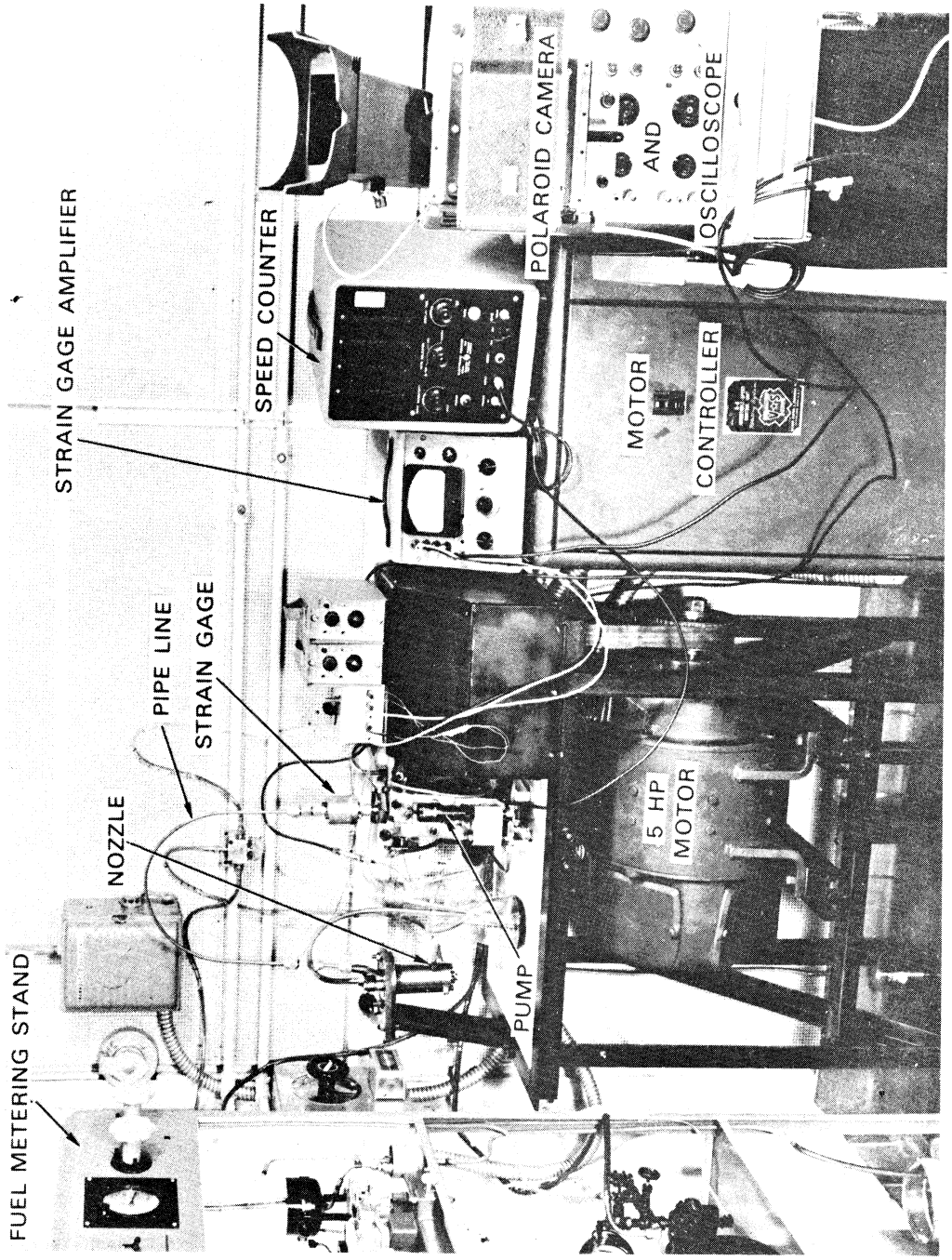

Figure 1. Diesel Fuel Injection System Test Equipment-General View.

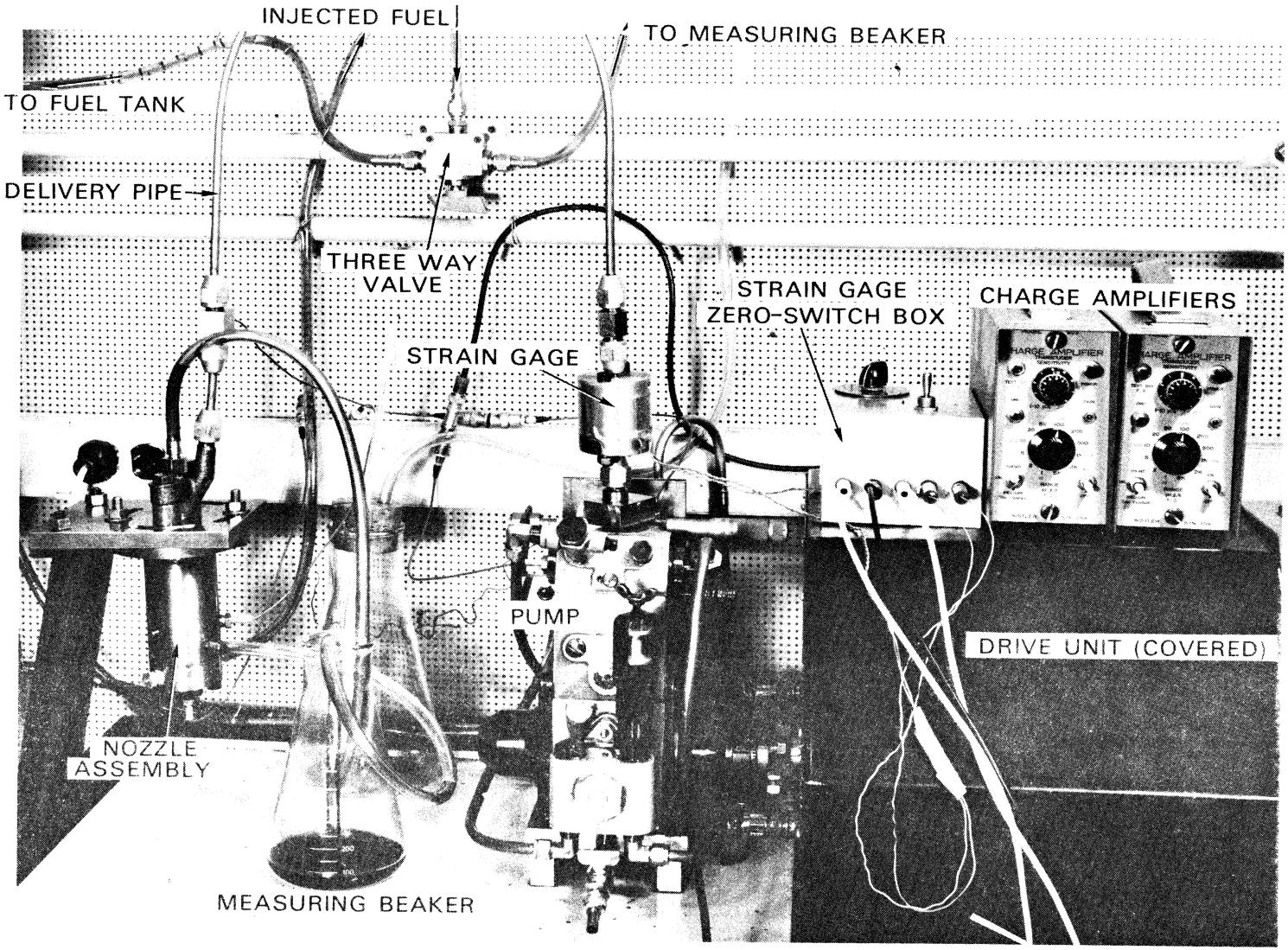

Figure 2. Diesel Fuel Injection System Test Equipment - Details of Pump, Pipe and Injector.

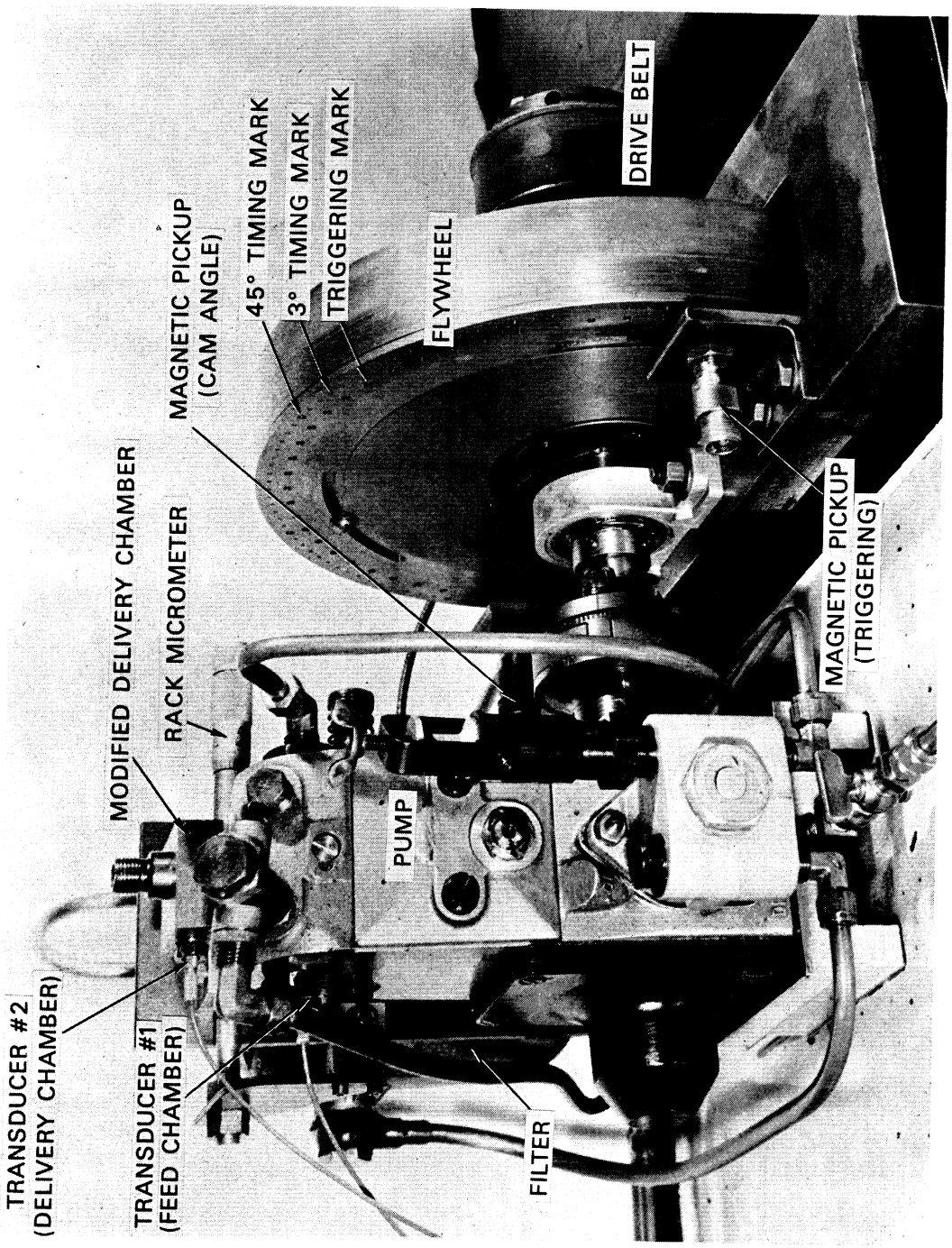

Figure 3. Diesel Fuel Injection System Test Equipment - Pump and Construction Details of Drive System.

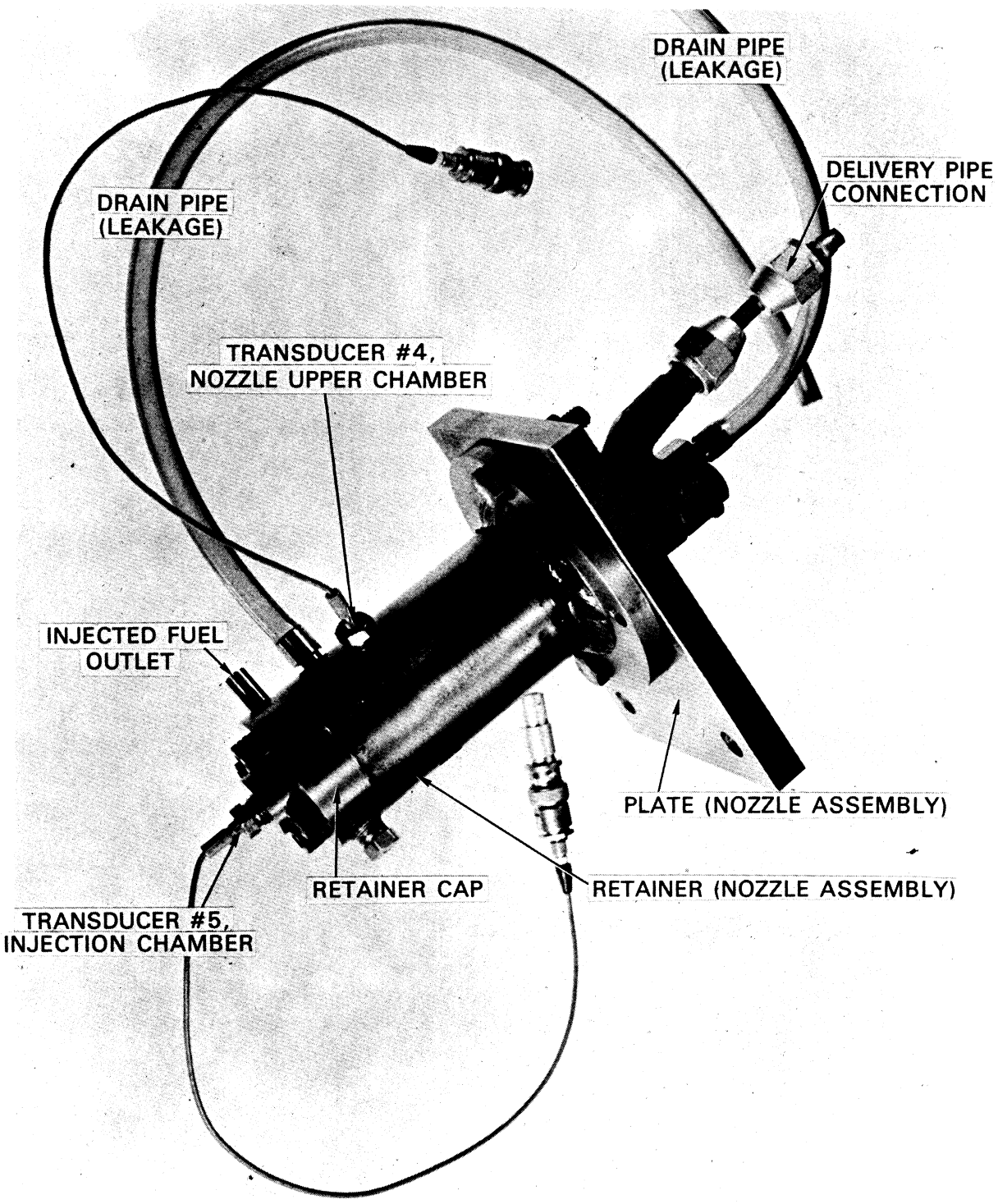

Figure 4. Modified Injector and Its Instrumentation.

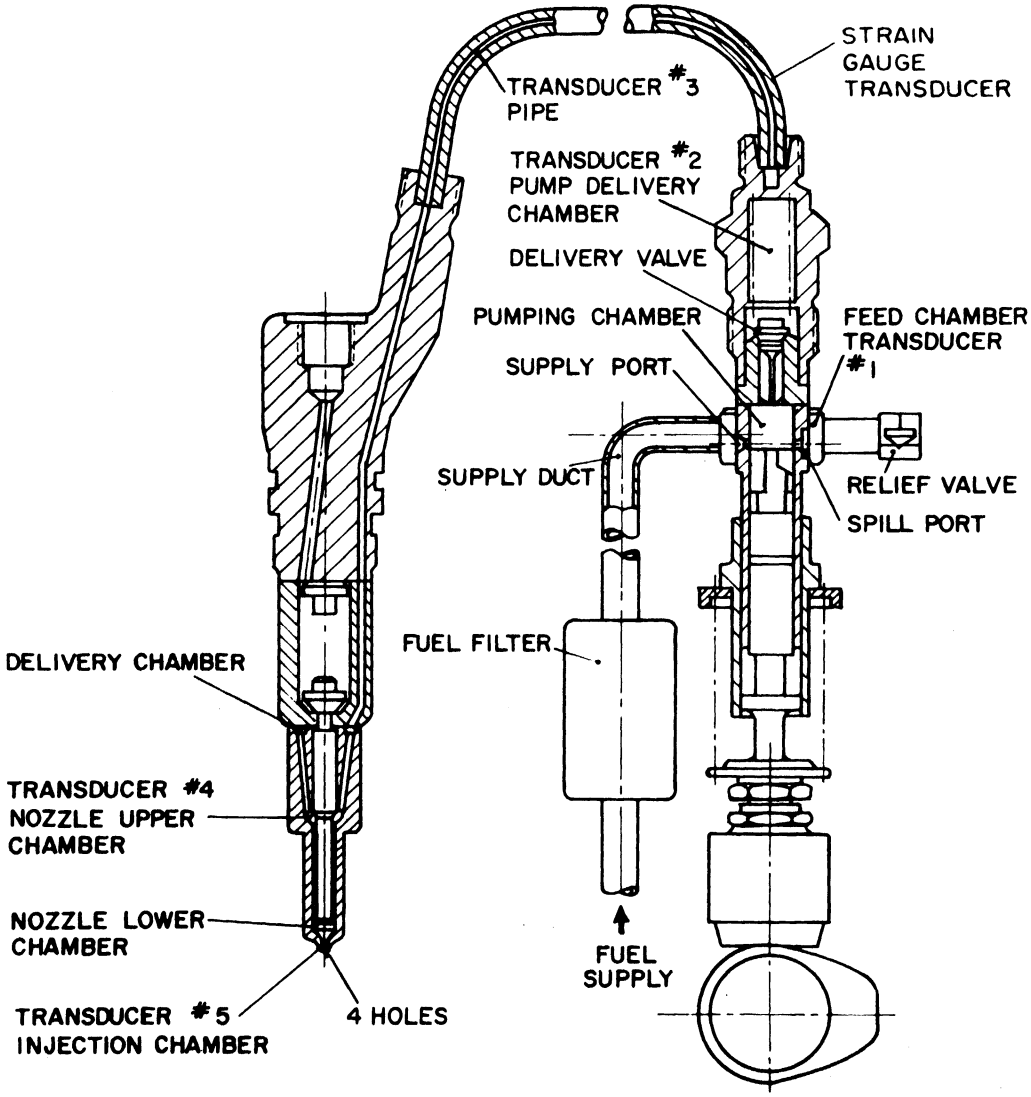

Figure 5. Schematic Representation of Diesel Injection System and Points of Pressure Measurement.

points of pressure measurement marked. The pump and injector general dimensions are given in Table I and II, respectively. The pump delivery valve had an equivalent weight of .013 lb.; the spring force on the seated valve was equal to 11 lbs.; the spring stiffness was equal to 40 lbs/in. The nozzle needle had an equivalent weight of .02706 lb.; the spring force on the seated needle was equal to 86 lbs.; the spring stiffness was equal to 857 lbs/in. The needle opening pressure was set under quasi-static conditions to 3000 lb/in.^{2} for all test runs. The injector nozzle discharged into a pressure region of one atmosphere. The fuel used in all tests was Standard Oil Company No. 2 diesel fuel, with a specific weight of .02986 lb/in.^{3} at atmospheric pressure and 60°F, a boiling point of 450°F and an API gravity of 39.5.

Most of the above dimensions and properties were measured and compared with the manufacturer's specifications. The measured values were used in most cases while the manufacturer's data were used only in cases where it was impractical to make an accurate measurement.

2.3 Instrumentation

The fuel pressure was measured using AVL piezo-quartz pressure transducers (type 7QP2500 a). The transducers were designed to measure dynamic pressures up to 1500 atmospheres and were claimed to be linear in this range within one percent of the full scale deflection.

TABLE I

GENERAL DIMENSIONS OF AMERICAN BOSCH APE1B INJECTION PUMP

Length of supply duct = 23 inch

Diameter of supply duct = .234 inch

Volume of pump feed chamber (inlet gallery) = .7 $in.^3$

Diameter of feed port = .107 in.

Diameter of spill port = .119 in.

Maximum volume of pumping chamber = .0808 $in.^3$

Diameter of delivery valve seat = .236 in.

Maximum volume of pump delivery chamber = .1637 $in.^3$

TABLE II

GENERAL DIMENSIONS OF ADB-150S AMERICAN BOSCH INJECTOR

Volume of injector delivery chamber = .00772 $in.^3$

No. of passages from delivery to nozzle upper chamber = 2

Length of passages = .76 in.

Diameter of passages = .069 in.

Volume of nozzle upper chamber = .004485 $in.^3$

Length of passage from upper to lower chamber = .925 in.

Inside diameter of passage = .80 in.

Outside diameter of passage = .198 in.

Volume of nozzle lower chamber = .001 $in.^3$

Volume of injection chamber = .001 $in.^3$

No. of injection holes = 4

Hole length = .035 in.

Hole diameter = .012 in.

Figure 5 shows the location of five pressure transducers which were designed to measure the pressures at the following points: the pump feed chamber, the pump delivery chamber, a location in the high pressure pipe line near the injector, the nozzle upper chamber and the injection chamber. The pump delivery chamber was modified to accommodate the pressure transducer, and the modification details are shown in Figure 6. Figure 7 illustrates the details of the connector used with pipe line transducer. The injector body and nozzle were modified to house transducers No. 4 and No. 5. The details of these modifications are given in Figure 8. To accommodate transducer No. 4, the injector body and its nozzle retaining nut were modified, and an injector retainer was added. To house transducer No. 5, the nozzle tip was modified and a cap was added as shown in Figures 8 and 9. The addition of transducer No. 4 added a volume of less than three percent to the nozzle upper chamber volume, and the addition of transducer No. 5 added a volume of less than 10 percent to the nozzle injection chamber. These volume additions were considered tolerable in view of the great accuracy in measuring the pressure in these very small volumes.

It was necessary to add a static pressure transducer to establish a reference pressure. This was needed since piezo-quartz transducers are of dynamic nature (measure pressure change only). This was especially important to measure the residual pipe line pressure between successive injections, commonly called the base pressure.

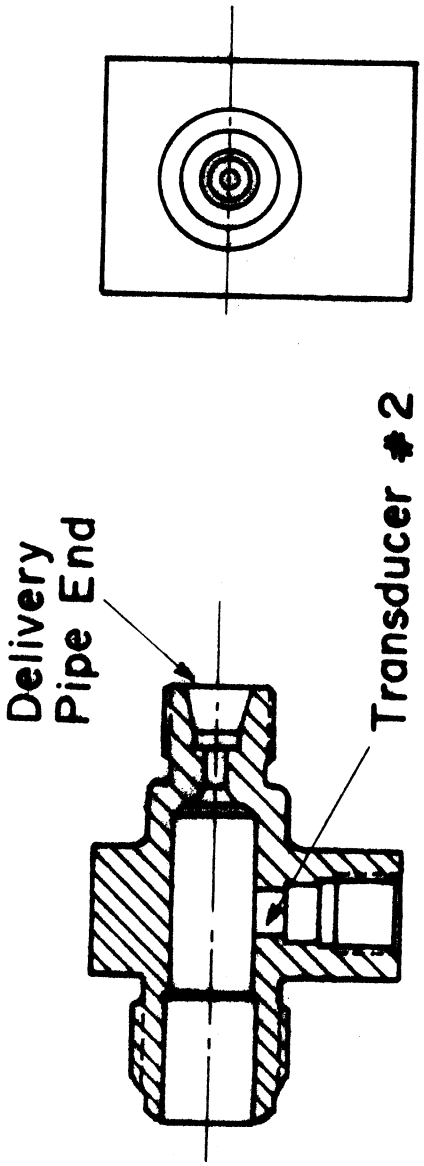

Figure 5. Modified Pump Delivery Chamber.

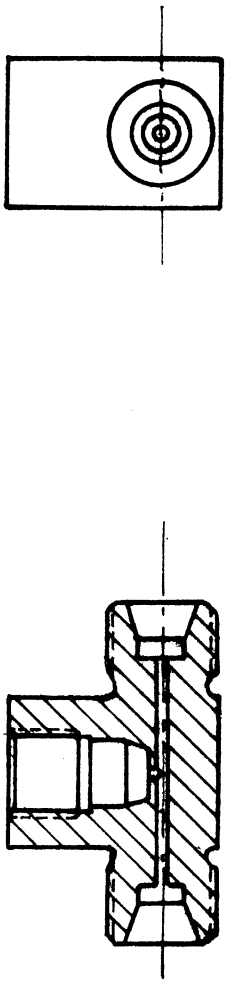

Figure 7. Transducer Holder for the Injection Pipe Line.

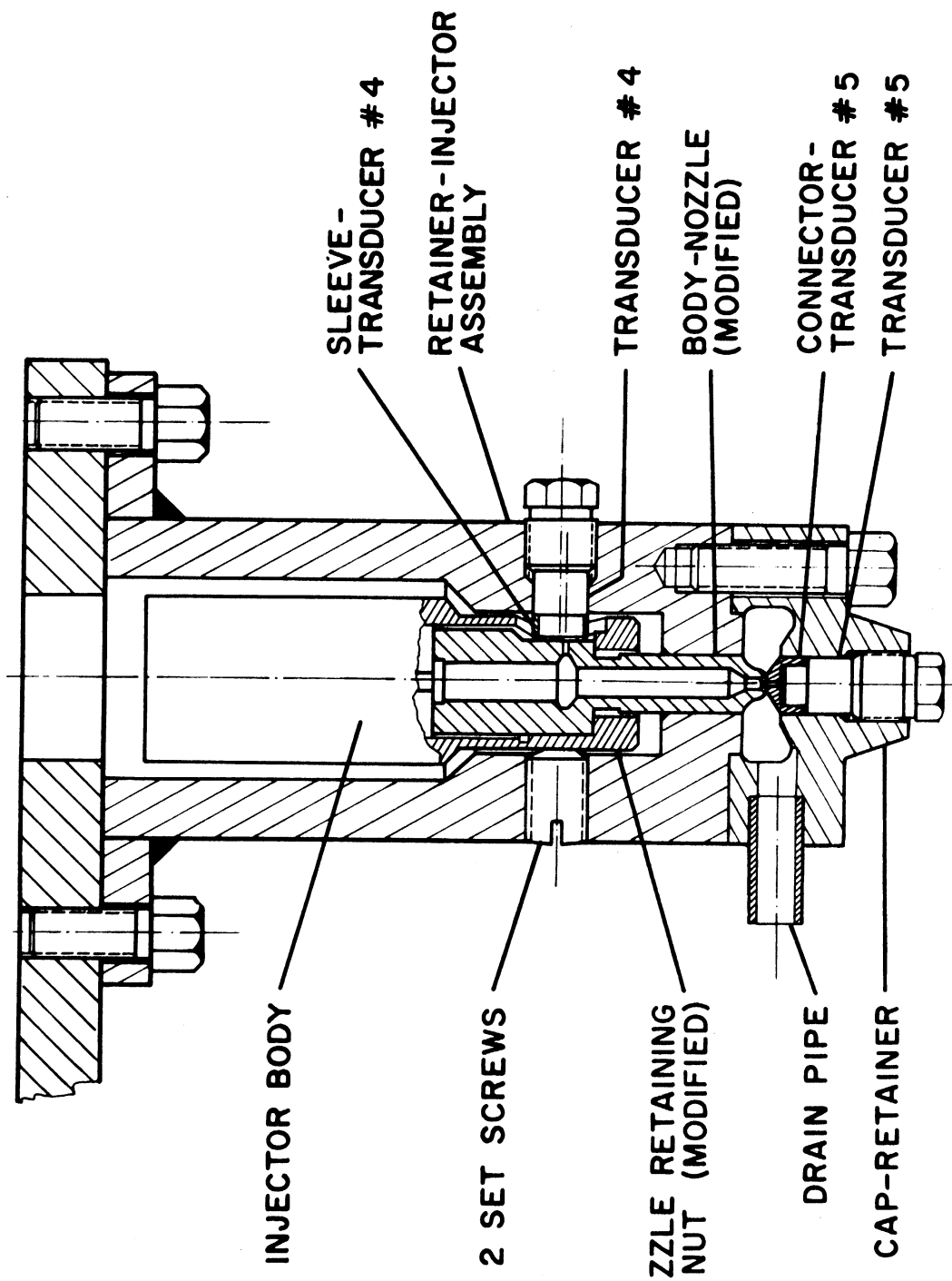

Figure 8. Modified Injector Body and Nozzle.

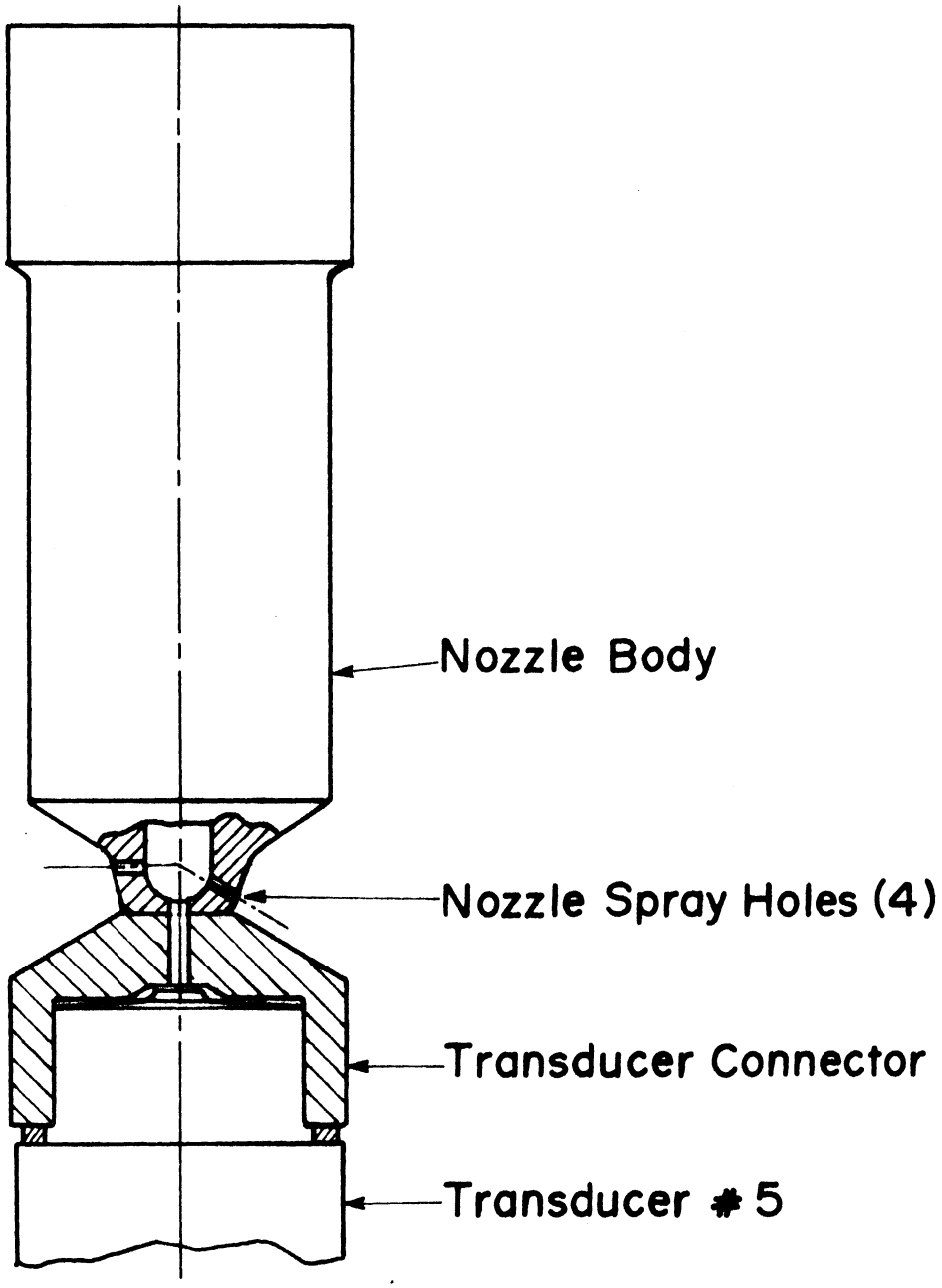

Figure 9. Sectional View of Connector and Nozzle Modification Details.

The static pressure transducer was of the strain gauge-type. It was constructed and inserted in the pipe line directly above the pump delivery chamber. This was done by reducing the pipe thickness through a one inch long section to .016 in. and measuring the circumferential strain on the outside diameter using four strain gauges connected in a four-arm bridge circuit. Some difficulties were encountered as a result of vibration and outside interference on the strain gauge circuit. This was overcome through building an outside structure to envelope the reduced section, and act as a vibration damper. All the pressure transducers were statically calibrated using a dead weight tester.

The pump speed was measured using a Hewlett-Packard electronic counter, Type 512A. The cam angles were recorded every three degrees using a disc with 120 equally spaced holes mounted on the flywheel and an electromagnetic pick up (type 3010-AN made by Electro-Mation Co.). Figure 3 shows some details of the cam angle measuring technique. A Tektronic 502A type dual beam oscilloscope fitted with a polaroid camera was used to record the pressure traces and the cam angle position.

The net fuel flow to the pump was measured using a metering stand made by Waukesha Motor Co. (left side of Figure 1) which consisted of a balance, a relay system and an electric clock. The fuel actually injected was collected and weighed, and the difference between the two measurements gave the overall system leakage.

2.4 Experimental Procedures

This section deals with two basic objectives. One is the measurement of parameters needed for the solution of the theoretical model of the injection system, namely, the residual pressure in the pipe line and the flow resistance through the nozzle holes. The other objective is to collect experimental data to compare with the theoretical model results.

The residual pressure in the pipe line was measured during each experiment by recording a dual trace representing the pressure from the strain gauge transducer together with the reference zero pressure. At the beginning and the end of each experiment, great care was taken to ensure that the bridge circuit was balanced and the zero reference line did not shift.

The average flow resistance coefficient through the nozzle holes C_t was defined as:

$$C_t = (C_d \times A_h)_t \qquad (2.1)$$

where C_d is the commonly known coefficient of discharge (ratio of actual measured flow to theoretical flow neglecting friction), A_h is the area of the nozzle holes, and the subscript t refers to averaging over the injection period. This definition simplifies the experimental procedure, since it requires the measurement of one parameter C_t instead of measuring both C_d and A_h. This is of special value if the area of the injection holes during

running conditions is in doubt. Figure 10 shows the details of the average flow resistance coefficient measurement. First the beginning and end of the injection period were defined with the difference in degrees being the injection period $\Delta\theta$. Then the injection chamber pressure trace was averaged during this injection period using the relation:

$$(p_i)_t = \frac{\int_0^{\Delta\theta} p_i d\theta}{\Delta\theta} \tag{2.2}$$

where p_i is the instantaneous pressure in the injection chamber in lb/in.^{2} and $(p_i)_t$ is the average pressure in lb/in.^{2}. Finally the average flow resistance coefficient, in in.^{2}, was calculated using the equation:

$$C_t = \frac{W}{((2g/\gamma)^{1/2}((p_i)_t - p_c)^{1/2}\ \Delta\theta/6N)} \tag{2.3}$$

where W is the injected mass flow rate in lbm/sec., g is the acceleration of gravity in in./sec.^{2}, γ is the fuel specific weight in lbm/in.^{3}, p_c is the pressure into which injection occurs, in psi, and N is the pump cam shaft speed in rpm.

For comparison with the theoretical model results, pressure traces from transducer No. 1 through No. 5 were recorded on the dual-beam oscilloscope. The upper beam showed the output of a particular transducer and the lower beam showed the cam angle position. The data collected included pictures of a complete cycle for each pressure transducer. Portions of the cycle during

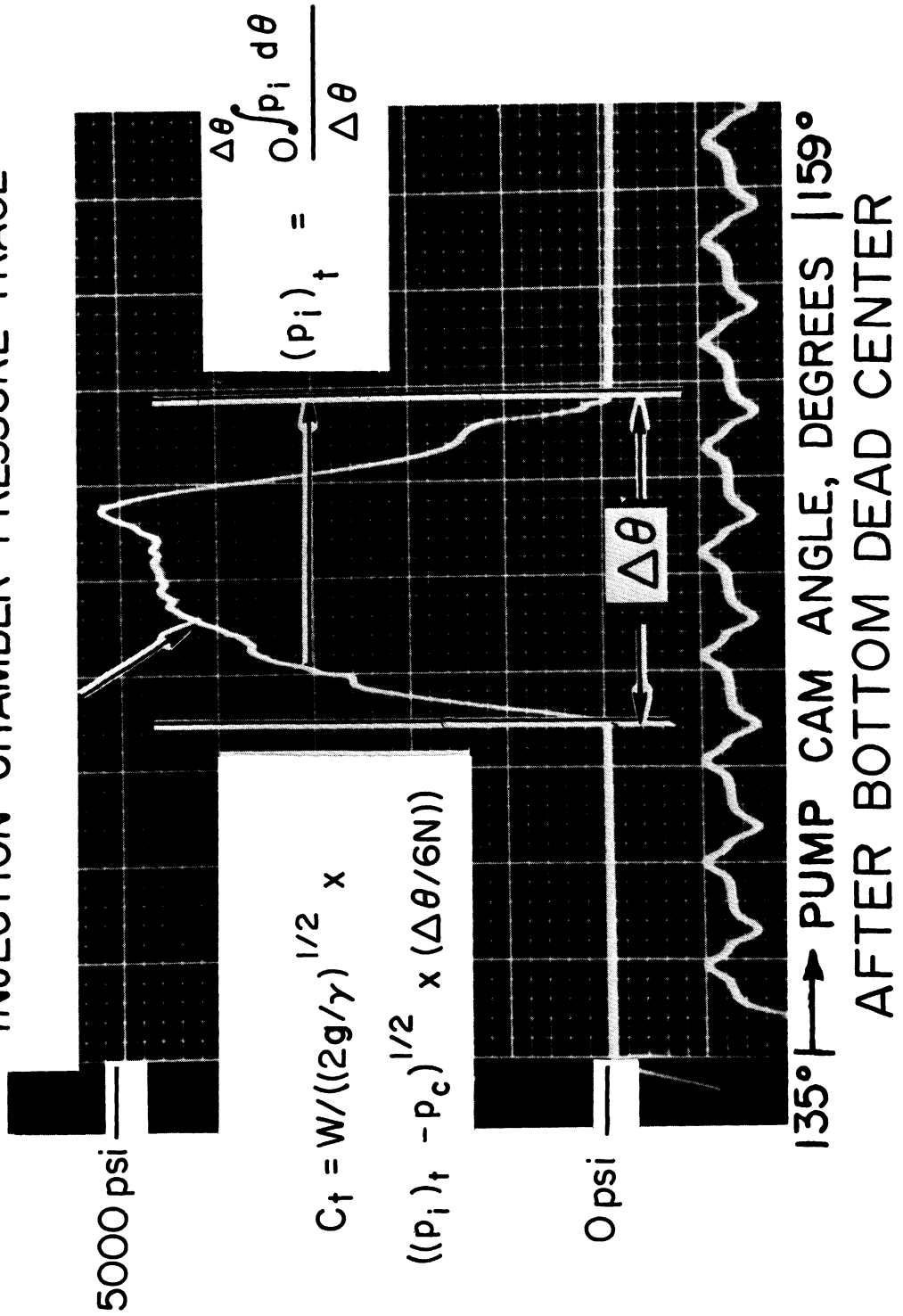

Figure 10. Oscilloscope Record of Transient Pressure in the Injection Chamber and the Calculation of C_t from the Trace.

which injection occurs were magnified to ease the data reduction process. During the pressure recording period the net fuel flow to the pump was measured and the net mass of the fuel injected was weighed. These two measurements were repeated several times during the course of running. The room and the injected fuel temperatures were also recorded. Usually the injected fuel had a higher temperature (around 120°F) due to viscous friction.

Several steps were necessary in processing the data. These included averaging the flows over the whole period of running, the calculation of the overall fuel leakage and the tabulation of pressures from each pressure trace. These tabular pressures were used for graphic representation of the results shown in this study.

2.5 The Experimental Results

The experimental data collected in this study can be divided into three parts. The first is data of running conditions needed for the purpose of comparisons between the experiment and the computer model. The second is data of running conditions needed for the theoretical study of the after-injection phenomenon and means of eliminating it. This data was used also for comparisons between the experiment and the computer model, and is presented together with the first data in Chapter IV. The third set of data which is presented in this chapter is the data needed for an experimental study of the injection system running under after-injection conditions.

2.5.1 The After-Injection Survey

Bradbury[7] gave a region on the speed-fuel delivery plane, Figure 11, in which after-injection occurs and outside of which it does not occur. In his description of Figure 11 he defined point X as the system design point. An increase in either fuel injected, or operating pressures due to increased pump speed results in after-injection. The after-injection is primarily cuased by occurrences at the pump, specifically with the manner in which the fuel is spilled near the end of the injection cycle. The lower limit line PAC results from a high spill rate due to the spill point being on the fast part of the cam. For high fuel deliveries, on the other hand, spilling occurs more toward the end of the cam lift (where the cam velocity is low). This results in a low spill rate, which in turn neutralizes the high pressures in the region above PBD. Bradbury also mentioned that line PBD will be vertical for pumps with constant cam speed near the end of the plunger lift. In addition the after-injection zone may be bodily moved to the right by increasing the area of the nozzle injection holes, or to the left by a partially plugged nozzle.

The previous discussion is of special value for the theoretical investigation of after-injection. It points to the important factors controlling this undesirable phenomenon. The injection system performance was therefore surveyed to identify the following two points:

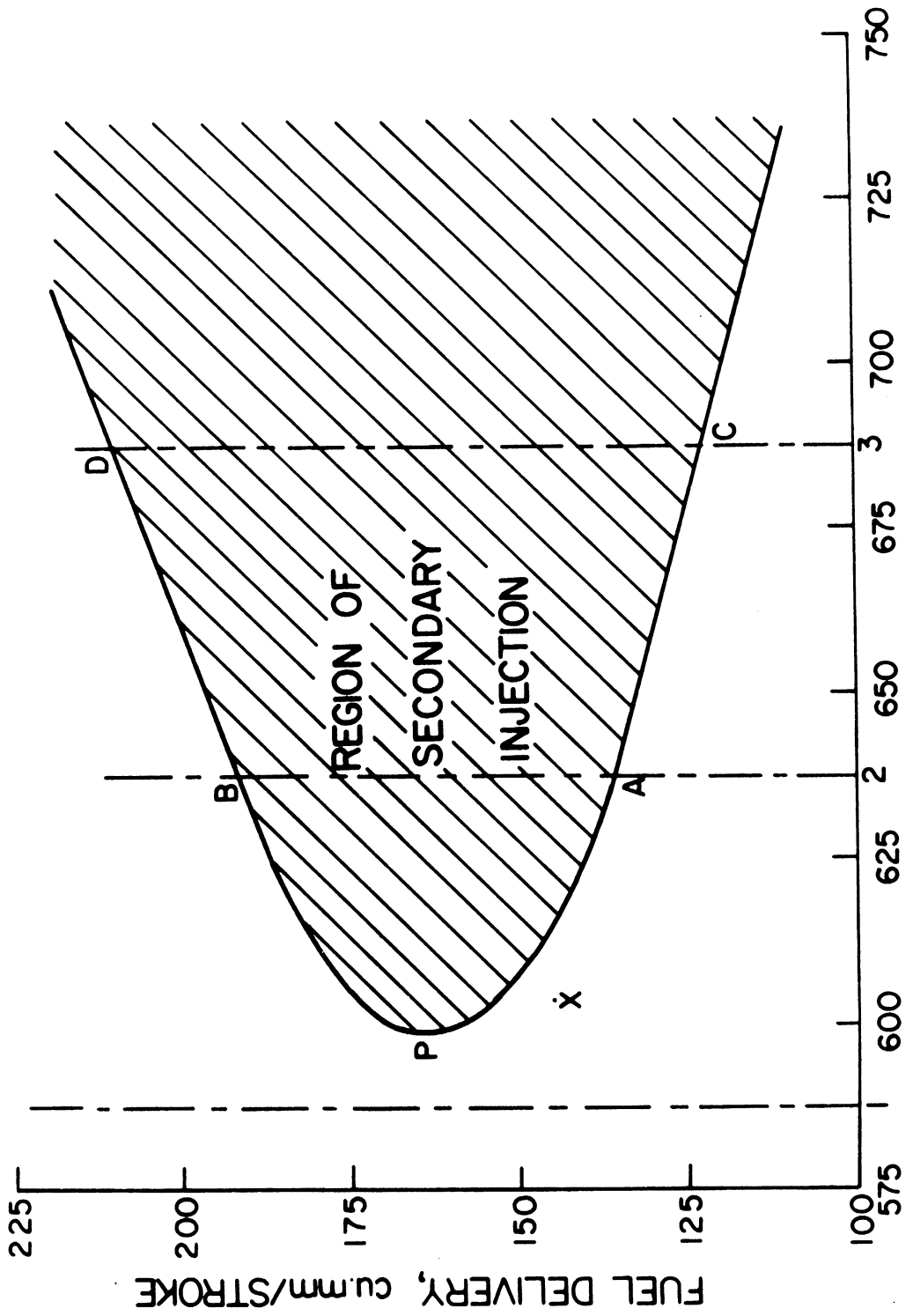

Figure 11. Secondary Injection Zone in a Speed, Fuel Delivery Plane.

1. The region of operation in which after-injection is certain to occur.

2. The magnitude of the after-injection problem.

In order to simulate after-injection conditions, the injection system described in Section 2.2 was tested with the injection holes partially blocked to reduce the injection area to about 2/3 of the original one. This condition commonly occurs in diesel engines after short periods of operation, usually due to carbon blocking of the injection holes.

The injection system was tested under a wide range of operating conditions. The pump cam speed was varied from 100 rpm to 1000 rpm with an increment of 100 rpm and the rack micrometer was varied from a condition representing 20 percent of maximum fuel delivery to a condition representing 80 percent of maximum fuel delivery, with an increment of 10 percent. Extremely high speed and high load conditions were not tested due to a fuel leakage problem around the injection chamber pressure transducer. Pressure measurements were taken in the pump delivery, injector upper and injection chambers. In addition the fuel flow to the pump and the total injected fuel were measured.

The average flow resistance coefficient through the nozzle holes was calculated in a manner similar to that described in Section 2.4. Figure 12 shows that the measured average flow resistance coefficient varied within $\pm$ 5 percent of .19 x 10^{-3} $in.^2$.

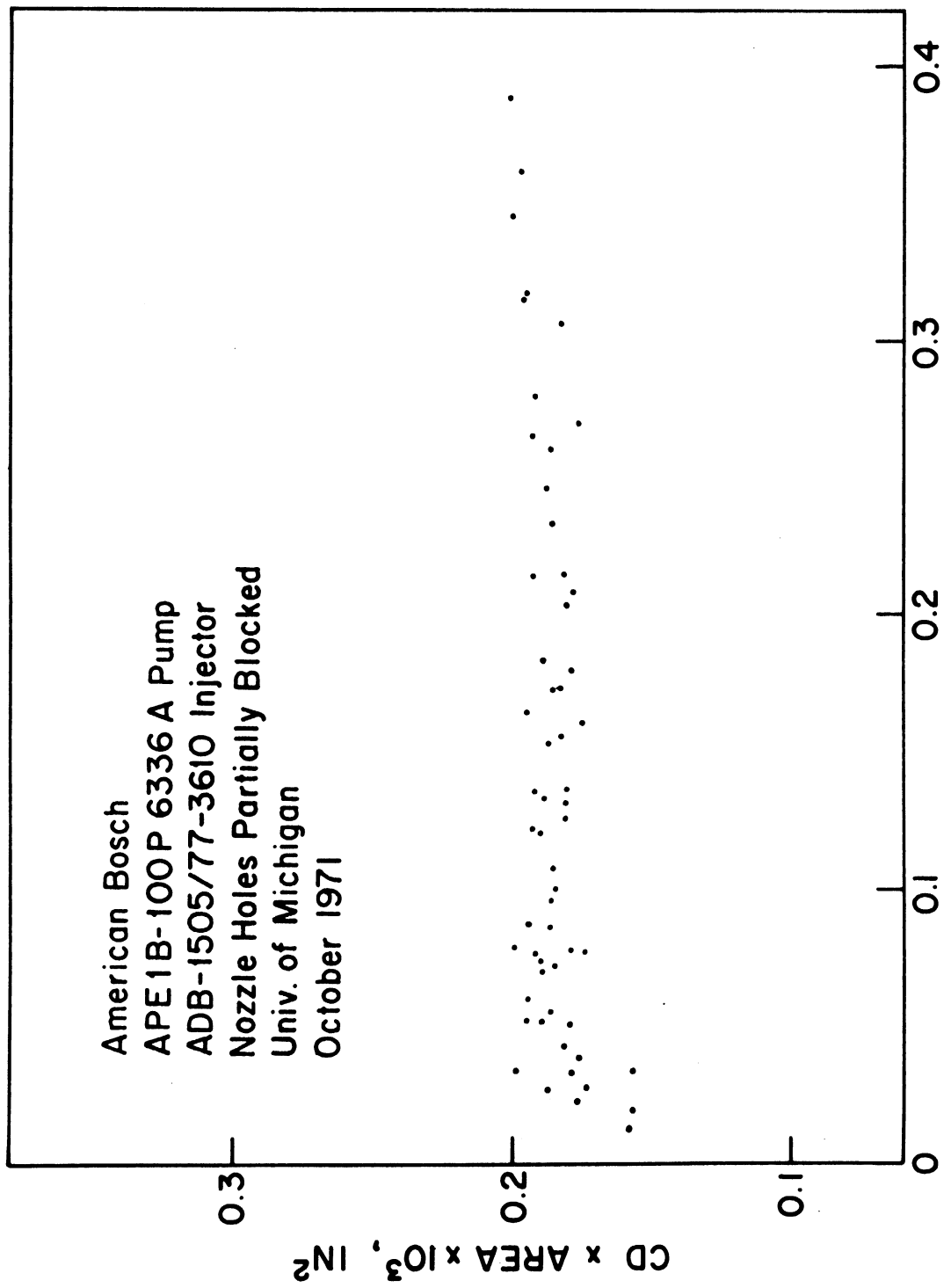

Figure 12. Variation of Flow Resistance Coefficient with Injected Flow Rate.

This variation is within the tolerance of the experimental measurement. Therefore, it is reasonable to conclude that the average flow resistance coefficient is constant under all test conditions.

Figure 13 shows the after-injection zone. The differences between Figure 13 and Figure 11 are due to the difference in nozzle injection areas, and because the pump used in the test rig had a constant cam speed near the end of the pumping stroke.

The relation between the total injection and the load is linear and is shown in Figure 14. Each trace on the figure represents a constant speed line. The slight differences between these lines are mainly due to a change in fuel leakage and throttling effect at the pump ports. High speed tests are characterized by short interval cycles; this results in lower fuel leakage and consequently higher total injection, when compared with lower speed tests. Figure 15 shows the effect of the pump speed on the total amount of fuel injected for various load conditions. The speed has little effect on the total amount of fuel injected per cycle. At low loads, an increase of speed results in a slight increase in the total amount of fuel injected per cycle. On the other hand, at high loads, an increase in speed results in a slight decrease in the total amount of fuel injected per cycle, due to the fact that more fuel is dumped at the spill port. This effect is more important at high loads than leakage.

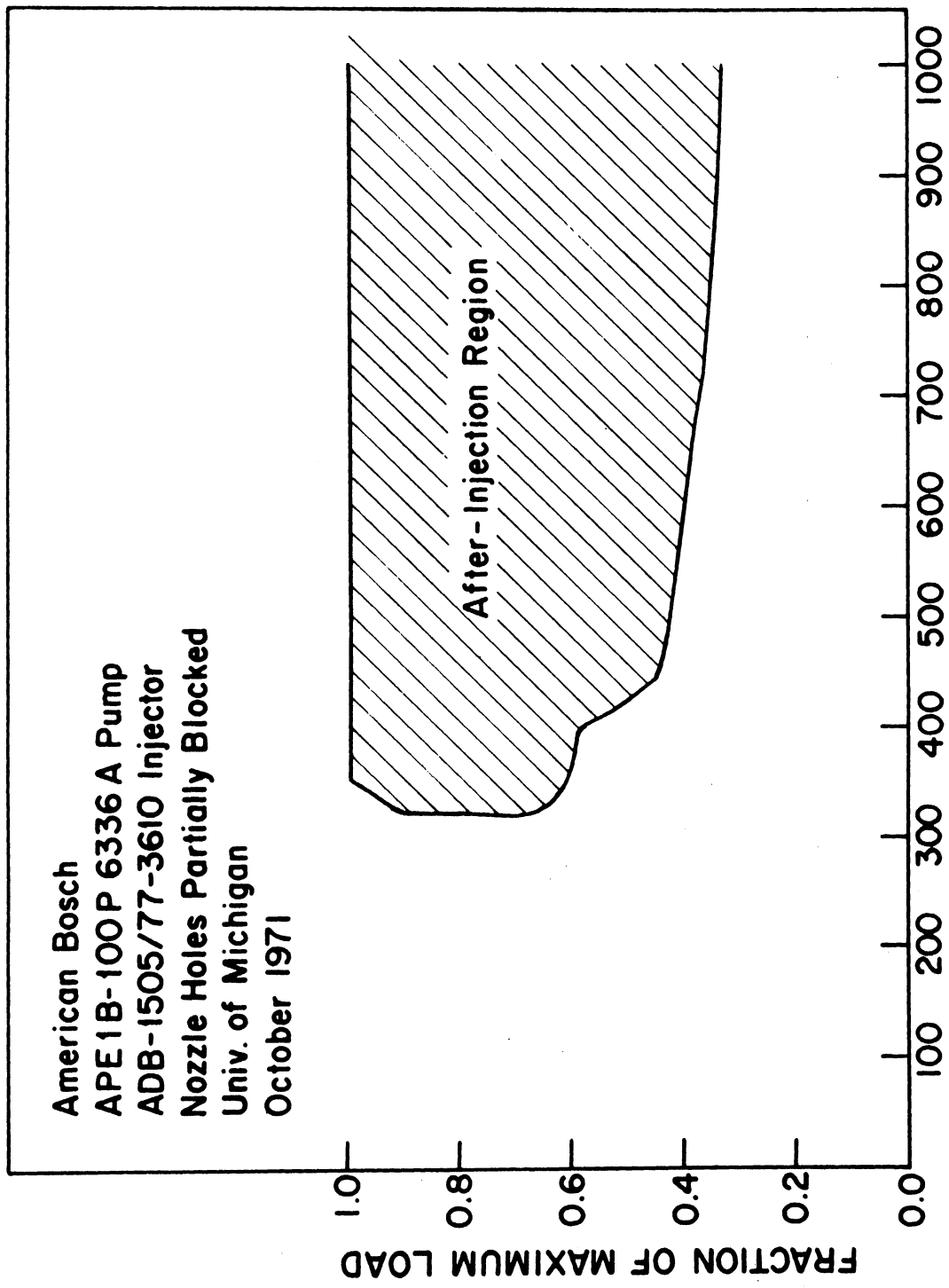

Figure 13. After-Injection Zone in a Speed, Load Plane.

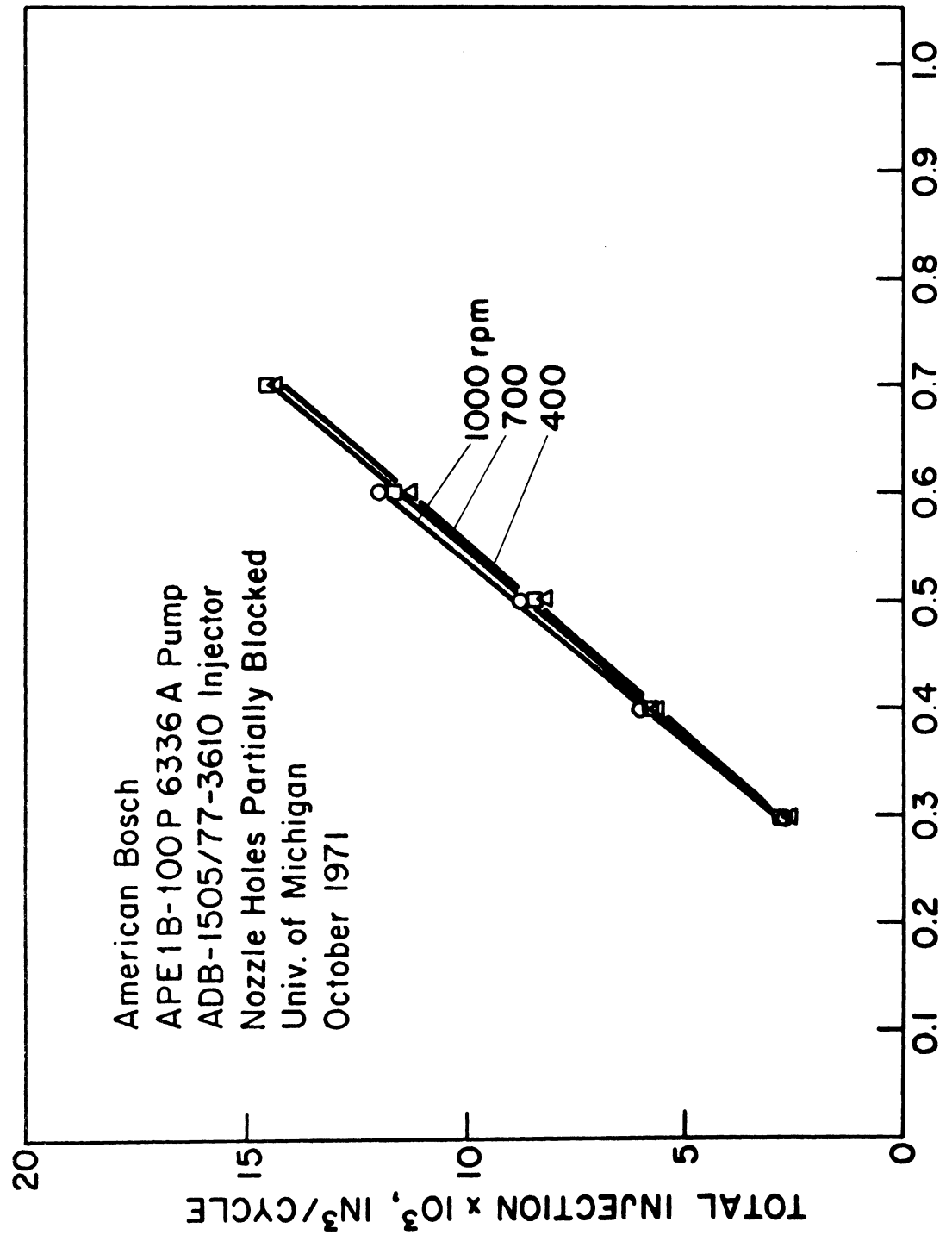

Figure 14. Effect of Load on Total Injection per Cycle for Various Pump Speeds.

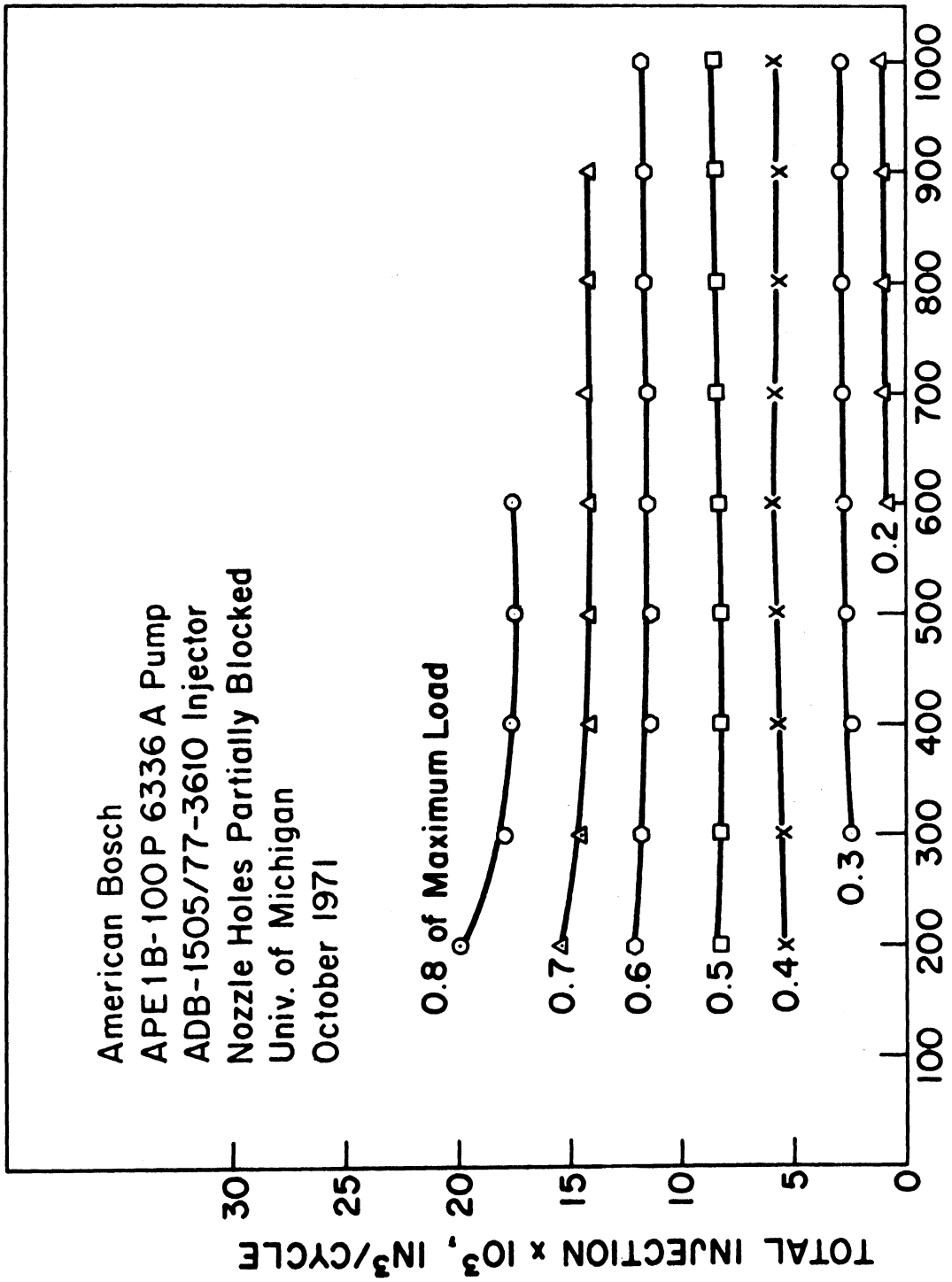

Figure 15. Effect of Pump Speed on Total Injection per Cycle for Various Load Conditions.

The amount of main injection is defined as the fuel injected during the first part of the cycle between the first nozzle needle opening and its first closing. The effect of load on the main injection/cycle is shown in Figure 16. Again each trace represents a constant speed test. At a fixed load, the lower the speed the higher the main injection. This is due to the fact that more after-injection occurs at high speeds, while the total injection is constant. In addition, Figure 17 displays the main injection as a function of pump speed for various load conditions. At low loads, there is very slight effect of speed on the main injection due to the fact that after-injection does not occur at these loads. This is contrasted with high load conditions where after-injection increases with increased speed and results in lower main injection.

The amount of after-injection is defined as the quantity of fuel injected after the main injection ends. Figure 18 shows the effect of load on the amount of fuel after-injected per cycle. It is seen from the lines of constant speed that after injection starts earlier as the speed increases. In addition, the rate of change of after-injection is smaller for lower speeds. In Figure 19 the data shown in Figure 18 is redrawn to show the effect of speed on the after-injection per cycle. At constant micrometer setting after-injection starts at a certain speed, after which it increases rapidly with speed. Finally, the rate of after-injection

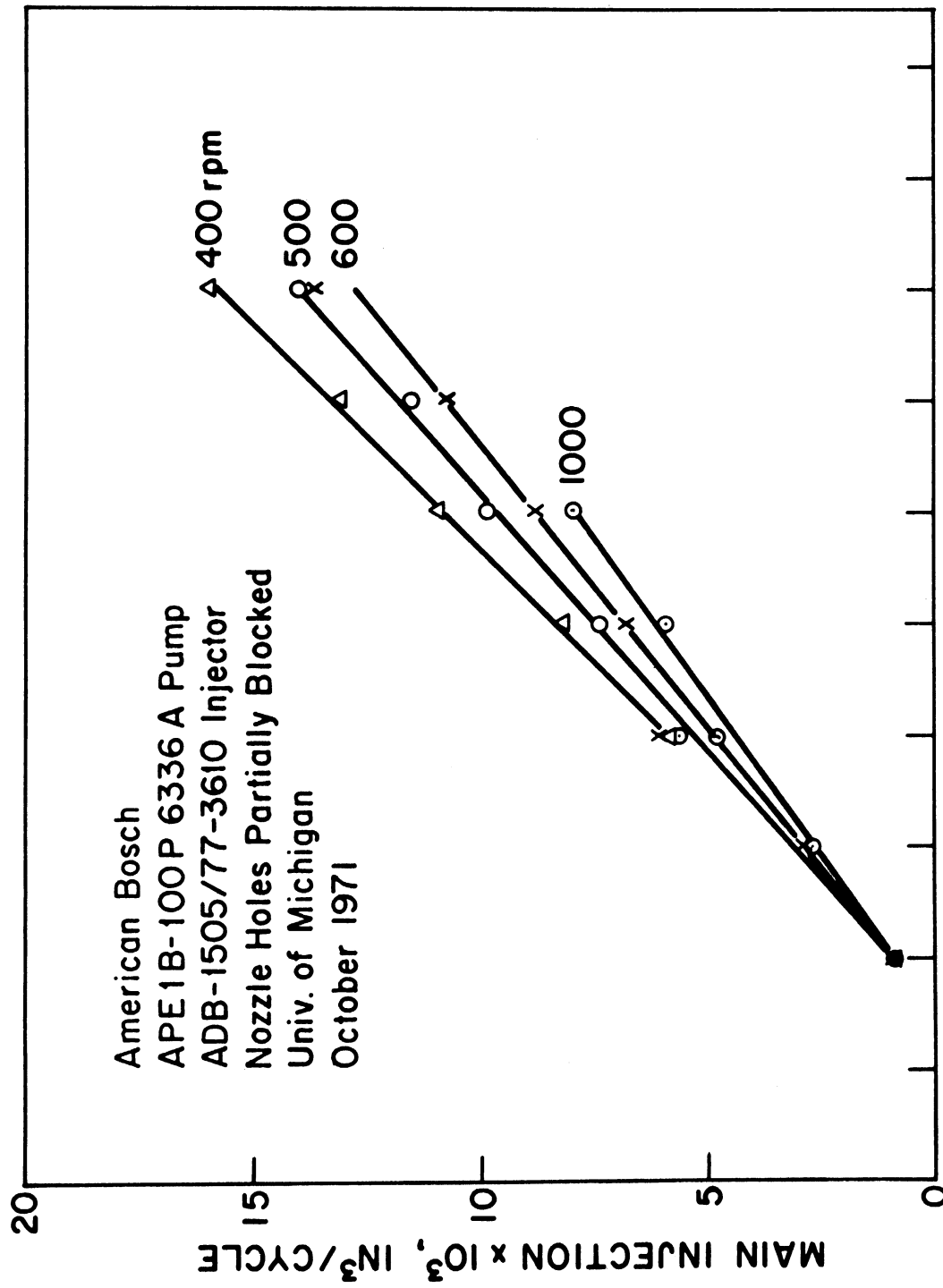

Figure 16. Effect of Load on Main Injection per Cycle for Various Pump Speeds.

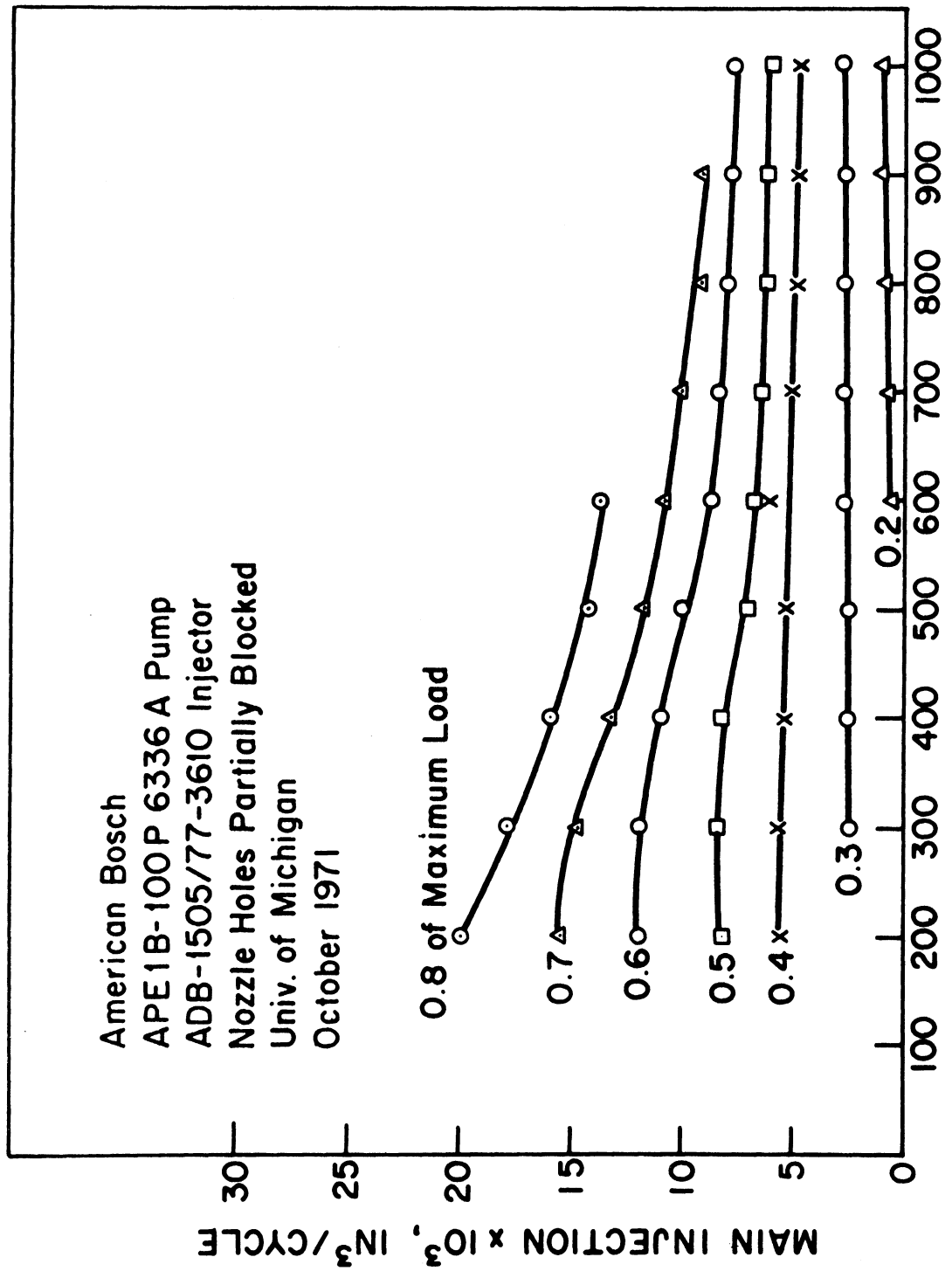

Figure 17. Effect of Pump Speed on Main Injection per Cycle for Various Load Conditions.

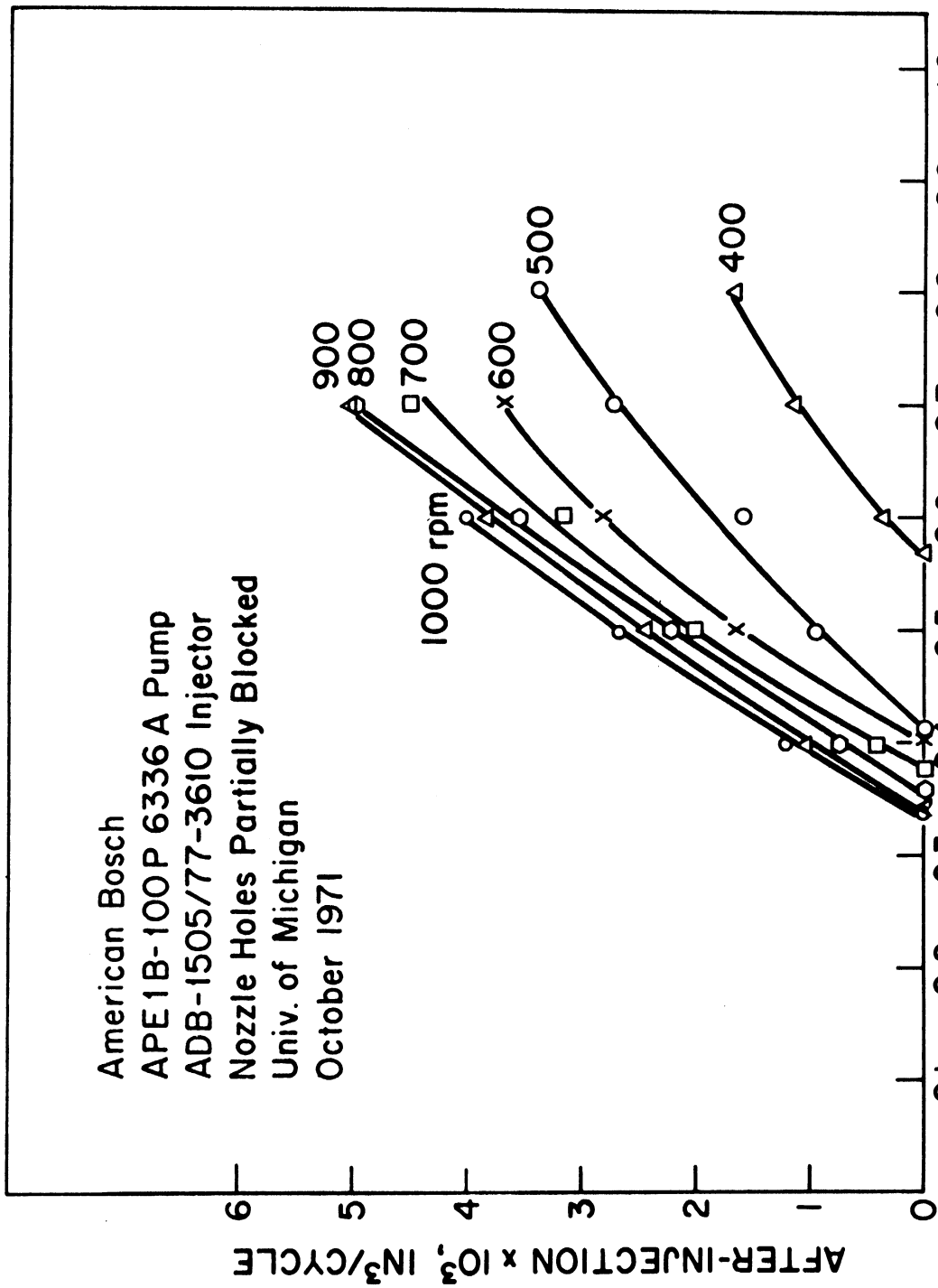

Figure 18. Effect of Load on After-Injection per Cycle for Various Pump Speeds.

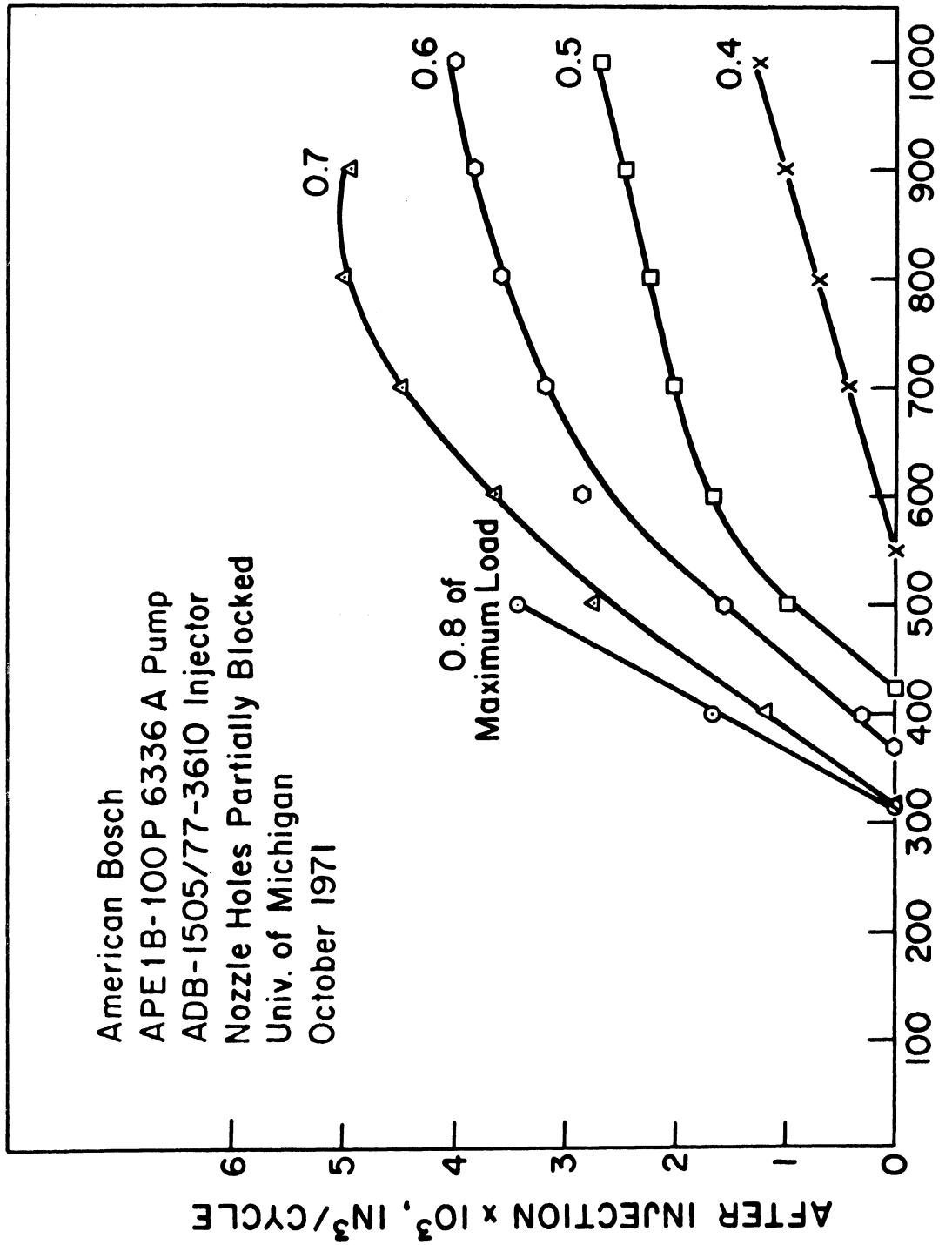

Figure 19. Effect of Pump Speed on After-Injection per Cycle for Various Load Conditions.

levels off at higher pump speeds. Figures 20 and 21 show the percentage of the after-injected fuel with respect to the total injection as a function of load and speed. Thirty-five percent of the total fuel was after-injected as a result of combining high speed and load conditions. Both figures show that the rate of increase of after injection decreases with increasing load at constant speed or increasing speed at constant load. This is mainly due to the fact that at constant speed, the total injection increases at higher rates with respect to changes in load than the after-injection. On the other hand at constant loads, the total injection is essentially independent of speed, while the after injection tends to go to a constant value only at high speeds.

The above survey of a diesel injection system indicates that many hydraulic limitations affect the performance of the system as a result of after-injection. These limitations and their effects are:

1. Injection systems are usually designed to operate at fuel deliveries and injection pressures considerably below their full capacities in order to avoid after-injection. These low injection pressures limit fuel atomization and penetration in the combustion chamber.
2. The optimum design point of injection systems is located critically close to the after-injection zone. Any accumulation of carbon or fuel impurities on the

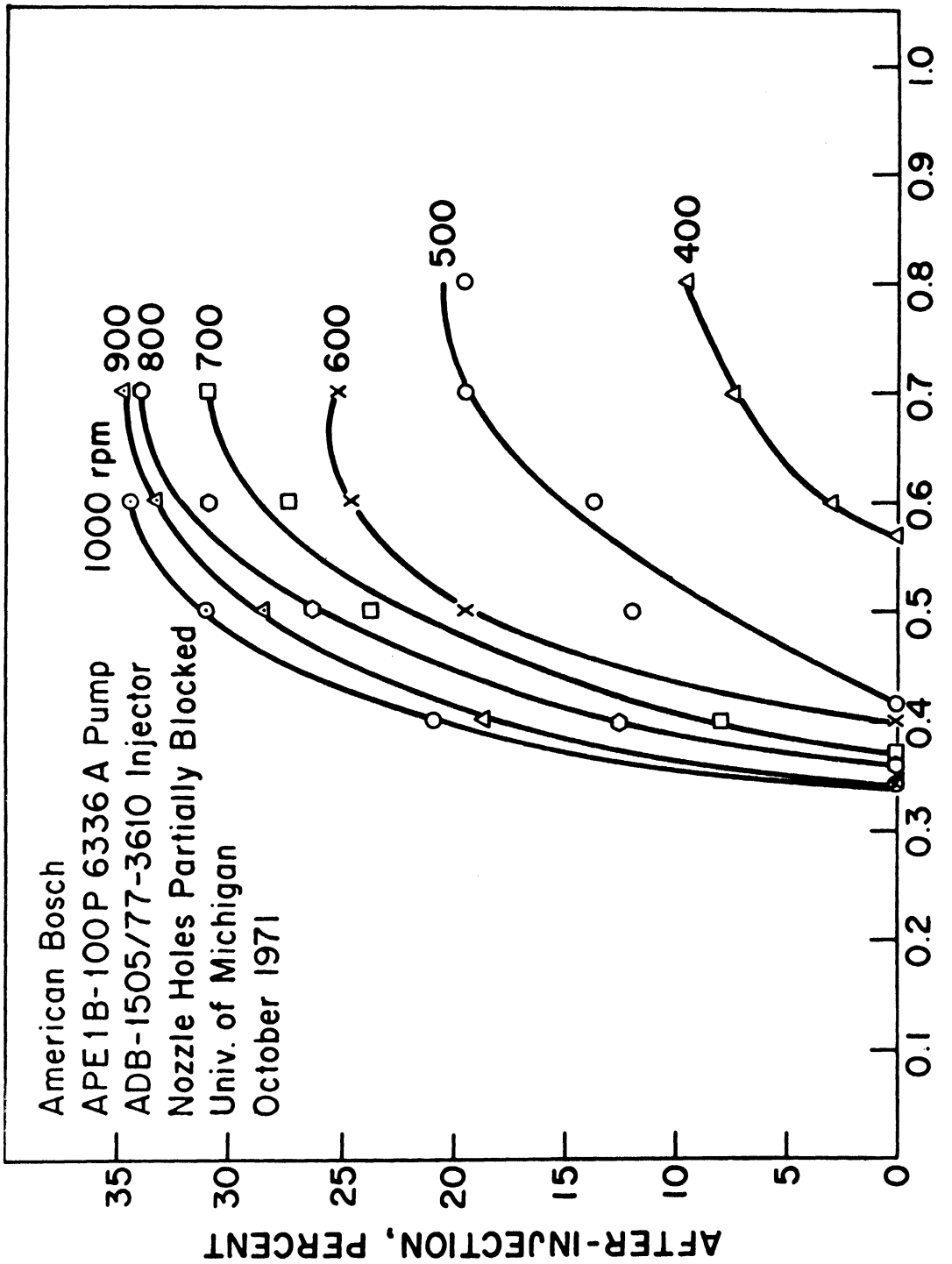

Figure 20. Effect of Load on Percent After-Injection for Various Pump Speeds.

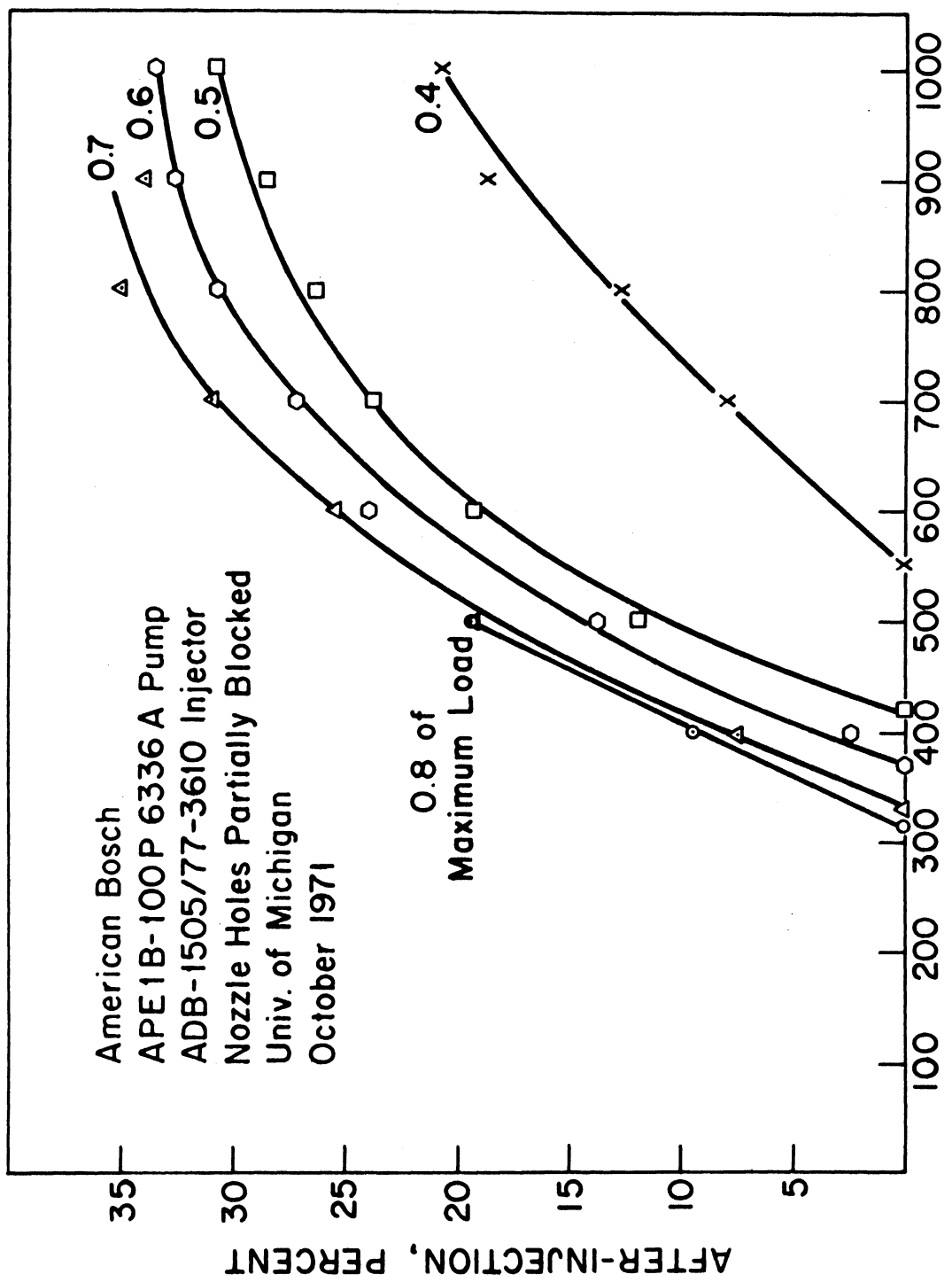

Figure 21. Effect of Pump Speed on Percent After-Injection for Various Load Conditions.

nozzle holes changes the system performance drastically and will introduce large amounts of after-injection. This results in a need for frequent servicing of the injection system.

From the above discussion it appears that the need is very urgent for a theoretical design approach that could eliminate after-injection by means other than increasing the nozzle injection area or reducing the maximum cycle pressure. The analytical method used in a design approach to eliminate after-injection by changing some of the system time varying properties is presented in Chapters V and VI.

III. BASIC EQUATIONS DESCRIBING THE DIESEL INJECTION SYSTEM

3.1 The Injection System Analysis

Until recently injection system design and modifications have been based on experimental trial-and-error methods. Experimental methods used to control some of the undesirable phenomena (after-injection and cavitation) that happen during the injection process are tedious, expensive and frustrating.

From the basic equations describing the fuel injection system, a computer model could be developed which would lessen the effort, time and expense of development work. The computer model could also be used as the basis for a design approach. The reliability of the design approach is dependent upon the accuracy of the computer simulation program. The basic assumptions underlying the simulation program should be fully understood and analyzed. The validity of such assumptions will be indicated by the correlation between the experimental data and the computer model results.

The diesel fuel injection system comprises four major components, namely: the fuel supply line, the pump, the delivery pipe line and the injector. It should be emphasized that the performance of each of these components depends on the other, i.e., a total system interaction takes place. Therefore, the equations describing the whole system should be solved in a simultaneous manner.

3.2 Basic Assumptions

The assumptions underlying the formulation of the injection system equations are:

a. The flow passages (supply line, chambers, etc.) were considered to be completely rigid. Elastic deformations of the different component parts of the system due to action of the fluid pressure are negligible. The error in the wave velocity as a result of neglecting pipe line deformation for the line defined earlier was found to be less than 0.5 percent for the maximum pressure variation (12,000 psi).

b. The effect of temperature and pressure on the fluid density and bulk modulus of elasticity, together with the effect of temperature on the fluid kinematic viscosity have been taken into account. References 25 and 31 were helpful toward the determination of those properties.

c. Fluid compressibility was introduced through the use of a pressure dependent bulk modulus of elasticity. This yielded a pressure dependent wave propagation velocity that is a function of fluid compressibility only.

d. Frictional effects were evaluated by considering the loss during unsteady flow to be the same as the loss

for steady flow with the same velocity and fluid property. A friction-factor-resistance formulation was used wherein the friction factor f is a function of the Reynolds number Re. For the laminar range ($Re < 2000$), Hagen-Poiseuille's equation gives:[28]

$$f = \frac{64}{Re} \tag{3.1}$$

For the turbulent range and transition zone ($Re \geq 2000$), the Blasius equation for smooth pipes gives:[28]

$$f = \frac{0.316}{Re^{1/4}} \tag{3.2}$$

The frictional pressure drop was calculated using the formula,[28]

$$\Delta p = f\left(\frac{8\gamma L}{\pi^2 D^5 g}\right) Q^2 \tag{3.3}$$

where Δp is the frictional pressure drop, γ is the fluid specific weight, L is the pipe length, D is the pipe diameter and Q is the rate of flow in the pipe.

e. A one-dimensional distributed parameter unsteady model was used to describe the flow in the fuel pipe lines. This implies that the parameters of system elasticity, inertia and frictional losses are distributed along the pipe length.

f. Whenever the pressure at any section on the pipe line tended to drop below vapor pressure it was maintained at vapor pressure and the formation of a vapor cavity was assumed. The vapor cavity was permitted to grow and collapse in accordance with the dynamic equations and a local mass continuity balance.

g. The flow through the orifices was assumed to be non-cavitating. Effects of fluid compressibility were neglected along the orifice length. Orifice discharge coefficients were based on steady-state data. References 14, 20 and 21 were used to give the coefficients of discharge as a function of length over diameter ratio and Reynolds number.

3.3 The Theoretical Formulation of the Model

The equations which describe the dynamic response of the diesel injection system include four effects, namely: compressibility of elastic volumes, flow through orifices and passages, dynamics of the moving parts and transient flow in the piping system. These equations are grouped in three categories as follows: the pipe lines (supply line and the high pressure delivery line), the pump and the injector.

3.3.1 Transient Flow in the Piping System

Figure 22a shows the control volume used in the derivation of the continuity equation. The net mass inflow through the control volume boundaries must equal the rate of increase of mass inside the control volume. This can be written in the following form:

$$\gamma AV - [\gamma AV + \frac{\partial(\gamma AV)}{\partial x} \delta x] = \frac{\partial}{\partial t}(\gamma A \delta x) \qquad (3.4)$$

where:

A = pipe cross sectional area in $in.^2$

V = fluid velocity in in./sec.

δx = incremental length of control volume

and x, t are the independent variables of distance and time, respectively.

Equation (3.4) can be expressed in the following form:[29]

$$\frac{\partial Q}{\partial x} + \frac{gA}{a^2\gamma} \frac{\partial p}{\partial t} = 0 \qquad (3.5)$$

where:

p = the fluid pressure in $lb/in.^2$

and a is the wave propagation velocity in the fluid which is given by:

$$a = \sqrt{gK/\gamma} \qquad (3.6)$$

where K is the fluid bulk modulus of elasticity - $lb/in.^2$

Figure 22b shows the control volume used for the equation of motion. The acting forces are the pressure and frictional forces. The force due to the deformation of the piping material and the

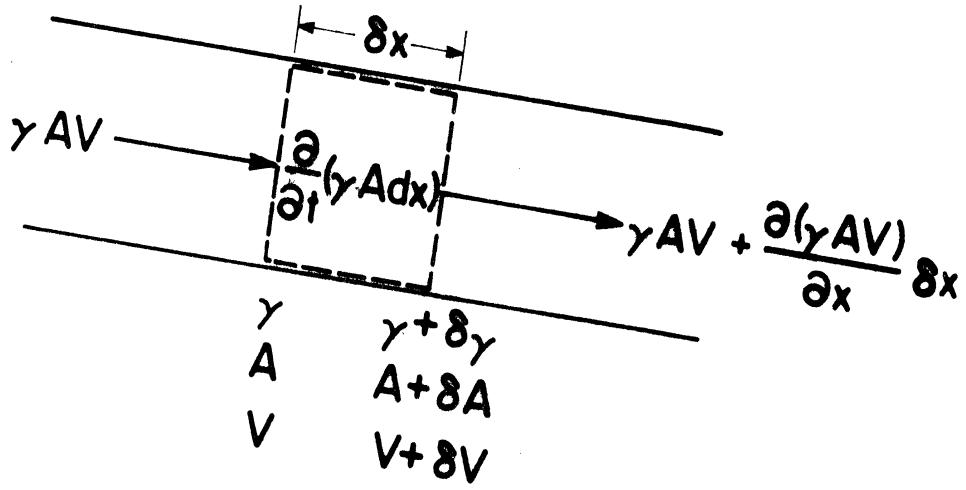

(a) Control Volume Used for the Continuity Equation

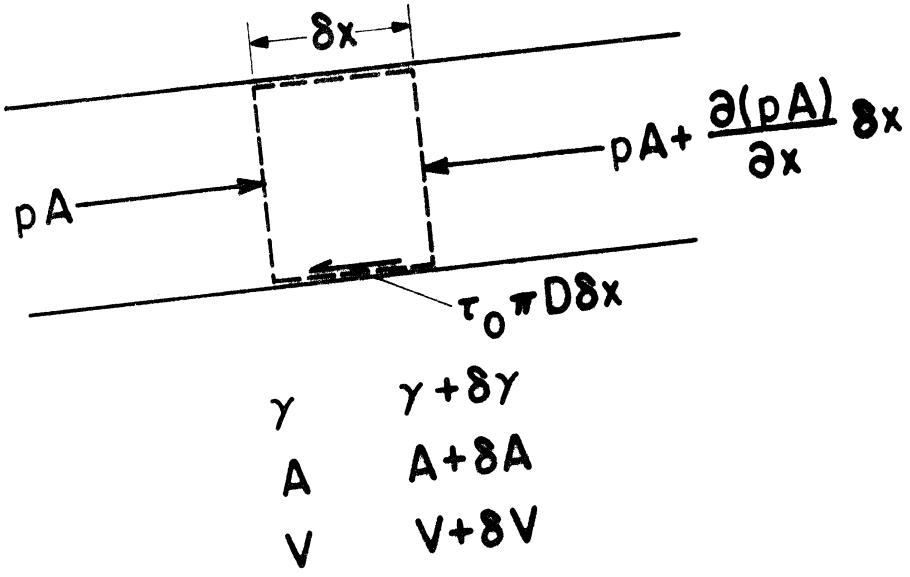

(b) Control Volume Used for the Equation of Motion

Figure 22. The Control Volume Used to Derive the Pipe Equations.

gravitational force are neglected due to their very small values compared to the pressure force. Therefore, the equation of motion can be written as:

$$pA - \left(pA + \frac{\partial(pA)}{\partial x}\,\delta x\right) - \tau_o \pi D\,\delta x = \frac{\gamma A}{g}\,\delta x\,\frac{dV}{dt} \qquad (3.7)$$

The following common expression for the steady state shear stress τ_o is used:[28]

$$\tau_o = \frac{f\,V|V|}{8} \qquad (3.8)$$

where

V = the fluid velocity.

Then Equation (3.7) can be expanded in the following form:[29]

$$\frac{\partial Q}{\partial t} + \frac{gA}{\gamma}\frac{\partial p}{\partial x} + \frac{f}{2DA}\,Q|Q| = 0 \qquad (3.9)$$

The absolute value of Q and V are introduced to maintain the correct direction of the shear stress with respect to the direction of motion. In the derivation of Equations (3.5) and (3.9) the convective acceleration terms are dropped because their values are very small compared to the other terms considered.

Equations (3.5) and (3.9) are partial differential equations with x and t as the independent variables, and p and Q as the dependent ones. These two equations are converted into four ordinary differential equations by use of the method of characteristics.[29] These ordinary differential equations can be transformed

into four algebraic equations by the use of a first-order finite difference approximation method which results in:

$$Q_Z - Q_W + \frac{gA}{\gamma_W a_W}(p_Z - p_W) + \frac{f_W \Delta t Q_W |Q_W|}{2DA} = 0 \qquad (3.10)$$

$$x_Z - x_W = a_W \Delta t \qquad (3.11)$$

$$Q_Z - Q_Y - \frac{gA}{\gamma_Y a_Y}(p_Z - p_Y) + \frac{f_Y \Delta t Q_Y |Q_Y|}{2DA} = 0 \qquad (3.12)$$

$$x_Z - x_Y = -a_Y \Delta t \qquad (3.13)$$

where Δt is the time increment. The pipe is divided into fixed equally spaced sections of length Δx each, and the subscripts W, Y and Z refer to positions in the x-t plane, as shown in Figure 23. It should be noted that Equation (3.10) is valid only along the forward characteristic line, W-Z, as described by Equation (3.11), while Equation (3.12) is valid only along the receding characteristic line, YZ, as described by Equation (3.13). For stability reasons it is necessary that the grid spacing Δx must be greater than or equal to the product of the wave speed a and the time increment Δt .

In general the analysis of any pipe line begins with known conditions of pressure and discharge at time $t=t_o$. Then the transient pressures and discharges are calculated for time $t_o + \Delta t$ at the equally spaced sections which are separated by the grid spacing Δx. By considering a pressure dependent wave speed, the slopes of

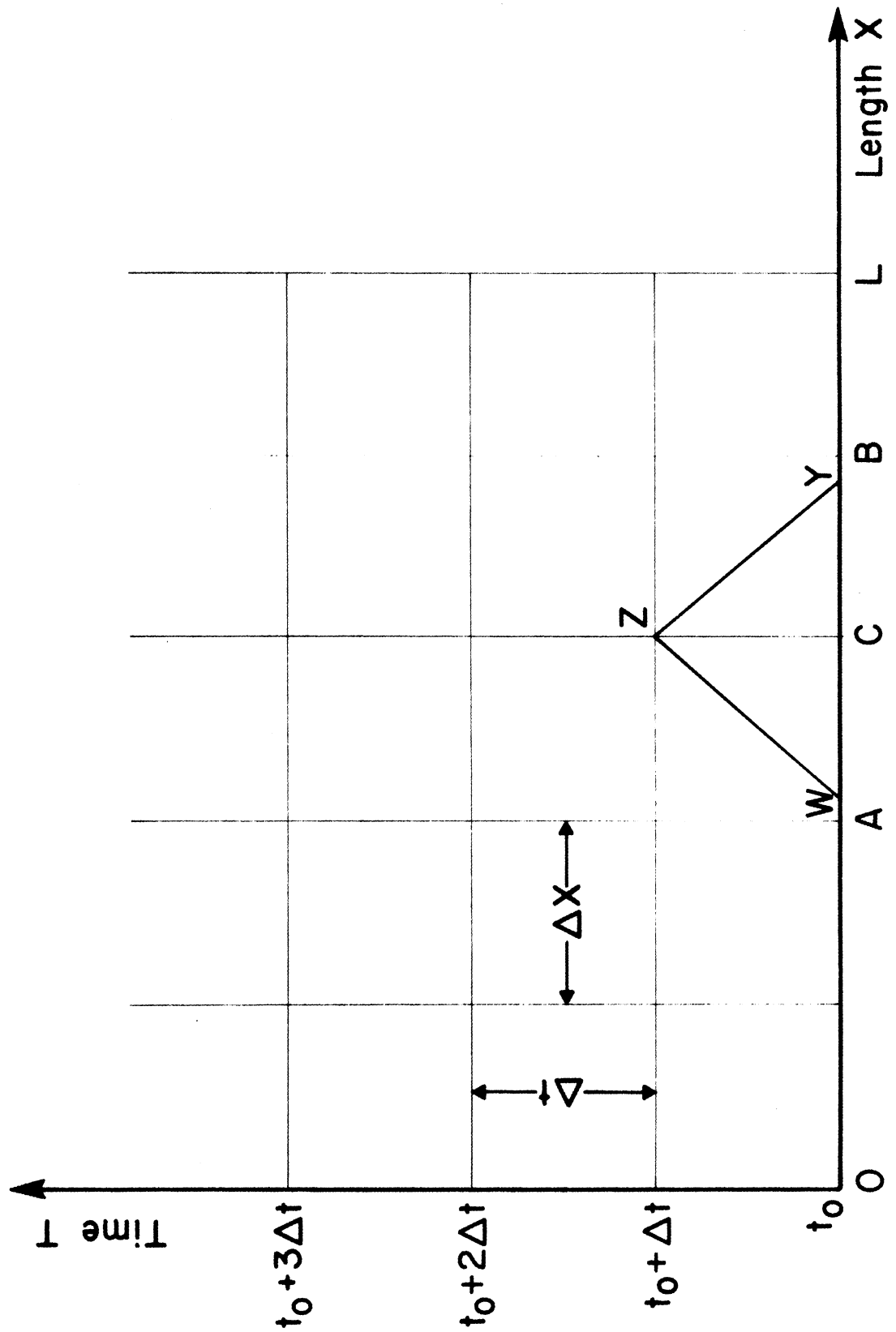

Figure 23. Characteristics in x-t Plane.

the characteristic lines W-Z and Y-Z are dependent on the value of the wave speeds at the points W and Y, respectively. In Figure 23, point W may be located at any place between A and C. Therefore, an interpolation between the known points A and C is required to find the conditions at point W. A similar interpolation is required at Y. In order to reduce errors resulting from interpolation, a variable time increment is helpful. The choice of the time increment, at a certain instant, is based on the maximum wave speed along the pipe line. As a result, the time increment may vary from one time to another.

In Figure 23 consider that the pressure and discharge are known at each grid intersection along the horizontal line $t = t_o$. The new values of pressure and discharge are calculated at a point Z by solving Equations (3.11) and (3.12). This procedure is valid for all interior points. At x=0, the C^- line is used together with the equations describing the boundary condition at x=0 to find the new boundary condition at $t = t_o + \Delta t$. Similarly for x=L the C^+ line is used together with the equation describing the boundary condition at x=L.

For the fuel supply pipe line, the conditions at the filter define the boundary equation at x=0. The large capacity of the filter implies that the pressure is constant at this point. On the other hand, the pump conditions define the pipe boundary equations at x=L. For the delivery pipe line, the pump equations

serve as the boundary equations at x=0. Similarly the injector equations serve as the boundary equations at x=L.

3.3.2 The Injection Pump

In order to formulate the equations describing the injection pump, it is necessary to describe the following effects:

a. The fluid compressibility in various volumes is calculated using the equation:

$$K = \frac{\Delta p}{\Delta \forall / \forall} \tag{3.14}$$

where

$\Delta\forall$ = change in fluid volume

$\forall$ = initial volume

Δp = change in fluid pressure

b. The fluid flow through the various orifices and passages is described by:

$$Q = C_d A \sqrt{\frac{2g}{\gamma}(p_1 - p_2)} \tag{3.15}$$

where p_1 and p_2 are the orifice upstream and downstream pressures respectively.

c. The equation of motion which describes the dynamic action of mechanical moving parts such as the delivery valve, is used in the following form:

$$F = m\, dV/dt \tag{3.16}$$

where

F = sum of all the forces in the direction of motion, including pressure, frictional and spring forces

m = mass of the mechanical part

V = velocity of the mechanical part

Figure 24 shows a cross sectional view of the injection pump, including the major elements. The continuity equations combined with Equation (3.14) for the feed, the pumping, and the pump delivery chambers are given by Equations (3.17) through (3.19), respectively.

$$\frac{dp_f}{dt} = \frac{K_f}{\forall_f}(Q_{Zs} - Q_1 + Q_2 - Q_4) \tag{3.17}$$

$$\frac{dp_p}{dt} = \frac{K_p}{\forall_p + A_v S_v - A_p S_p}(A_p V_p - A_v V_v + Q_1 - Q_2 - Q_3) \tag{3.18}$$

$$\frac{dp_d}{dt} = \frac{K_d}{\forall_d - A_v S_v}(A_v V_v + Q_3 - Q_{Zd}) \tag{3.19}$$

S represents the valve or pump plunger displacement, and the subscripted Q's represent the flow rates at different points of the injection pump as illustrated in Figure 24. The subscripts f, p, d and v refer to conditions at the pump feed, pumping and delivery chambers and the pump delivery valve respectively. The denominator on the right hand side of Equation (3.18) represents the instantaneous volume of the pumping chamber due to the effect of the plunger and delivery valve motions. Similarly the one in Equation (3.19)

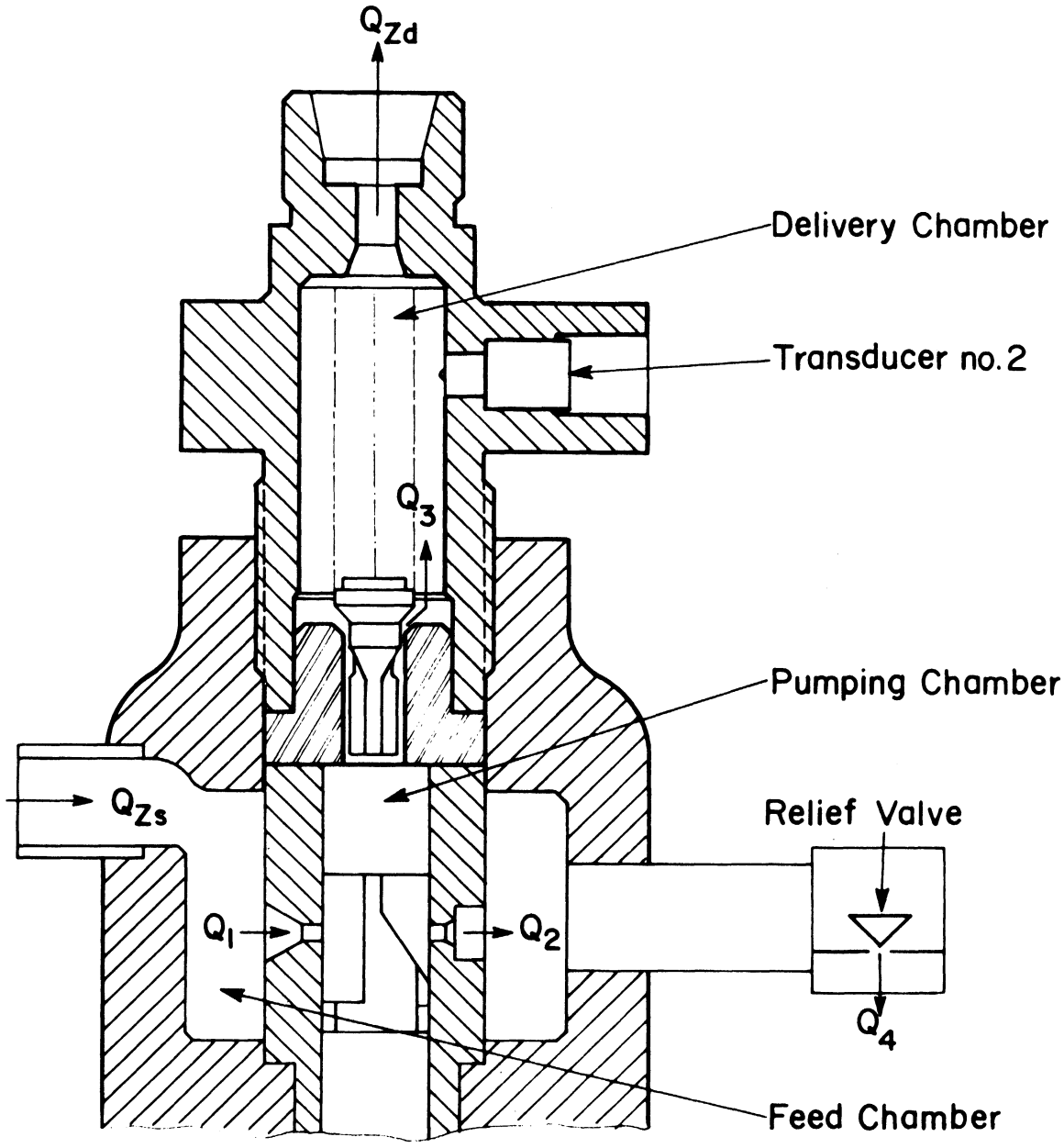

Figure 24. Sectional View of Injection Pump.

gives the instantaneous volume of the pump delivery chamber due to the effect of the delivery valve motion. The flow rates through different pump orifices are defined by:

$$Q_1 = C_{d_1} A_1 \sqrt{2g(p_f - p_p)/\gamma} \tag{3.20}$$

$$Q_2 = C_{d_2} A_2 \sqrt{2g(p_p - p_f)/\gamma} \tag{3.21}$$

$$Q_3 = C_{d_3} A_3 \sqrt{2g(p_p - p_d)/\gamma} \tag{3.22}$$

$$Q_4 = C_{d_4} A_4 \sqrt{2g\ p_f/\gamma} \tag{3.23}$$

The numerical subscripts 1 through 4 refer to the pump intake port, spill port, flow area around the delivery valve and pump relief valve area, respectively.

Equation (3.16) applied to the pump delivery valve takes the following form:

$$\frac{dV_v}{dt} = \frac{g}{w_v}(A_v(p_p - p_d) - k_v - r_v S_v - f_v V_v) \tag{3.24}$$

where

$$\frac{dS_v}{dt} = V_v \tag{3.25}$$

In the above equations the quantities k, r, f_v and w_v represent the spring static force, spring stiffness, valve viscous friction coefficient and valve weight, respectively.

The flow leaving the supply line and entering the pump feed chamber, Q_{Zs}, is described by Equation (3.10) in the following form:

$$Q_{Zs} - Q_{Ws} + \frac{gA}{\gamma_{Ws} a_{Ws}}(p_{Zs}-p_{Ws}) + \frac{f_{Ws}\Delta t\, Q_{Ws}|Q_{Ws}|}{2DA} = 0 \qquad (3.26)$$

where the subscript Ws refers to known conditions in the supply pipe at an earlier time increment and defined in a fashion similar to Figure 23. Similarly the flow leaving the pump delivery chamber and entering the fuel delivery pipe, Q_{Zd} is described by Equation (3.13) in the following form:

$$Q_{Zd} - Q_{Yd} - \frac{gA}{\gamma_{Yd} a_{Yd}}(p_{Zd}-p_{Yd}) + \frac{f_{Yd}\Delta t\, Q_{Yd}|Q_{Yd}|}{2DA} = 0 \qquad (3.27)$$

where the subscript Yd refers to the known conditions in the supply pipe at an earlier time increment and defined in a fashion similar to Figure 23.

3.3.3 The Fuel Injector

The major elements of the fuel injector are shown in Figure 25. The continuity equations combined with Equation (3.14) for the delivery and nozzle upper chambers combined, nozzle lower chamber and injection chamber are:

$$\frac{dp_u}{dt} = \frac{K_u}{\forall_u + A_u S_n}(Q_{Zu} - Q_5 - Q_8 - A_u V_n) \qquad (3.28)$$

$$\frac{dp_l}{dt} = \frac{K_l}{\forall_l + A_l S_n}(Q_5 - Q_6 - A_l V_n) \qquad (3.29)$$

$$\frac{dp_i}{dt} = \frac{K_i}{\forall_i + A_i S_n}(Q_6 - Q_7 - A_i V_n) \qquad (3.30)$$

The subscripts u, l, i, and n refer to the nozzle delivery and upper chambers, the nozzle lower chamber, the injection chamber,

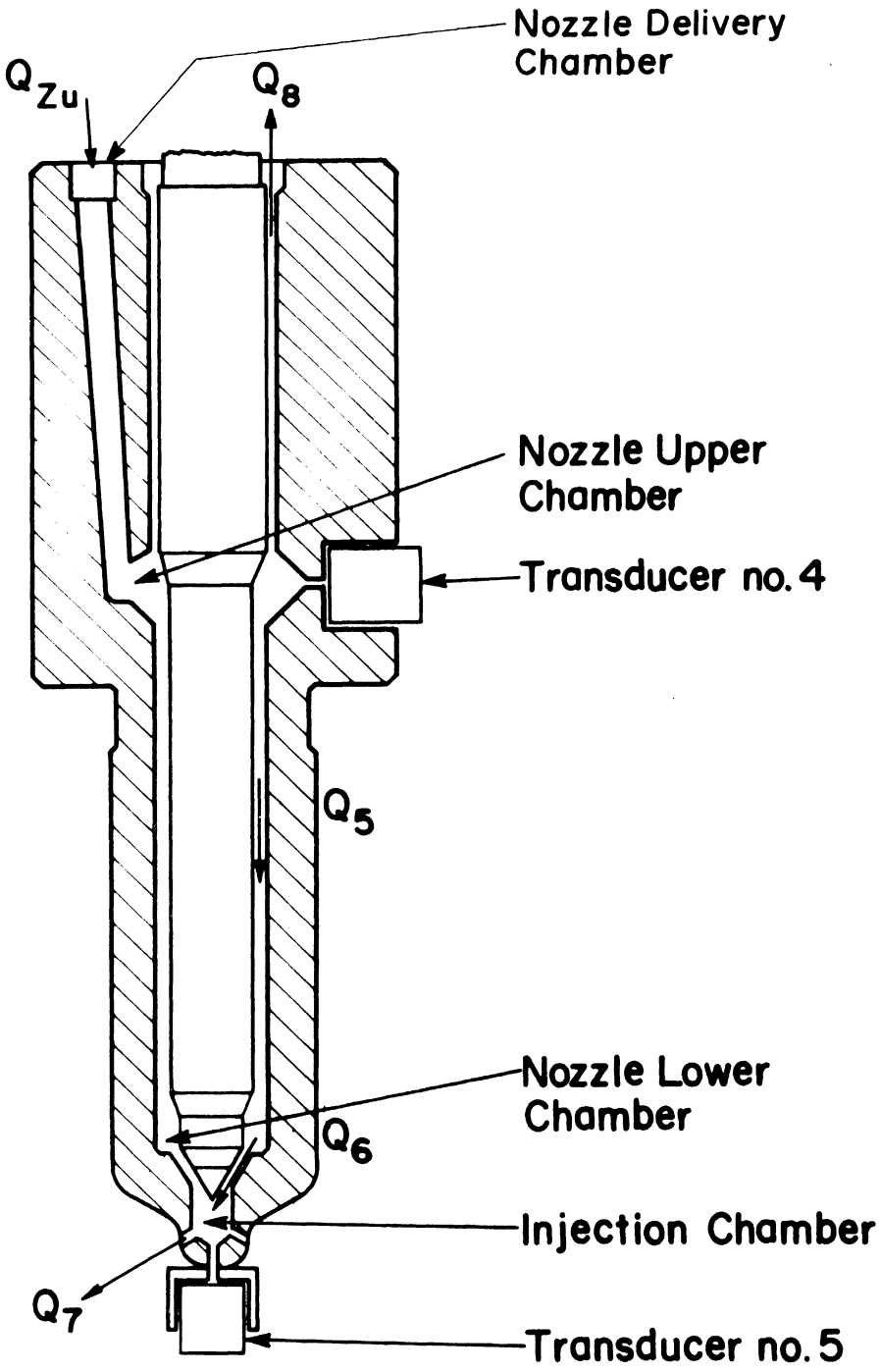

Figure 25. Sectional View of Injection Nozzle.

and the injector needle. In the above equations the term $\forall + AS$ is the instantaneous volume due to the needle motion.

Flow rates with numerical subscripts refer to the orifice flows shown in Figure 25 and are given by:

$$Q_5 = C_{d_5} A_5 \sqrt{2g(p_u - p_1)/\gamma} \tag{3.31}$$

$$Q_6 = C_{d_6} A_6 \sqrt{2g(p_1 - p_i)/\gamma} \tag{3.32}$$

$$Q_7 = C_{d_7} A_7 \sqrt{2g(p_i - p_c)/\gamma} \tag{3.33}$$

The leakage past the needle is given by

$$Q_8 = C_{Vf} p_u \tag{3.34}$$

where C_{Vf} is a viscous flow coefficient which can be calculated from Equations (3.1) and (3.3). The equations that describe the needle dynamics take the following forms:

$$\frac{dV_n}{dt} = \frac{g}{w_n}(A_u p_u + A_1 p_1 + A_i p_i - k_n - r_n S_n - f_n V_n) \tag{3.35}$$

$$\frac{dS_n}{dt} = V_n \tag{3.36}$$

The subscript n refers to conditions at the nozzle needle.

The flow leaving the delivery pipe line and entering the injection delivery chamber, Q_{Zu}, is described by Equation (3.10) in the following form:

$$Q_{Zu} - Q_{Wd} + \frac{gA}{\gamma_{Wd} a_{Wd}}(p_{Zu}-p_{Wd}) + \frac{f_{Wd}\Delta t Q_{Wd}|Q_{Wd}|}{2DA} = 0 \qquad (3.37)$$

where the subscript Wd refers to known conditions in the delivery pipe line at an earlier time increment and defined in a fashion similar to Figure 23.

IV. COMPARISON AND DISCUSSION OF THE SIMULATION AND EXPERIMENTAL RESULTS

The previous chapter dealt with the basic equations describing the injection system. This chapter considers the method of solution of these equations. In addition, the computer simulation results are presented and compared with the experimental data. A discussion of the parameters affecting the accuracy of the simulation model is given at the end of the chapter.

4.1 The Solution Technique

This section describes the method used to determine the theoretical system response. This is achieved by solving three sets of simultaneous equations representing the conditions at the supply and delivery pipe lines, the pump and the injector. Equations (3.10) and (3.12) describe the conditions in the pipe lines. The conditions at the pump are expressed by Equations (3.17), (3.18), (3.19), (3.24) and (3.25). The unknown time dependent variables in these equations are: the pressures in the pump feed, pumping and delivery chambers, the delivery valve displacement and velocity, the flow at the inlet of the pump feed chamber, and the flow at the exit of the pump delivery chamber. Similarly Equations (3.28) through (3.30), (3.35) and (3.36) represent the conditions at the injector.

The unknown time dependent variables in these equations are: the pressures in the nozzle upper, lower and injection chambers, the needle displacement and velocity, and the flow at the inlet of the nozzle upper chamber.

The solution of the system equations begins with known initial conditions in the pipe line, the pump, and the injector at time t. The interior points for both the intake and delivery pipes are calculated at time $t + \Delta t$ using Equations (3.10), (3.12) and the known initial conditions in the pipe line. The pump conditions are determined by solving the pump equations in conjunction with Equations (3.26) and (3.27). The last two equations are the C^+ and C^- equations at the pump-supply line boundary and the pump-delivery line boundary, respectively. Similarly, Equation (3.37) is used together with the injector equations to determine the conditions at the injector. It should be noted that Equation (3.37) is the C^+ equation at the delivery line-injector boundary.

The procedure for the numerical solution of Equations (3.10), (3.12) is well documented in the literature.[29] The pump and injector equations are solved numerically. Particular care should be exercised to assure a true solution of each set of differential equations because the boundary conditions at both the pump and injector are changing extremely rapidly. A modified predictor-corrector method by Hamming[26] is used in this model. This method is a numerical integration method which makes use of

the knowledge of the system response at earlier times. It requires information from the pipe line during the step change. This information is available by interpolation between known conditions in the pipe and by the use of Equations (3.10) and (3.12). In this method the time step for solving the system differential equations can be reduced below the fixed characteristic method time step. The size of this reduction depends on a prescribed accuracy level. Therefore, a relatively small time step is used in that part of the cycle in which the transient contains high frequency components, and the characteristic time step is used over the major part of the cycle. This improves the computer program efficiency, an advantage which is not readily available in either an iterative method or a Runge-Kutta method. The characteristic time step used in the simulation program was of the order of 0.0001 second, corresponding to a cam angle of about 0.48 degree at 800 rpm.

The input data required for the solution of the injection system must include a total description of the system geometric configuration, properties of the system components and fluid properties described in Section 2.2. The forcing function of the entire system is the specified cam motion which drives the pump plunger.

4.2 Experimental Data for Comparison with the Simulation Program Results

This section deals with the test conditions used to compare the experimental data with the theoretical simulation results. The object of the theoretical model is to be able to predict the performance of the diesel injection system and the phenomena associated with its operation. Therefore, the test conditions should cover different speeds and loads. Numerous experimental tests have been conducted to cover experimentally the range of conditions. Some of these cases are presented in Tables III and IV. Table III shows the testing conditions used to compare the experimental data with the simulation results.[32] Test No. 1 had a high speed, low load conditions and cavitation showed up in the pipe and injector pressure traces. On the other hand, Test No. 2 had a lower speed and a higher load. In this test neither cavitation nor after-injection occurred. Test No. 3 had combined high speed and load conditions and after-injection was detected. It is seen from Table III that the average flow resistance coefficient C_t is reasonably constant under all test conditions. Figure 26 shows a sample of recorded traces for Test No. 3. The upper trace in each frame is the pressure trace taken at each transducer location. The lower trace correlates the pressure trace with the instantaneous position of the cam during the pumping cycle.

TABLE III

RESUME OF TESTING CONDITIONS USED TO COMPARE WITH THE SIMULATION PROGRAM

Test No.	Speed rpm	Rack Micr.* Setting in.	Total Fuel Injected lb/min.	Base Pressure psi	C_t $in.^2$	Cavitation	After-Injection
1	800	.675	.0818	1100	.000185	Yes	No
2	400	.509	.0966	-	.000186	No	No
3	800	.509	.191	1400	.000178	No	Yes

*Rack Micrometer setting, in. = $1. - \frac{\text{Test load}}{\text{Maximum load}}$

TABLE IV

RESUME OF TESTING CONDITIONS USED TO COMPARE WITH THE SIMULATION PROGRAM AND USED TO STUDY THE AFTER-INJECTION PHENOMENON

Test No.	Speed rpm	Rack Micr. Setting in.	Total Fuel Injected lb/min.	Base Pressure psi	C_t in.^{2}	After-Injection lb/min.	% After Injection of Total Injection
4	365	.608	.054	1300	.000127	.0055	10.19
5	405	.350	.148	2000	.000126	.0343	23.18
6	700	.426	.216	2500	.000128	.0796	36.85

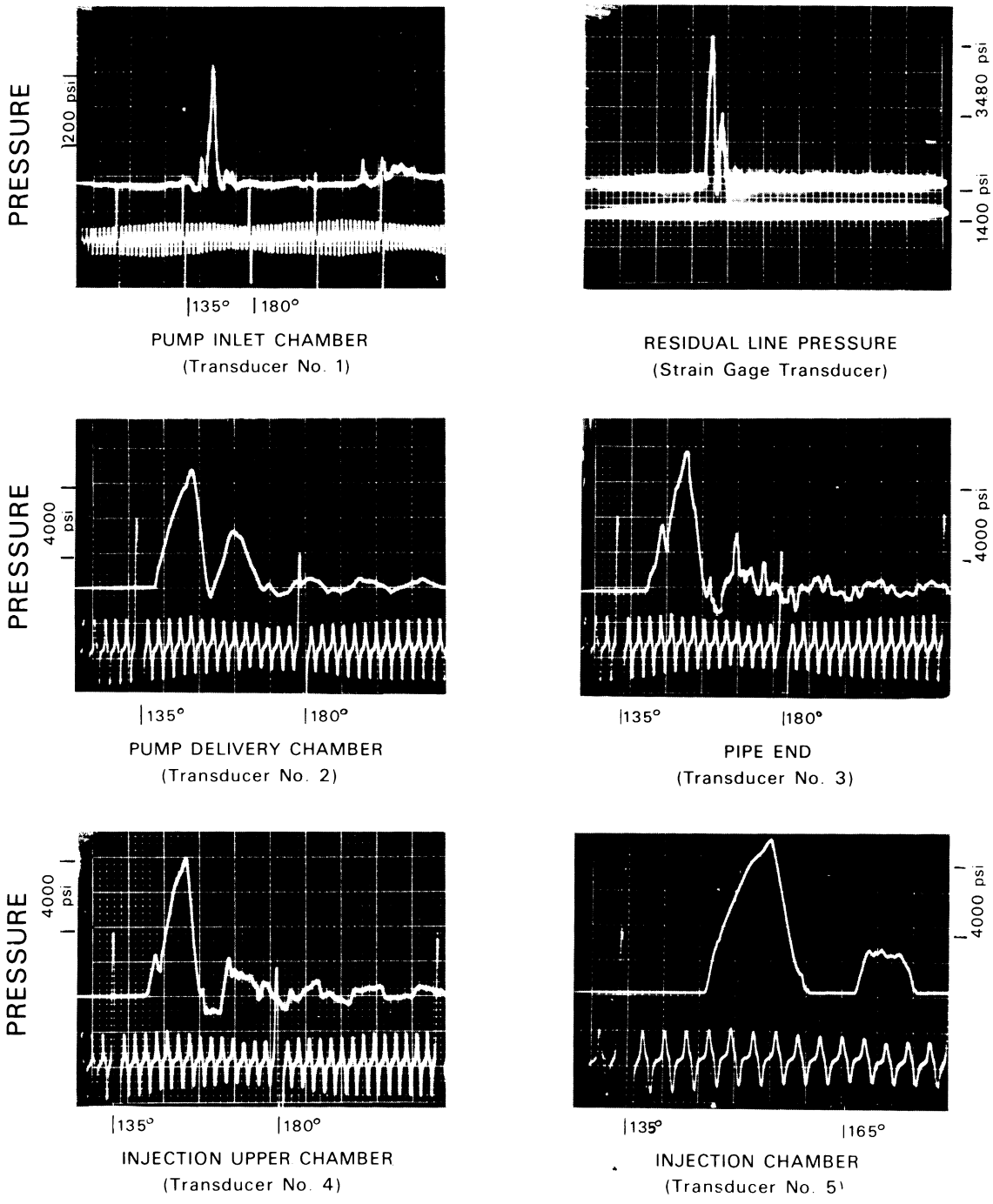

Figure 26. Oscilloscope Records of Transient Phenomena in the Diesel Injection System.

A smaller injection area was used for the tests presented in Table IV. This was necessary to produce after-injection so that this phenomenon could be simulated and then theoretically investigated. Test Nos. 4, 5, and 6 were chosen to represent low, medium and high speed and load conditions, respectively. It is seen from the table that a simultaneous increase of speed and load results in an increase in after-injection.

The experimental data obtained with this equipment were highly reproducible. This includes not only the system residual pressure and injected volume in each cycle but also individual pressure spikes in the recorded traces. These spikes may at first appear to be random. After injection and temporary conditions of vapor pressure were also very reproducible traits of certain operating condition.

As indicated in Section 4.1, the forcing function of the entire system is specified by the cam motion driving the pump plunger. Figure 27 shows the pump plunger lift during the pumping part of the cycle, together with the uncovered area of the spill port for Test No. 3.

4.3 Comparison of Results and Discussion

A comparison between experimental data and the theoretical model results for the six testing conditions listed in Tables III and IV is presented in this section. The results for the pressure

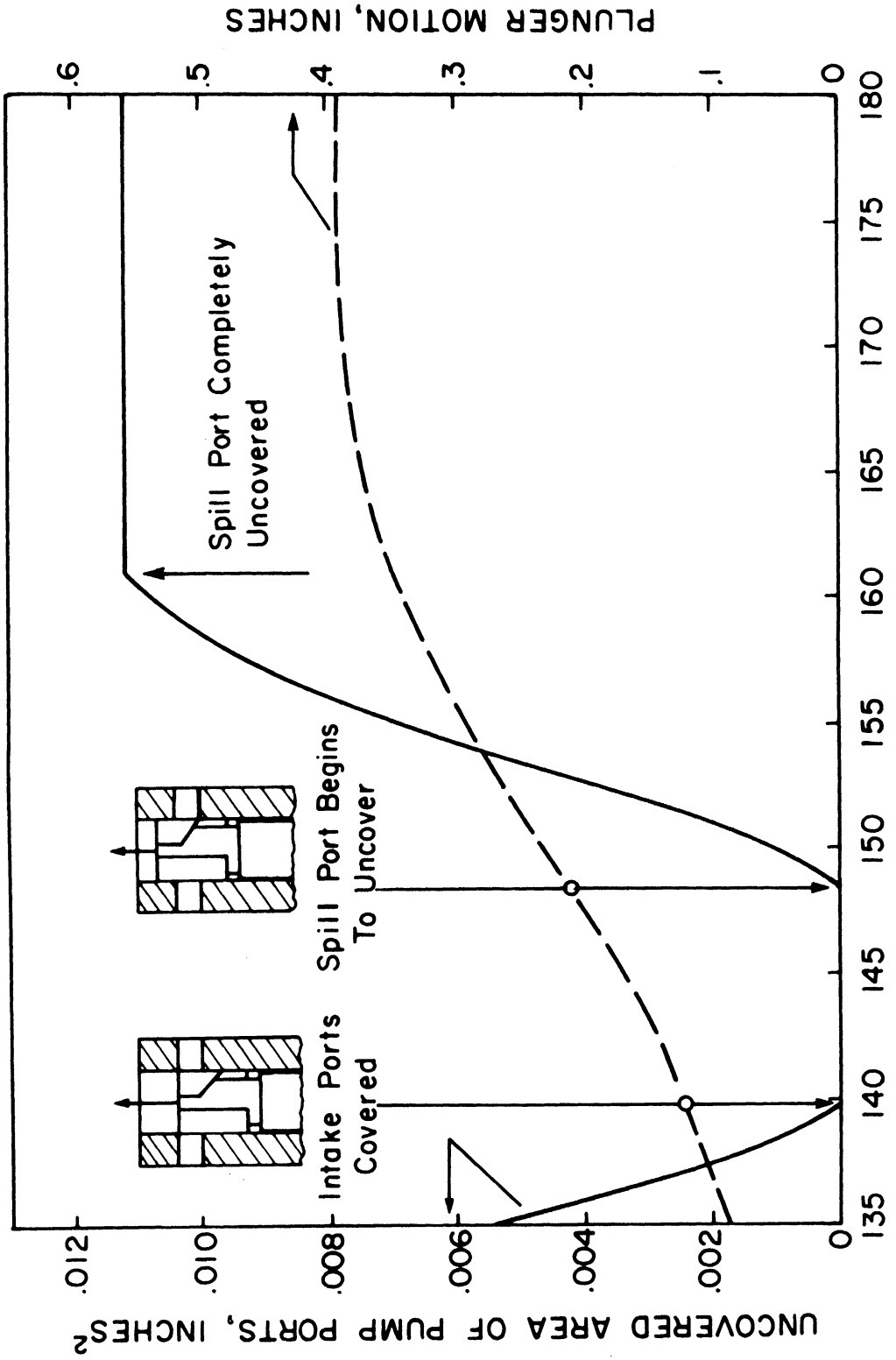

Figure 27. Pump Plunger Motion and Pump Port Areas; Rack Control Setting = 0.850 in.

variation at four locations, namely: the delivery chamber, the pipe end, the nozzle upper chamber and the injection chamber are given in Figures 28 through 33. Also, theoretical results for the pressure variation at the pumping chamber and the pump delivery valve and nozzle needle motion are included in the same set of figures. In addition, a comparison of experimental and simulated results in the pump delivery chamber for a larger pump cam angle is shown in Figure 34. These results are from the same test conditions as those shown in Figure 30. All the injection system variables are presented as functions of the pump cam angle for the portion of the cycle in which fuel injection occurs. The computer model results, together with the experimental data for the system residual pressure and the injected fuel for each of the six cases considered, are listed in Tables V and VI.

It is seen from the previous comparisons that the analytical model agrees reasonably well with the experimental data. This generates confidence in the underlying assumptions and techniques used in developing the model.

A cause and effect study of the injection system response is possible by examining any of the presented cases (Figures 29 through 34). For example, the pressure in the pumping chamber begins to rise slowly because the ports are still partly uncovered. When the ports are covered, the pressure rises rapidly. The pressure in the pump delivery chamber rises when the delivery valve

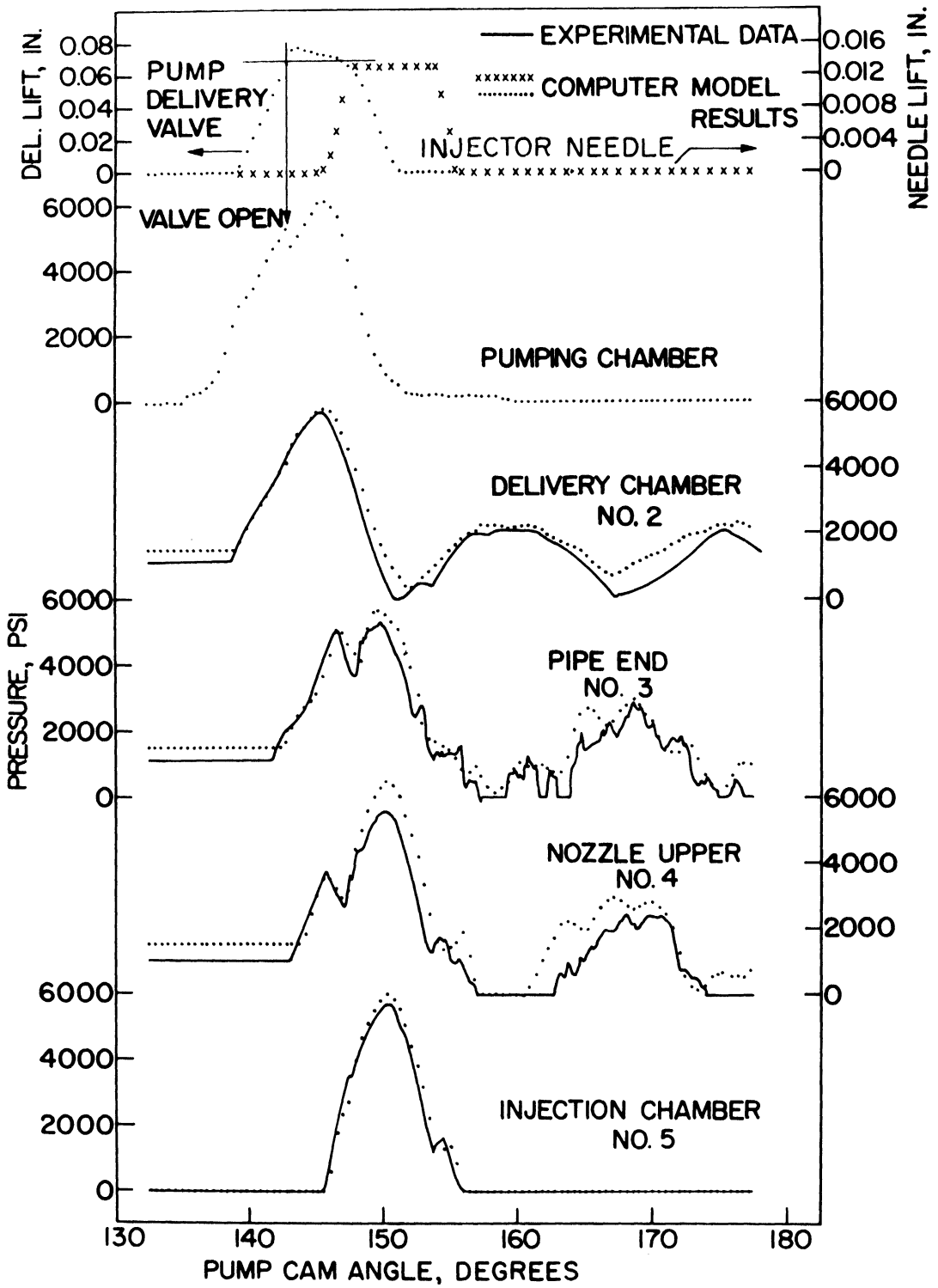

Figure 28. Comparison of Injection System Hydraulic Characteristics—Experimental and Computer Results, 800 RPM Pump Speed and 0.675 Rack Micrometer (0.0818 lb. fuel injected/min.).(32)

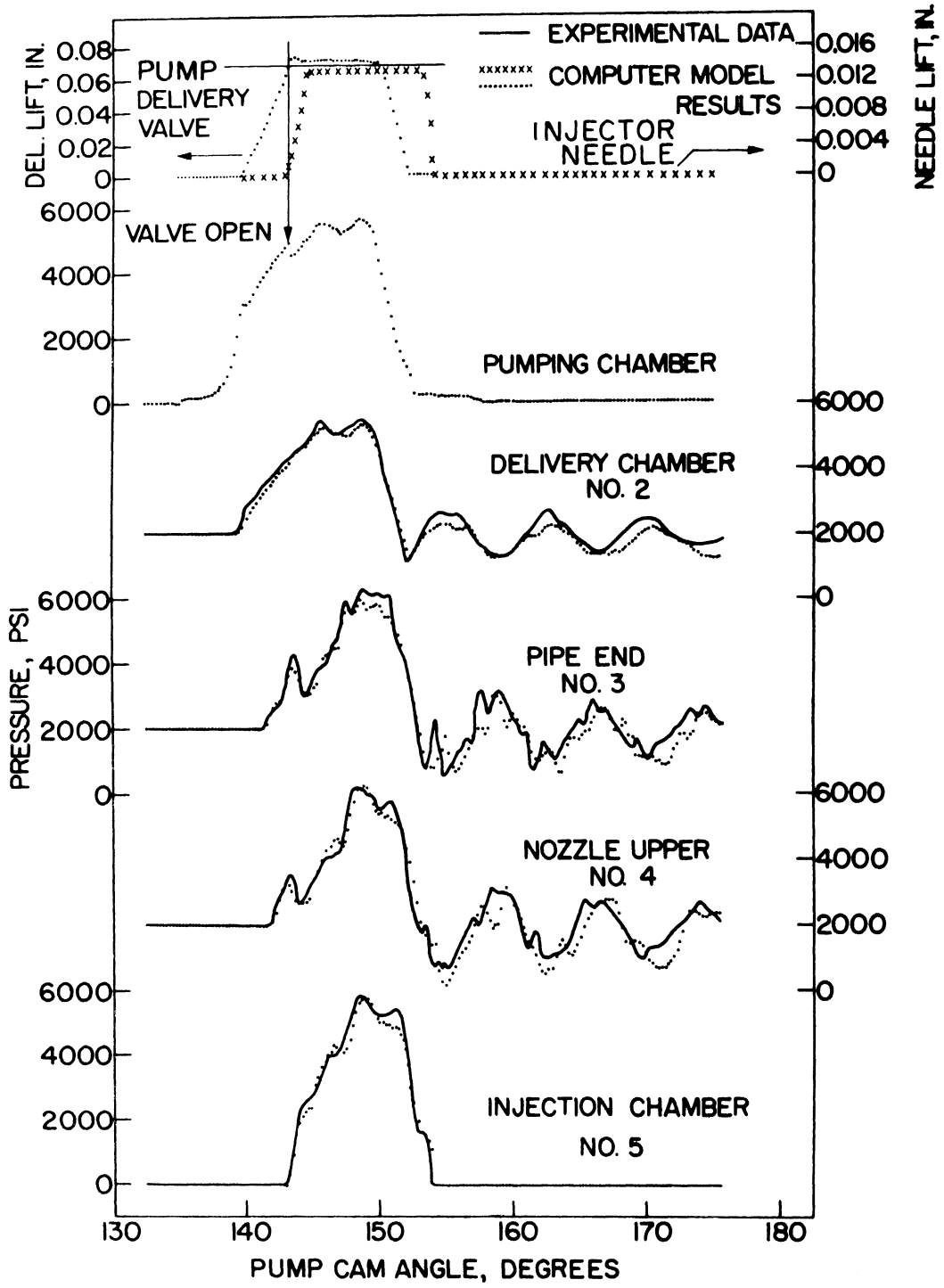

Figure 29. Comparison of Injection System Hydraulic Characteristics—Experimental and Computer Results, 400 RPM Pump Speed and 0.509 Rack Micrometer (0.0968 lb. fuel injected/min.).(32)

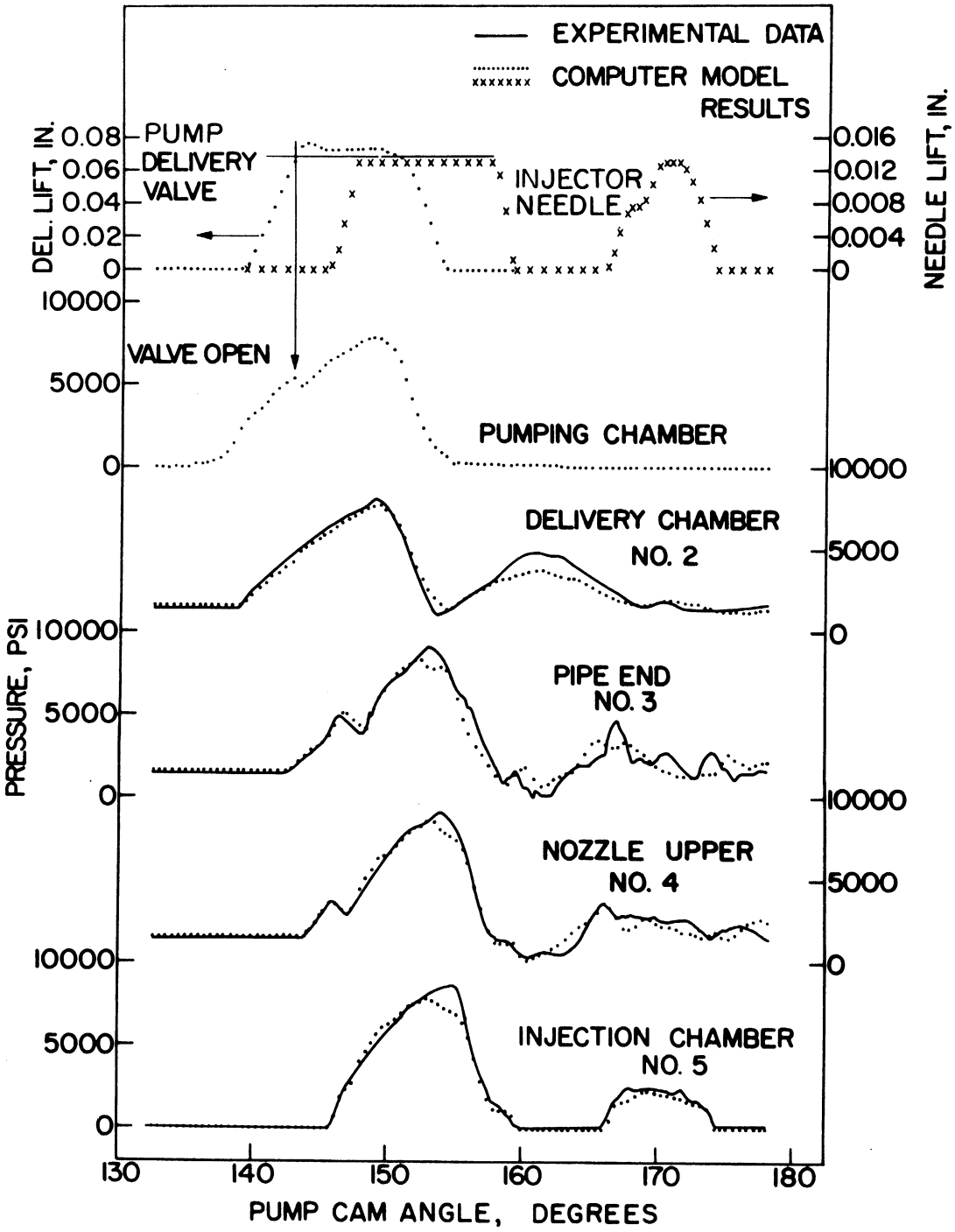

Figure 30. Comparison of Injection System Hydraulic Characteristics—Experimental and Computer Results, 800 RPM Pump Speed and 0.509 Rack Micrometer (0.1910 lb. fuel injected/min.).[32]

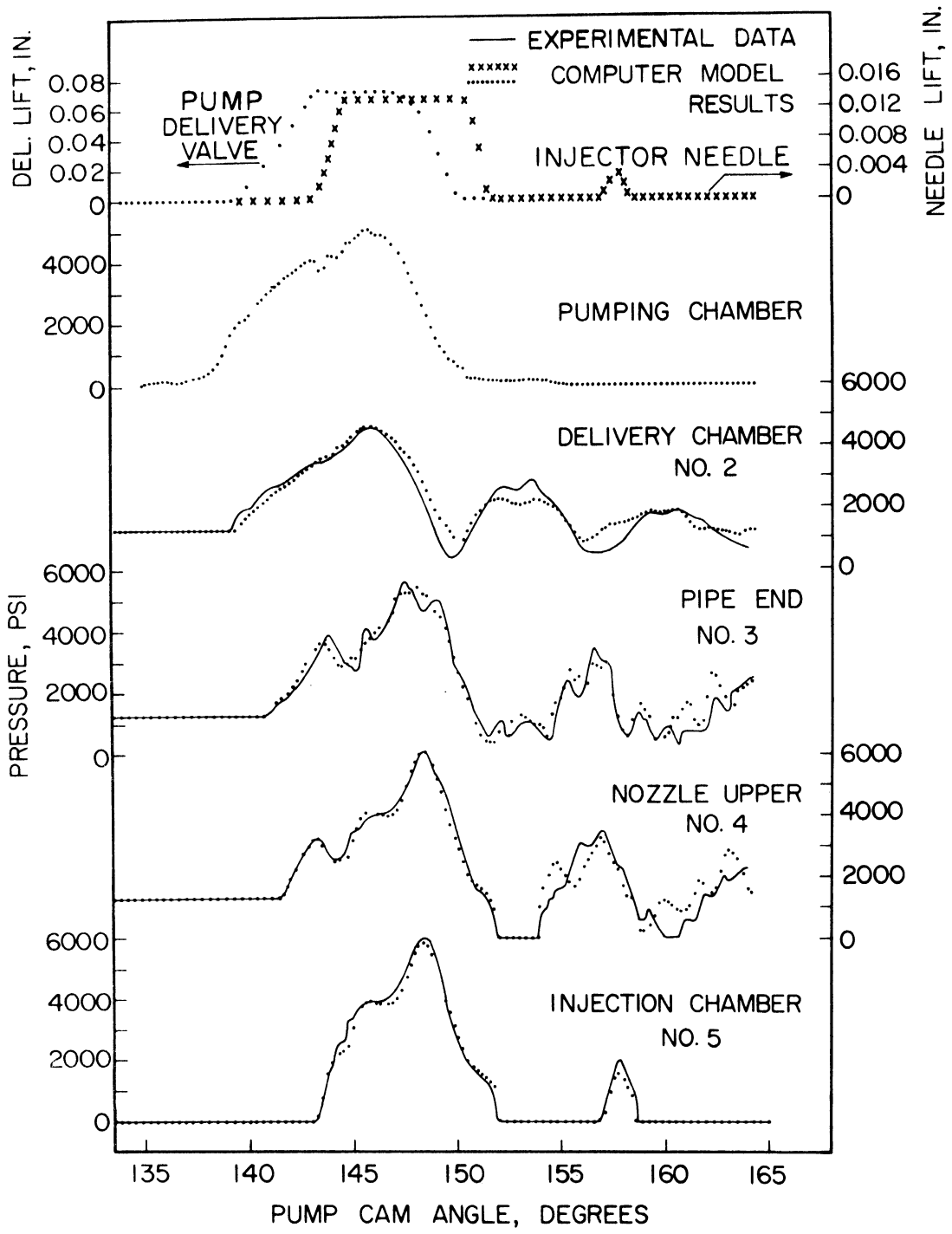

Figure 31. Comparison of Injection System Hydraulic Characteristics—Experimental and Computer Results, 365 RPM Pump Speed and 0.608 Rack Micrometer (0.054 lb. fuel injected/min.).

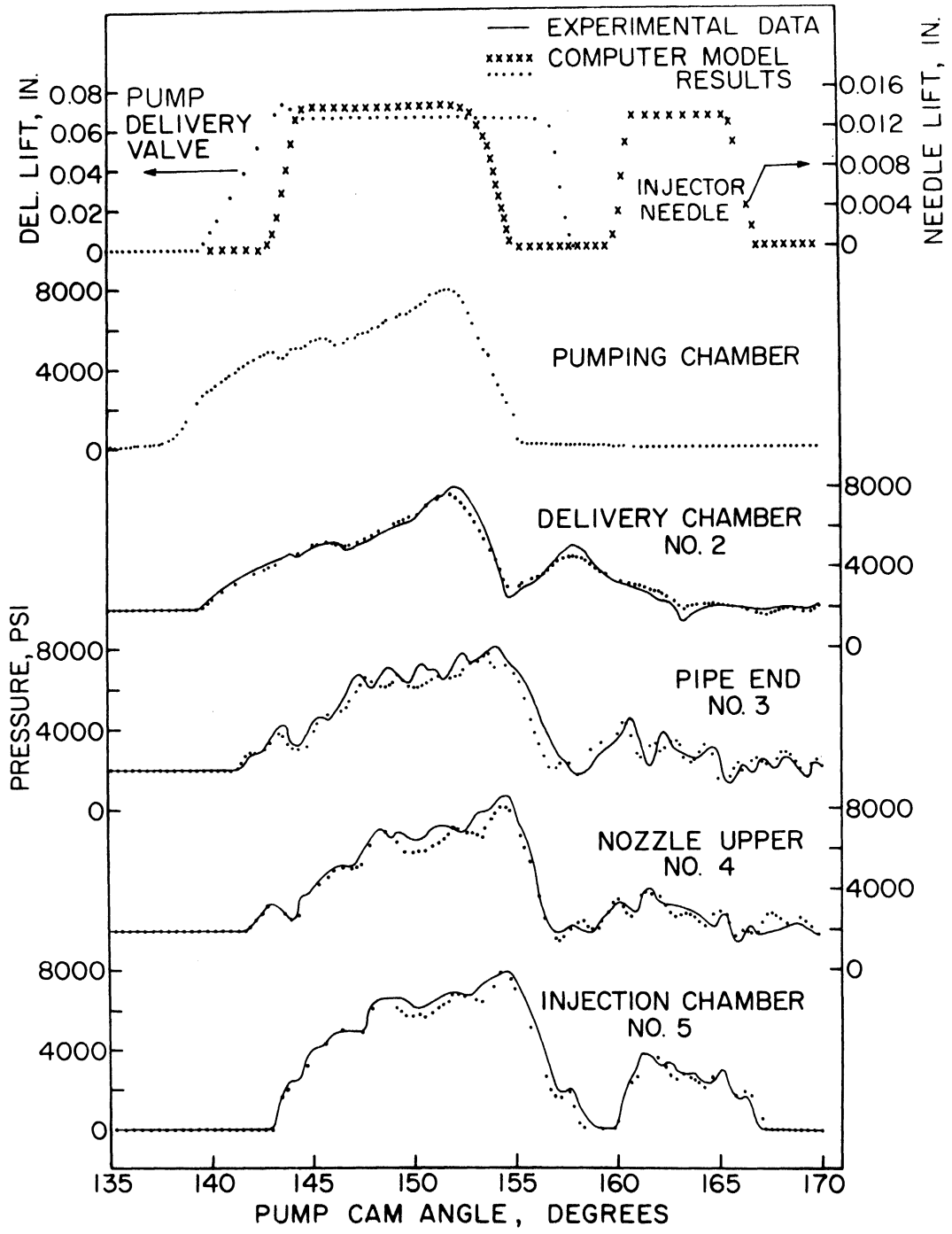

Figure 32. Comparison of Injection System Hydraulic Characteristics—Experimental and Computer Results, 405 RPM Pump Speed and 0.339 Rack Micrometer (0.1480 lb. fuel injected/min.).

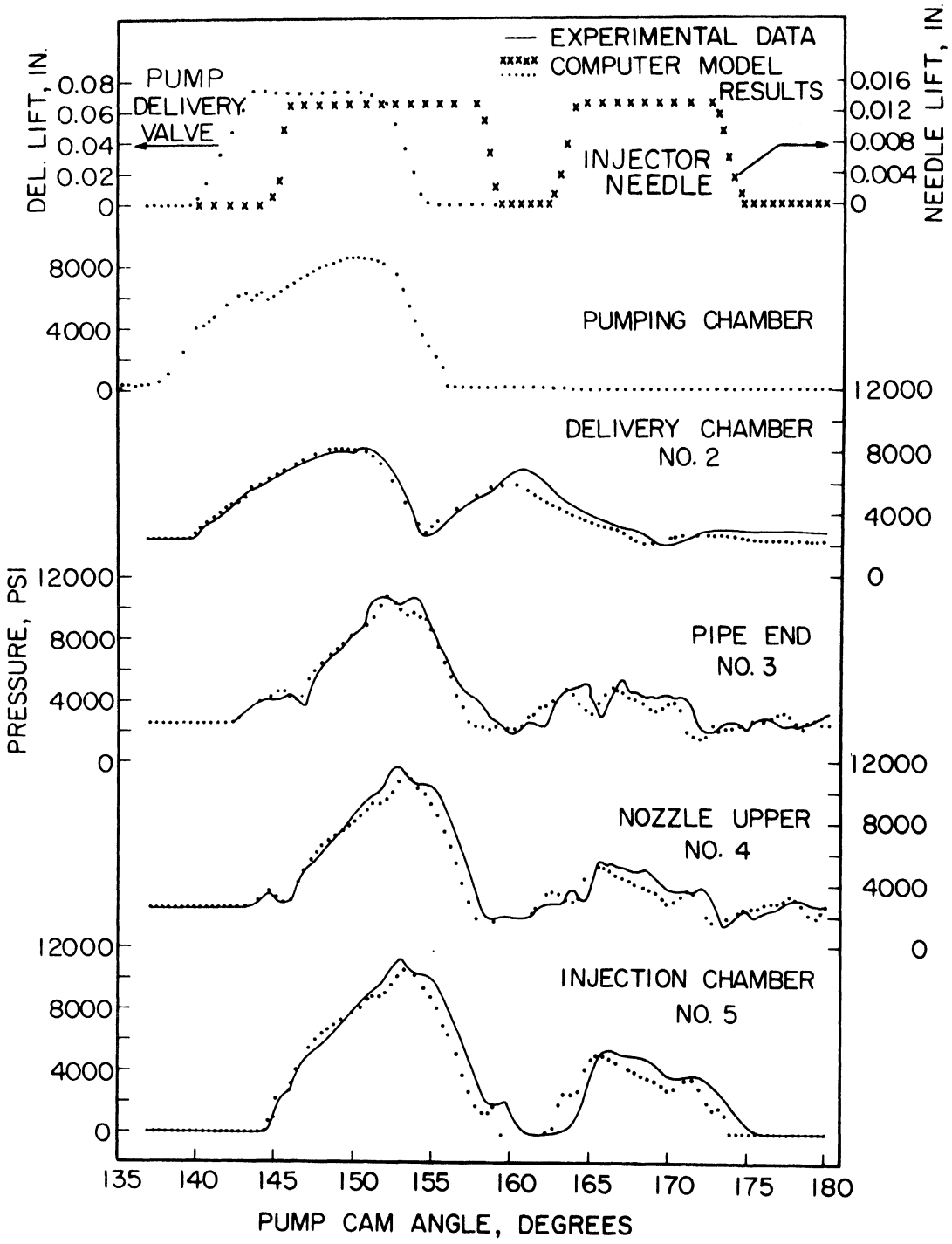

Figure 33. Comparison of Injection System Hydraulic Characteristics—Experimental and Computer Results, 700 RPM Pump Speed and 0.426 Rack Micrometer (0.216 lb. fuel injected/min.).

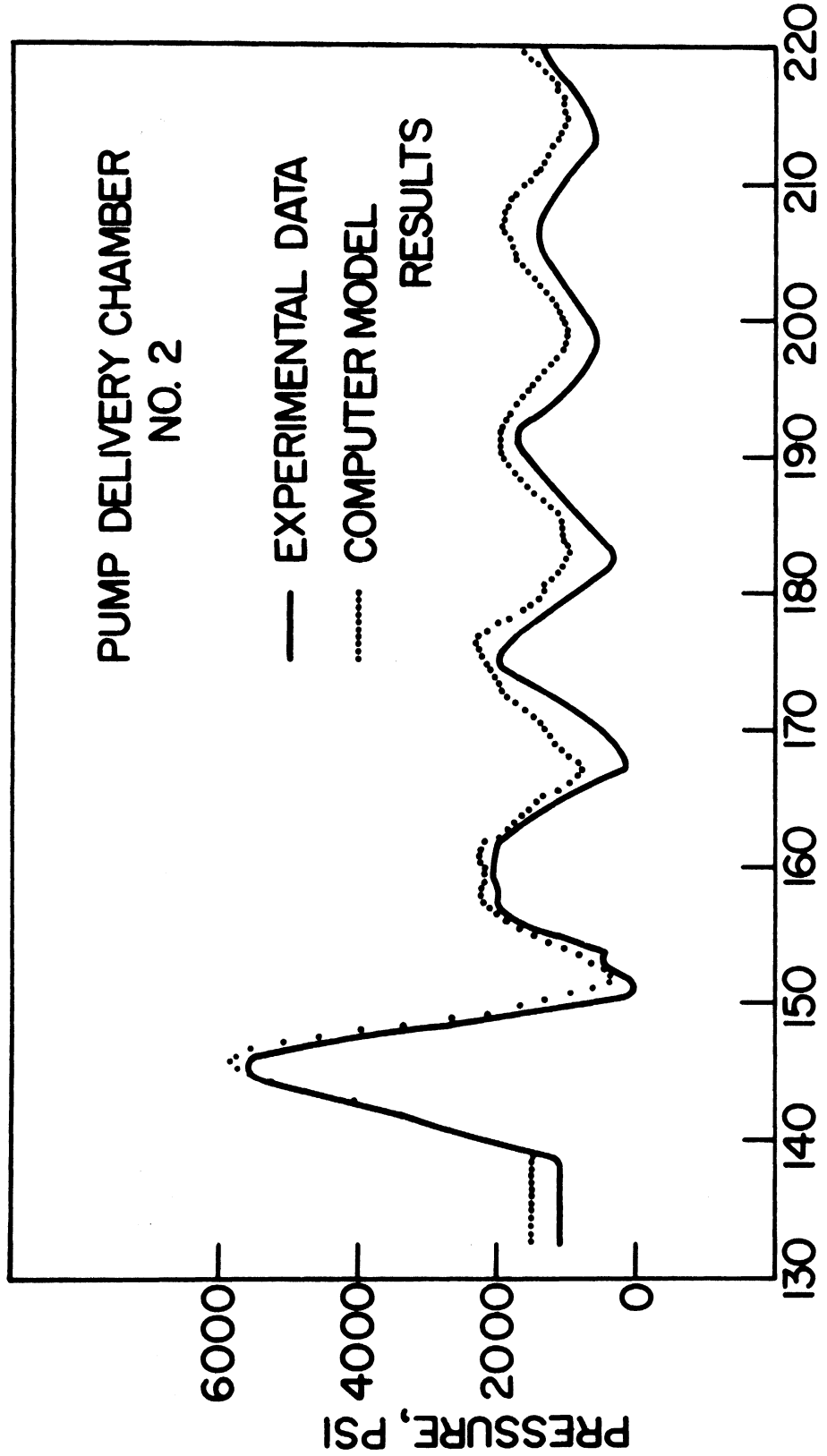

Figure 34. Comparison of Pressure in Pump Delivery Chamber, Experimental and Computer Results for a Large (90°) Portion of Cam Shaft Angle.

TABLE V

COMPARISON BETWEEN THEORETICAL AND EXPERIMENTAL RESULTS FOR DATA PRESENTED IN TABLE III

Test No.	Speed rpm	Rack Micr. Setting in.	Experimental Data		Simulation Data	
			Injected Fuel $in.^3$/cycle	Base Pressure psi	Injected Fuel $in.^3$/cycle	Base Pressure psi
1	800	0.675	0.00340	1100	0.00357	1490
2	400	0.509	0.00805	-	0.00840	2000
3	800	0.509	0.00796	1400	0.00789	1600

TABLE VI

COMPARISON BETWEEN THEORETICAL AND EXPERIMENTAL RESULTS FOR DATA PRESENTED IN TABLE IV

Test No.	Speed rpm	Rack Micr. Setting in.	Experimental Data		Simulation Results	
			Injected Fuel $in.^3$/cycle	Base Pressure psi	Injected Fuel $in.^3$/cycle	Base Pressure psi
4	365	0.608	0.00493	1300	0.00511	1400
5	405	0.350	0.01218	2000	0.01193	1988
6	700	0.426	0.01029	2500	0.01011	2430

opens, and drops with the delivery valve closing. The nozzle needle opens after the pressure in the nozzle upper chamber exceeds the injector opening pressure of 3000 psi. This causes the nozzle upper chamber pressure to drop temporarily and the injection chamber pressure to begin to rise at the instant of needle opening. The needle motion and nozzle pressure are easily correlated for cases with after-injection. The wave reflection phenomena and the time delay in pressure wave travel are made clear by comparing pressures at different locations.

4.3.1 The Base Pressure

The base pressure is the steady state pressure in the delivery pipeline between two consecutive cycles. It is important to establish this pressure as a known reference value. A suitable reference is established if vapor pressure is reached during any part of the cycle since this value is readily determined. In cases where vapor pressure does not occur, the base pressure was measured by the use of the strain gauge transducer mounted on the delivery pipe line. The experimentally determined base pressure was used to start each computer run. The simulation ends after the pump delivery valve and the nozzle needle close with no possible reopening in the considered cycle. At this point it is possible to evaluate the average pressure in the system by the use of pressures along the pipe line, in the pump delivery chamber and in the injector.

Figure 35 illustrates the method used for the base pressure evaluation. In this figure L_{PUMP} and L_{INJ} are additional lengths equivalent to the corresponding volume in the pump and injector, respectively. If the average system pressure after the cessation of fuel supply and injection is different from the initially used base pressure, a new value of base pressure is estimated and the run is repeated. Usually one extra trial was needed to satisfy the condition that the assumed base pressure is equal to the resulting one.

For a meaningful agreement between the model and the experiment the measured base pressure should be within a limited error bound from the theoretically determined one. In Tables V and VI the error bound is of the order of 300 psi. This value is within the tolerance of the experimental measurement, taken with this particular strain gauge transducer.

4.3.2 The Mass Continuity

A gross mass continuity balance provides a good check on any fluid transient problem solved with numerical techniques. The experimental data included a measurement of the fuel supply to the pump and the injected fuel. Actual leakage that occurs in the system is available by subtraction. The leakage usually did not exceed three percent of the injected fuel. Similarly, the computer model accumulates the volume pumped, injected, and the leakage volume. A comparison between the experimental and computer model results of

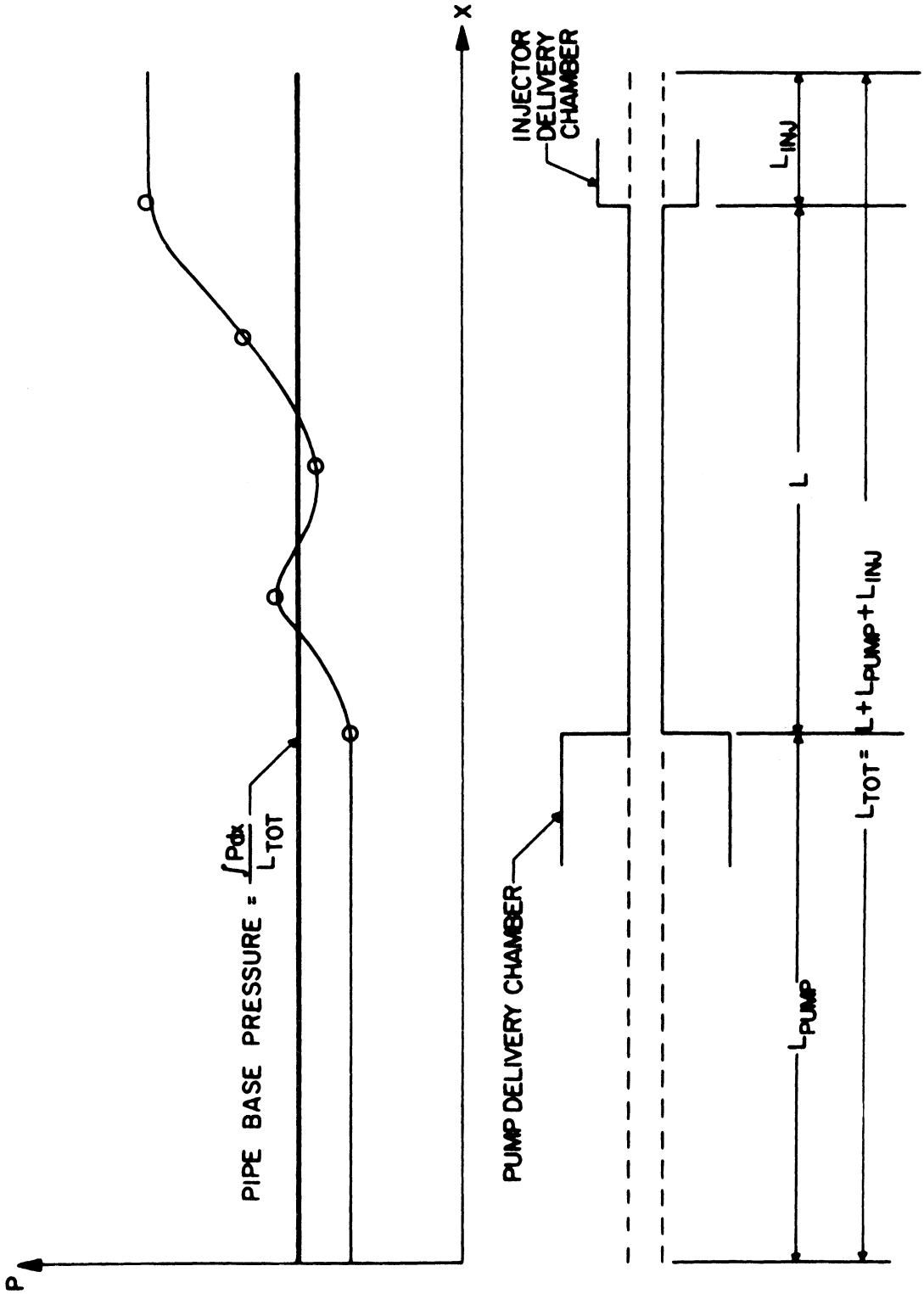

Figure 35. Sketch Showing the Method for Calculating the Pipe Base Pressure.

the injected fuel is shown in Tables V and VI, where it is seen that the mass continuity checked well within less than 4.5 percent of the injected fuel. Any discrepancy between the assumed and resulting base pressure in a simulation run usually gives rise to continuity errors in the simulation.

4.3.3 The Effect of Variable Wave Speed

The variation in wave speed is due to the variation in the bulk modulus of elasticity. A reference modulus is found from the experimental recordings of the initial operating conditions in the test runs. The variation in the modulus is used as cited in the literature.(31) A change in pressure between 0 and 12,000 psi results in a change of wave speed between 4017 and 4391 ft/sec. Very little improvement in the timing of pressure peaks was achieved using variable wave speed. Therefore, it is justifiable to use constant wave speed values in the simulation program for the above pressure range.

4.3.4 The Effect of Distributed Friction

Friction is present as viscous losses, and it controls the rate of attenuation of the residual pressure waves in the system after the end of injection. Friction has a slight effect on the shape of the initial pressure build-up in the system during the injection period. Also the variations in the friction factor with Reynolds number slightly affect the simulation results.

4.3.5 The Coefficient of Discharge

Simulation results are greatly affected by values of the coefficient of discharge at some key locations. The most important of these is the coefficient of discharge of the nozzle holes. The coefficients of discharge of flow past the pump delivery valve and the nozzle passage leading to the injection chamber are also important. The value of these coefficients are difficult to estimate from the literature due to their unusual geometric configurations. Best results in simulation are obtained by the use of factors determined where possible from the measured pressure transient response as described in Section 2.4. The variation of the coefficients of discharge with Reynolds number has a slight effect on the simulation results. It was shown experimentally (Section 2.5.1) that the coefficient of discharge of the injection nozzle holes is reasonably constant during all test conditions.

4.3.6 The Vapor Pressure

Vapor pressure is detected on the recorded pressure traces by a flat-bottom-trace for a short period of time. The computer model was able to reproduce the same condition by not permitting the pressure to drop below vapor pressure, and by assuming a local vapor cavity formation. The size of this cavity is computed from a mass continuity balance. The vapor pocket collapses when the pressure exceeds vapor pressure. At this point homogeneous fuel is assumed at the former pocket.

V. THE DESIGN CONTROL PARAMETER AND FORMULATION OF THE DESIGN PROGRAM

5.1 Introduction

After-injection is usually caused by uncontrolled transients after the end of the main injection. A survey of this phenomenon, together with the factors affecting it, were presented in Chapter II. Many experimental trial and error methods have been used to control this phenomenon with limited success. These methods included changing the nozzle injection area or the delivery pipe diameter with the goal of reducing the injection pressures, and consequently, after-injection. The lack of success in using these methods can be attributed to the fact that these design changes are time invariant and hence do not suit the transient nature of the problem. More success could be achieved by studying the time varying parameters of the system. Examples of these parameters are: the instantaneous area of the spill port during the spill period and the cam motion.

Prior to the 1960's, control of objectionable transients in hydraulic systems was achieved by using simulation methods in which the performance of time varying control devices (i.e., valves) are assumed and the system resulting performance is obtained. The control device characteristics are changed until acceptable performance is achieved. These methods proved to be inconvenient, tedious and many times inadequate even for simple systems.

Recently new design procedures referred to as "Valve Stroking"[29] have been developed. In these procedures, hydraulic systems

are synthesized by specifying a transient enabling the calculation of a desired time varying boundary condition which is then used to determine the required design changes. This is a more direct approach which leads to sophisticated control techniques not attainable by the previous methods.

This work included a study to apply valve stroking techniques to the diesel injection system in order to control residual transients after the uncovering of the pump spill port. This study centered around the investigation of the desired pressure and flow boundary conditions required to eliminate after-injection. The concept provided a better understanding of the controlling parameters in the system. However, it did not lead to feasible design changes. This is mainly due to the rapidly varying nature of the system pressure and flow boundary conditions, and to the passive type elements in the system which respond to internal driving forces rather than to externally forced conditions.

The difficulties encountered in trying to achieve feasible design changes by using valve stroking techniques led to the seeking of a design parameter which does not exhibit erratic behaviour. It was noted that the variation of the system stored elastic energy during the injection cycle is a smooth function of time. This characteristic makes it a good candidate for a system control parameter. An investigation using the system stored elastic energy as a control parameter is presented in the remaining sections of this

chapter. The results of this investigation are presented in Chapter VI.

5.2 Average Elastic Energy--The Control Parameter

In this study the term average elastic energy will be used to define the average pressure stored in the injection system at an instant of time. It should be noted that this pressure has the units of energy per unit displaced volume at the boundaries. Two examples are given to illustrate this definition. First, a moving frictionless piston in a liquid filled cylinder exerts work on the liquid. This energy is stored in the elastic deformation of the liquid. The same energy could be used to drive the piston back to its initial position. The second example is drawn from unsteady liquid flow in a frictionless pipe. In this example, elastic energy is stored in a liquid column due to the compression of the column. This energy is released as kinetic energy by the expansion of the column.

The dotted system in Figure 36 is the system used to calculate the injection system average elastic energy. This system includes the fluid in the pump delivery chamber, in the injector delivery, upper and lower chambers and in the delivery pipe line. In this figure, p and L_{TOT} are the same as defined in Figure 35. The average elastic energy at an instant is calculated in the same manner in which the base pressure was calculated in Secion 4.3.1.

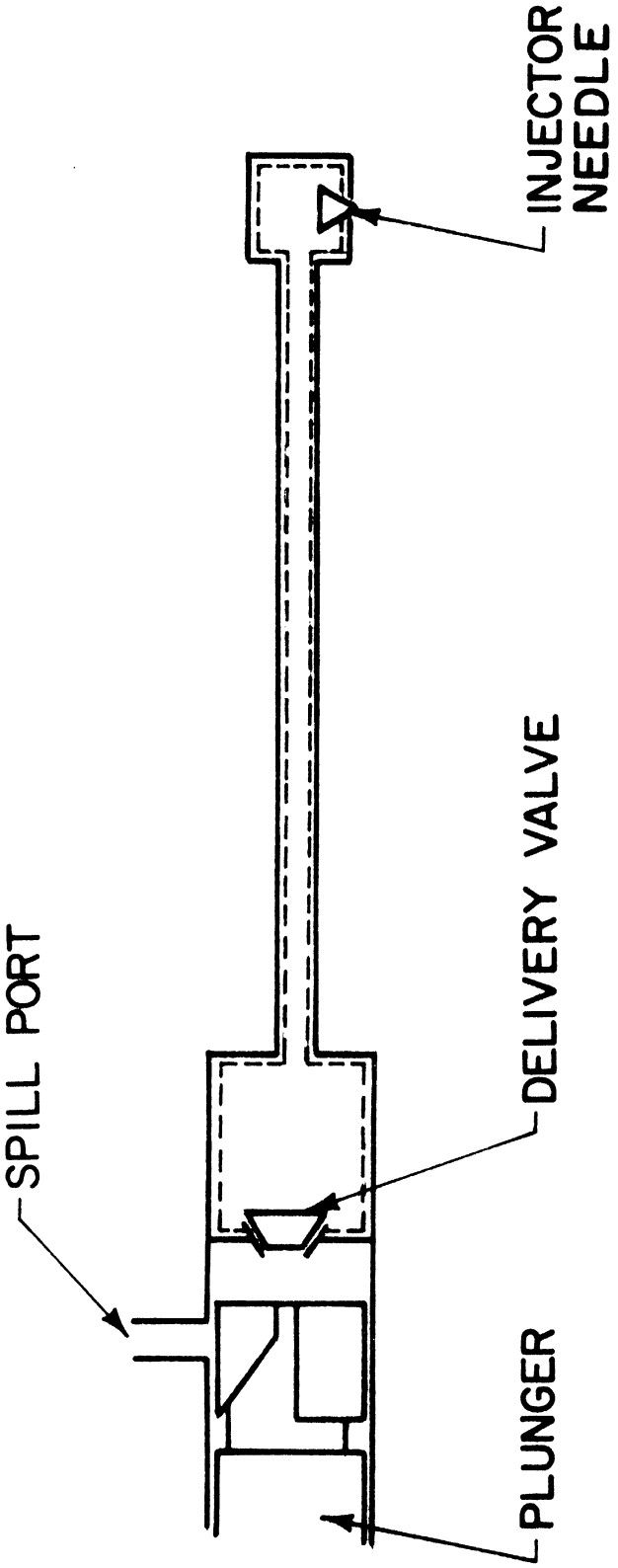

$$\text{AVERAGE ELASTIC ENERGY} = \frac{\int p\,dx}{L_{TOT}}$$

Figure 36. Schematic Representation of System Used to Calculate the Average Elastic Energy.

It can be visualized that the pump adds energy in the form of flow work at the delivery valve end. This energy is stored in the pipe line and volumes of the system as elastic energy. Part of this energy is released at the injection nozzle during the injection period. If excessive uncontrolled elastic energy remains in the system following the closure of the pump delivery valve, it will be released at the nozzle resulting in after-injection.

The average elastic energy, together with pressures in the pump delivery chamber and nozzle upper chamber for Test No. 3, (Table III) are displayed in Figure 37. All the traces begin at the point when the spill port begins to open. In Region I, the average elastic energy drops because of spilling at the pump spill port plus the energy release due to injection at the nozzle. Region II begins when the delivery valve closes. The energy-drop in this region is due to injection at the nozzle only. Region II ends when the nozzle needle begins to close, while Region III coincides with the period of needle closure. For this region slight increase in elastic energy might occur due to the effect of work done by the needle compressing the fuel during its downward motion. When the needle finally closes, the nozzle upper chamber pressure is lower than the needle opening pressure. However, the intermediate elastic energy in Region IV is high, thus causing the pressure at the nozzle upper chamber to increase as the pressure wave reflects in the closed system. When this pressure reaches the

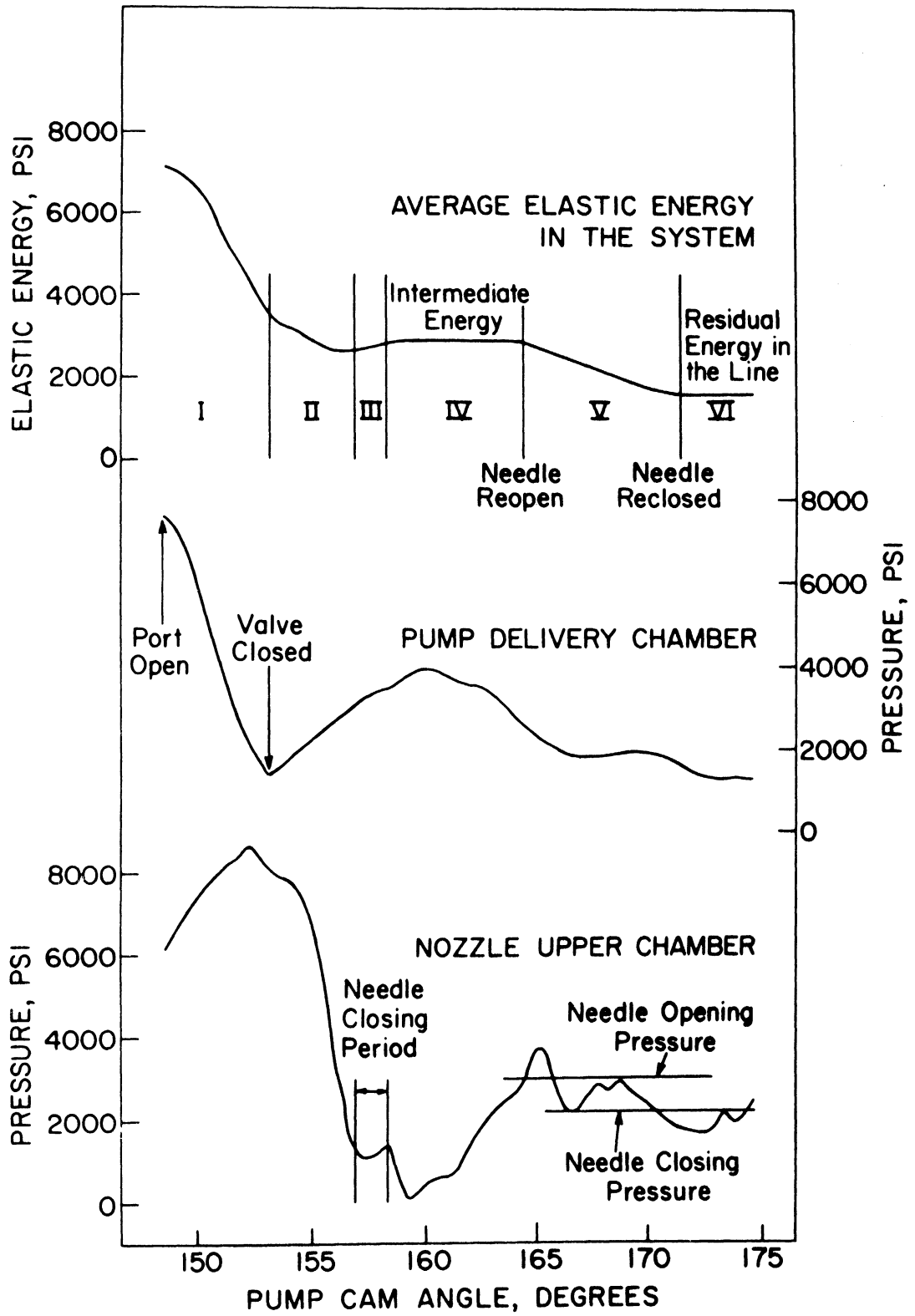

Figure 37. Transient Pressures and Average Elastic Energy Versus Pump Cam Angle for Test No. 3 (Table III).

needle opening pressure, the needle opens and the system elastic energy drops during Region V. Later on, the upper chamber pressure drops below the needle closing pressure and the needle closes. At this point, the system elastic energy finally reaches the residual energy. The elastic energy stays constant during Region VI until the next cycle begins.

The average elastic energy trace in Figure 37 gives a better understanding of the after-injection phenomenon. The manner in which this energy drops during the spill period seems to control the behavior of residual transients in the injection system. For example, a rapid energy drop in Region I will cause a rapid closing of the delivery valve, which means a higher intermediate energy and therefore an increased after-injection. On the other hand, a very slow drop during the spill period will lead to prolonged injection periods. Control of undesirable transients seems possible by releasing the average elastic energy in a controlled manner.

5.3 Description of the Design Method on the Pipe Characteristic Plane

The investigation of a specific case of after-injection begins with recording experimental data of the actual test condition. Then the simulation program is used to simulate this condition. Comparisons are made between theoretical results and experimental data to check the validity of the assumptions and

techniques used in this study. The results and comparisons of four cases of after-injection (Tests No. 3 through 6) were presented in Chapter IV. The design program presented in this section serves the purpose of finding means to eliminate after-injection. This is achieved by utilizing a controlled release of the stored elastic energy in the system. The resulting alterations in pressure and flow patterns are calculated and translated into feasible design changes, using the design program.

Figure 38 represents the pipe characteristic plane (x-t plane). An instant of time is represented by a horizontal line, while a vertical line represents a specific location along the pipe. The line AJ represents the location of the pump delivery chamber, and the line BI represents the location of the injector delivery chamber. On the other hand, line ED represents the instant of time at which the negative wave, resulting from the spill at the pump, reaches the injector. Also line HG represents the instant of nozzle needle closing. Three important events characterize the performance of the diesel injection system and are given on Figure 38. First, the plunger helix begins to uncover the spill port at point C. Then the pump delivery valve is totally closed at F. Finally, the nozzle needle is totally closed at G. On this figure, the distance AC is the wave travel time and BD is twice the wave travel time.

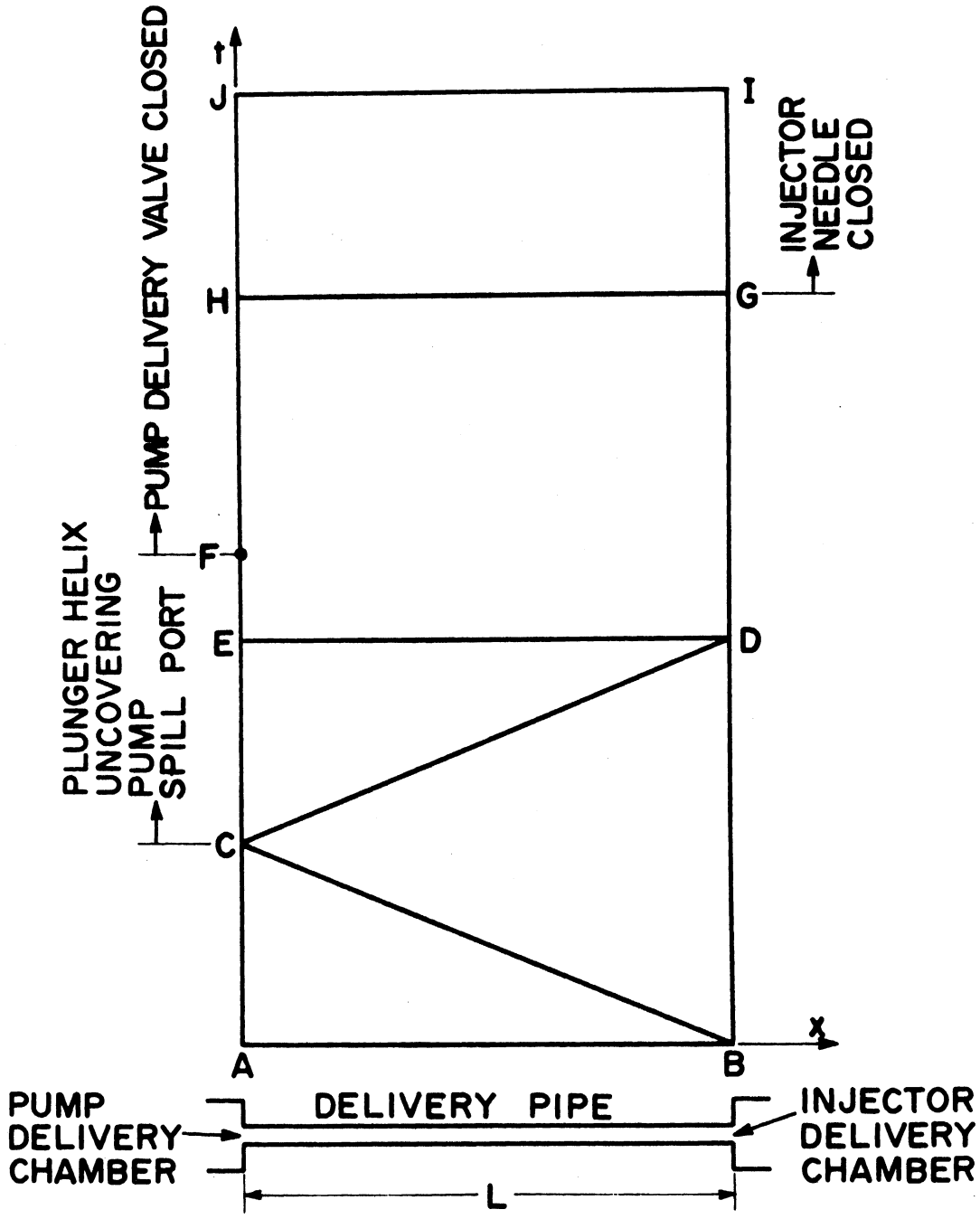

Figure 38. Injection System Performance on the Pipe x-t Plane.

The design method is illustrated on Figure 39, which is similar to Figure 38, but includes more details of the solution procedure. In this figure, the distance between the vertical lines represents a pipe section of length Δx, while the distance between the horizontal lines is the characteristic method time step Δt. The data needed by the design program includes a complete description of the injection system geometric configuration and properties. Simulation program results of pressure and flow along the line BD are specified for the design program. Also a control period beginning at point C together with a controlled average elastic energy function are specified. The choice of the length of the control period and the energy function during this period depend on the injection system properties and the choice of the controlling device. Further discussion of this subject will be presented in Chapter VI.

Several regions are given on Figure 39 to simplify the presentation of the solution method. The solution procedure in Region I begins with known pressure and flow conditions at all points along the vertical line BD. Conditions at points lying on another vertical line adjacent to BD are calculated by the use of the pipe characteristic equations in a manner illustrated by the triangle $Z_1Y_1W_1$. In this triangle, pressure and flow conditions are known at Y_1 and W_1 and are not known at Z_1. It should be noted that Z_1W_1 is the C^+ characteristic line

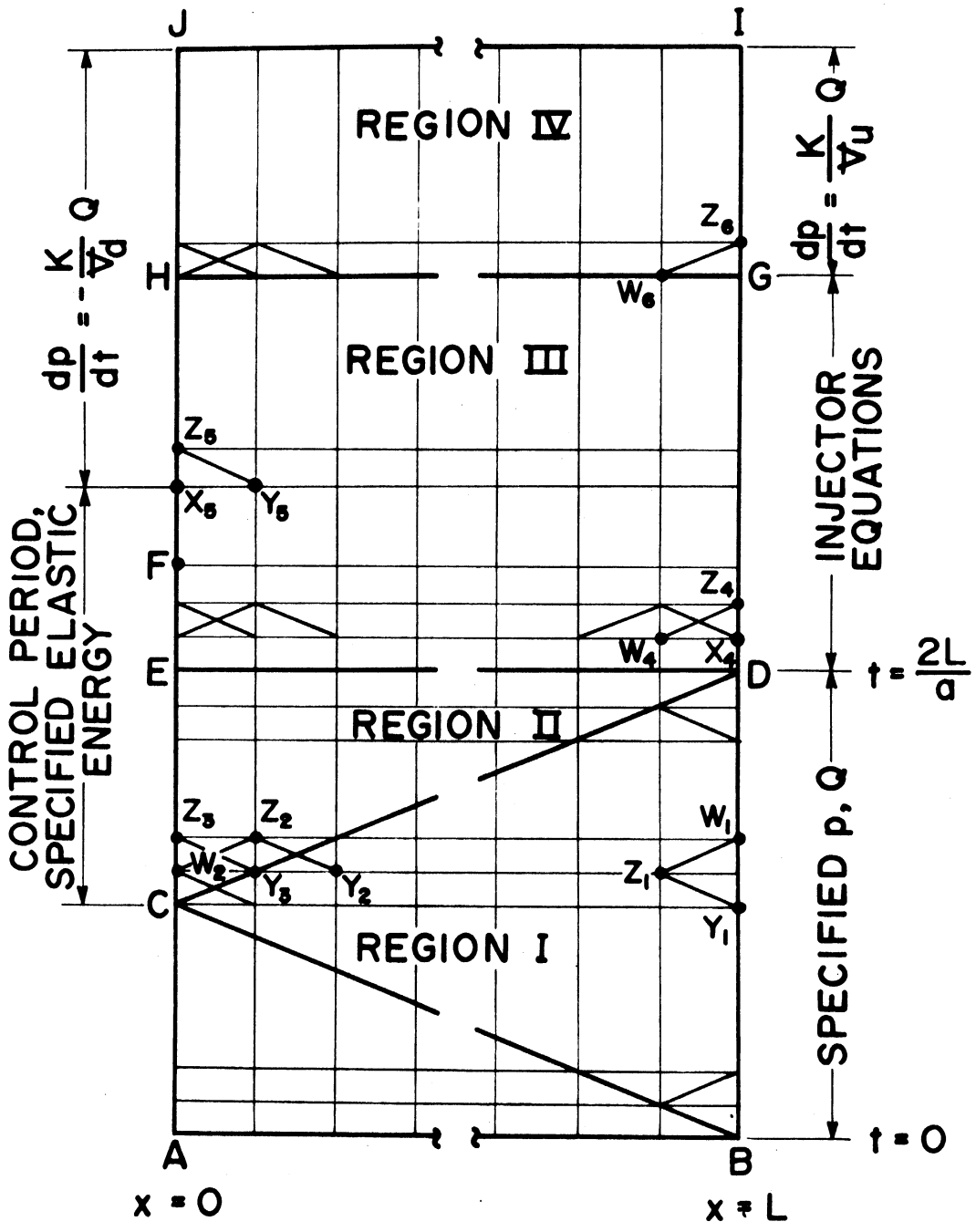

Figure 39. Design Method on the Pipe x-t Plane.

and Y_1Z_1 is the C^- characteristic line. When the conditions at all points lying on a vertical line are calculated, the calculation proceeds to points on the next adjacent vertical line. Calculations in Region I end when the pressure and flow at point C are known.

In Region II, calculations begin at $t = L/a + \Delta t$. At this instant, pressure and flow conditions are known for all pipe locations except the boundary point W_2 . Conditions at this boundary point are calculated by making use of the assumed instantaneous average elastic energy together with an equation from the pipe C^- characteristic line. At $t = L/a + 2\Delta t$, pressures and flows are known at all points except at Z_2 and Z_3 . At this point of time, conditions at the interior point Z_2 are calculated by utilizing the known pressures and flows at W_2 and Y_2 together with the pipe characteristic equations along the C^+ line W_2Z_2 and the C^- line Y_2Z_2 . Conditions at Z_3 are calculated in the same manner described for W_2 . This procedure continues by advancing to the next step, calculating the interior points, and then calculating the boundary point along the line CE. Calculations in this region end by calculating pressures and flows at all points along the horizontal line ED .

Calculations in Region III proceed by calculating all pressures and flows at time t prior to calculating these conditions at time $t + \Delta t$. This is done by first calculating the

interior points in the same manner previously described for point Z_2 in Region II. Then, conditions at the injector boundary point along the line DG are calculated by solving the injector equations (previously described in Section 3.3.3) together with the pipe characteristic equation along the C^+ line illustrated by the line W_4Z_4. Finally the pump boundary point along EH is calculated. During the control period, this calculation is performed in the same manner described for W_2. After the end of the control period, the compressibility equation [Equation (3.14)] describes the conditions in the pump delivery chamber and is used together with the pipe C^- characteristic equation to determine the pressure and flow at the pump boundary. This C^- line is illustrated by the line Y_5Z_5. Similarly, the compressibility equation [Equation (3.14)] relates the pressure and flow in the combined injector chambers after the needle is completely closed. This equation is used together with the pipe C^+ characteristic equation to determine the pressure and flow at the injector boundary in Region IV. In this region, the interior points and pump boundary point are calculated in the same manner described for Region III. Since the design program objectives are to eliminate undesirable system characteristics (after-injection and cavitation), no provision has been made to simulate these characteristics.

5.4 Formulation and Solution of the Equations Used in the Design Program

Having described the solution procedure on the x-t plane, attention is now given to the formulation and solution of equations used in the design program. These equations are divided into four major groups; namely, interior point equations, pump-pipe boundary equations, injector-pipe boundary equations, and equations of design changes at the pump.

5.4.1 Equations and Method of Solution at Interior Points

On Figure 39, Z_1 represents an interior point in Region I at time t and pipe location x with known pressure and flow conditions at W_1 and Y_1. W_1 is located at time $t + \Delta t$ and distance $x + \Delta x$, while Y_1 is located at time $t - \Delta t$ and distance $x + \Delta x$. The pressure and flow conditions at Z_1 are found by using Equations (3.10) and (3.12). Equation (3.10) represent the C^+ characteristic line Z_1W_1 and is written in the following form:

$$Q_{W_1} - Q_{Z_1} + \frac{gA}{\gamma_{Z_1} a_{Z_1}}(p_{W_1} - p_{Z_1}) + \frac{f_{Z_1}\Delta t Q_{Z_1}|Q_{Z_1}|}{2DA} = 0 \qquad (5.1)$$

Also, Equation (3.12) represent the C^- characteristic line Y_1Z_1 and is written in the following form:

$$Q_{Z_1} - Q_{Y_1} - \frac{gA}{\gamma_{Y_1} a_{Y_1}}(p_{Z_1} - p_{Y_1}) + \frac{f_{Y_1}\Delta t Q_{Y_1}|Q_{Y_1}|}{2DA} = 0 \qquad (5.2)$$

For convenience, the variables M and J are defined in the following forms:

$$M = \frac{gA}{\gamma a} \tag{5.3}$$

and

$$J = \frac{f\Delta t}{2DA} \tag{5.4}$$

M and J are functions of the pressure and flow conditions. Therefore the subscripts are associated with them to identify these conditions. It should be noted that these variables are positive and have an order of magnitude of 0.001 for the particular system under consideration. Eliminating p_{Z_1} from Equations (5.1) and (5.2) yields:

$$B_1 - B_2 Q_{Z_1} + B_3 Q_{Z_1} |Q_{Z_1}| = 0 , \tag{5.5}$$

where

$$B_1 = M_{Y_1} Q_{W_1} + M_{Z_1} Q_{Y_1} + M_{Z_1} M_{Y_1} (p_{W_1} - p_{Y_1}) - M_{Z_1} J_{Y_1} Q_{Y_1} |Q_{Y_1}| , \tag{5.6}$$

$$B_2 = (M_{Z_1} + M_{Y_1}) \tag{5.7}$$

and

$$B_3 = M_{Y_1} J_{Z_1} \tag{5.8}$$

For positive Q_{Z_1} the general solution of Equation (5.5) is:

$$|Q_{Z_1}| = \frac{B_2 \pm \sqrt{B_2^2 - 4B_1B_3}}{2B_3} \tag{5.9}$$

and for negative Q_{Z_1}, the solution becomes:

$$|Q_{Z_1}| = \frac{B_2 \pm \sqrt{B_2^2 + 4B_1B_3}}{2B_3} \tag{5.10}$$

It should be noted that B_3 is much less than B_2, B_2 and B_3 are always positive and the product B_1B_3 is much less than the square of B_2. In order to avoid very high orders of magnitude of Q_{Z_1}, Equations (5.9) and (5.10) become:

$$Q_{Z_1} = \frac{|B_1|}{B_1} \frac{B_2 - \sqrt{B_2^2 - 4|B_1|B_3}}{2B_3} \tag{5.11}$$

In Equation (5.11), the sign of B_1 describes the sign of the flow Q_{Z_1}. Then the pressure p_{Z_1} is calculated by substituting Q_{Z_1} in Equation (5.1) or Equation (5.2).

The calculation procedure at the interior points in Regions II, III and IV is essentially the same. This procedure is illustrated by the calculation of pressure and flow conditions at point Z_2, (Figure 39). Z_2 represents an interior point at a time t and a pipe location x. The pressure and flow conditions at the adjacent points W_2 and Y_2 are known. W_2 is located at time $t - \Delta t$ and distance $x - \Delta x$, while Y_2 is located at time $t - \Delta T$ and, distance $x + \Delta x$. Equations (3.10) and (3.12) are used to calculate the pressure and flow at Z_2 and can be written in the following form:

$$Q_{Z_2} - Q_{W_2} + M_{W_2}(p_{Z_2} - p_{W_2}) + J_{W_2}Q_{W_2}|Q_{W_2}| = 0 \tag{5.12}$$

$$Q_{Z_2} - Q_{Y_2} - M_{Y_2}(p_{Z_2} - p_{Y_2}) + J_{Y_2}Q_{Y_2}|Q_{Y_2}| = 0 \tag{5.13}$$

Subtracting Equation (5.12) from Equation (5.13) results in:

$$p_{Z_2} = \frac{J_{Y_2} Q_{Y_2} |Q_{Y_2}| - J_{W_2} Q_{W_2} |Q_{W_2}| + M_{W_2} p_{W_2} + M_{Y_2} p_{Y_2} + Q_{W_2} - Q_{Y_2}}{M_{Y_2} + M_{W_2}} \tag{5.14}$$

The flow Q_{Z_2} is calculated by substituting for p_{Z_2} from Equation (5.14) into Equation (5.12) or Equation (5.13).

5.4.2 Equations and Method of Solution at the Pump-Pipe Boundary

Calculation procedure of the pressure and flow conditions at this boundary takes advantage of computed pressure and flow conditions in the remainder of the pipe length. Calculation of these conditions, at a point Z_3, (Figure 39), is given as an illustrative example for this procedure. Assume that Z_3 is located on the horizontal line $t = t_3$. The pressure at Z_3 is calculated from the average elastic energy defined in Section 5.2 and by Figures 35 and 39 and is expressed as:

$$p_{Z_3} = (E_{t_3} \times L_{TOT} - \int_{L_{PUMP}}^{L_{TOT}} p_{t_3} \, dx)/L_{PUMP} \tag{5.15}$$

where E is the specified instantaneous average elastic energy, and the other variables are previously defined. The flow at Z_3 is calculated by substituting p_{Z_3} in the pipe C^- characteristic equation [Equation (3.12)], and is given by

$$Q_{Z_3} = Q_{Y_3} + M_{Y_3}(p_{Z_3} - p_{Y_3}) - J_{Y_3} Q_{Y_3} Q_{Y_3} \, . \tag{5.16}$$

Outside the control period interval, the compressibility equation [Equation (3.14)] relates the pressure and flow in the pump delivery chamber. The calculation procedure at the pump boundary is illustrated by calculating the pressure and flow at the point Z_5 (Figure 39). The finite difference form for the compressibility equation at this point is given by:

$$\frac{p_{Z_5}-p_{X_5}}{\Delta t} = -\frac{K}{2V_d}(Q_{Z_5}+Q_{X_5}) \quad . \tag{5.17}$$

In addition, the C^- characteristic equation [Equation (3.12)] can be written as:

$$Q_{Z_5} = Q_{Y_5} + M_{Y_5}(p_{Z_5}-p_{Y_5}) - J_{Y_5}Q_{Y_5}|Q_{Y_5}| \tag{5.18}$$

In the above equations subscripts refer to locations on the x-t plane (Figure 39). Equations (5.17) and (5.18) are two algebraic equations in two unknowns, and can be solved simultaneously to give p_{Z_5} and Q_{Z_5} .

5.4.3 Equations and Methods of Solution at the Injector-Pipe Boundary

The injector equations were presented in Chapter III. They were solved using the predictor corrector method in the simulation program. From the simulation results presented in Figures 28 through 33, the following observations are noted: (1) The nozzle needle stays at its highest position (0.013 inch) until the negative wave that results from the opening of the spill port reaches the injector. (2) The needle begins to close when the

pressure at the injector reaches the needle closing pressure. (3) During the needle closing period, the needle velocity is fairly constant. Therefore, it was decided to simplify the solution procedure in the design program by assuming a needle motion in accordance with the above three observations.

In the design program, it is assumed that the needle lift is 0.13 inch at the point D, in Figure 39. The needle stays at that lift until the pressure at the injector in Region III starts to drop below the needle closing pressure. At this point, the needle starts to close. The needle velocity is constant during its closing period. The magnitude of this velocity was taken from the above-mentioned simulation results. Therefore, a prescribed needle motion dependent on the pressure at the injector is given in Region III, Figure 39, and the needle equations are dropped. It should be stated that this procedure is not necessary and was used only to expedite the solution procedure.

The remaining injector equation [Equations (3.28), (3.29) and (3.30)] are of the following form:

$$\frac{dp}{dt} = \varphi(t) \tag{5.19}$$

where $\varphi(t)$ is a function of time representing the right-hand side of these equations. Such equations can be written in the following finite difference form:

$$\frac{p_2-p_1}{\Delta t} = \frac{\varphi(t_1) + \varphi(t_2)}{2} \tag{5.20}$$

where the subscripts 1,2 refer to the beginning and end of the time period Δt . The left-hand side of Equation (5.20) is the pressure slope, while the time function on the right-hand side is averaged during the time period. The algebraic equations expressed by Equation (5.20) are solved together with the pipe C^+ characteristic equation [Equation (3.37)] using an iterative method. This method is illustrated by using the points W_4, X_4 and Z_4 on the x-t characteristic plane (Figure 39). On this figure pressure and flow conditions are known at W_4, X_4 and are to be calculated at Z_4 . First, the pressure at Z_4 (nozzle upper chamber pressure) is assumed. As a first approximation, this pressure is assumed to be the same as that at X_4 . Substituting this value, Equation (3.37) can be solved for the flow at Z_4 (flow entering the injector upper chamber). Similarly, substituting p_{Z_4} and Q_{Z_4} , the finite difference form of Equation (3.28) can be solved for the nozzle lower chamber pressure. Using the above known pressures and flow, it is possible to calculate the pressure in the nozzle injection chamber by two means. The first is by using Equation (3.29) and the second is through solving Equation (3.30). If the assumed pressure at Z_4 happens to be the same as the true solution of these equations, the two calculated values of the pressure in the injection chamber should be the same. However, this is a very uncommon situation. Therefore, the difference between the two calculated pressures is used as an error function and the

solution is repeated by assuming a new pressure at Z_4 , which is obtained by adding an increment of $\pm$ 200 psi to the previously assumed value of pressure. The sign of the increment depends on the sign of the error. This procedure is repeated until a change in the error sign is indicated. At this point a Newton-Raphson converging method[15] is used to obtain the solution. This technique proved to be very efficient. It greatly improves the convergence of the solution; in most cases no more than five iterations to reach a solution were needed.

After needle closing, the injector equations are dropped. The compressibility equation [Equation (3.14)] for the combined injector chambers (delivery, upper and lower) at point Z_6 (Figure 39) is given in the following finite difference form:

$$\frac{p_{Z_6} - p_G}{\Delta t} = + \frac{K}{2(\forall_u + \forall_l)}(Q_{Z_6} + Q_G) \qquad (5.21)$$

Equation (5.21) is solved with the pipe C^+ characteristic equation:

$$Q_{Z_6} - Q_{W_6} + M_{W_6}(p_{Z_6} - p_{W_6}) + J_{W_6} Q_{W_6} |Q_{W_6}| = 0 \qquad (5.22)$$

The solution of Equations (5.21) and (5.22) gives the pressure and flow at Z_6 . In this equation the subscripts G, W_6 and Z_6 represent points on the x-t characteristic plane (Figure 39).

5.4.4 Equations and Method of Solution of Design Changes at the Pump

So far, the design program has used an assumed average elastic energy profile and known initial conditions to calculate pressure and flow conditions in the whole x-t plane given in Figure 39. To make use of these conditions, they must be translated into feasible design changes in the injection system.

Two design changes aimed at the elimination of after-injection are suggested at the pump. The first example is a controlled relief valve in the pump delivery chamber which opens to release the excessive elastic energy at the correct instant. The second is a redesign of the pump spill port area to release the elastic energy in a controlled manner. In both examples, the calculated pressure and flow data at the pump-pipe boundary during the control period are used as added boundary conditions to the pump equations. The solution of these equations provides the required design change. The equations used in both examples are given in this section. Design program results of these examples are given in Chapter VI.

The control valve used in the first example is illustrated by Figure 40. It is assumed that this valve does not open while the delivery valve is open. Therefore, the equation representing the pump delivery chamber [Equation (3.19)] is modified to:

$$\frac{dp_d}{dt} = - \frac{K_d}{\forall_d}(Q_{c.v.} + Q_{Zd}) \qquad (5.23)$$

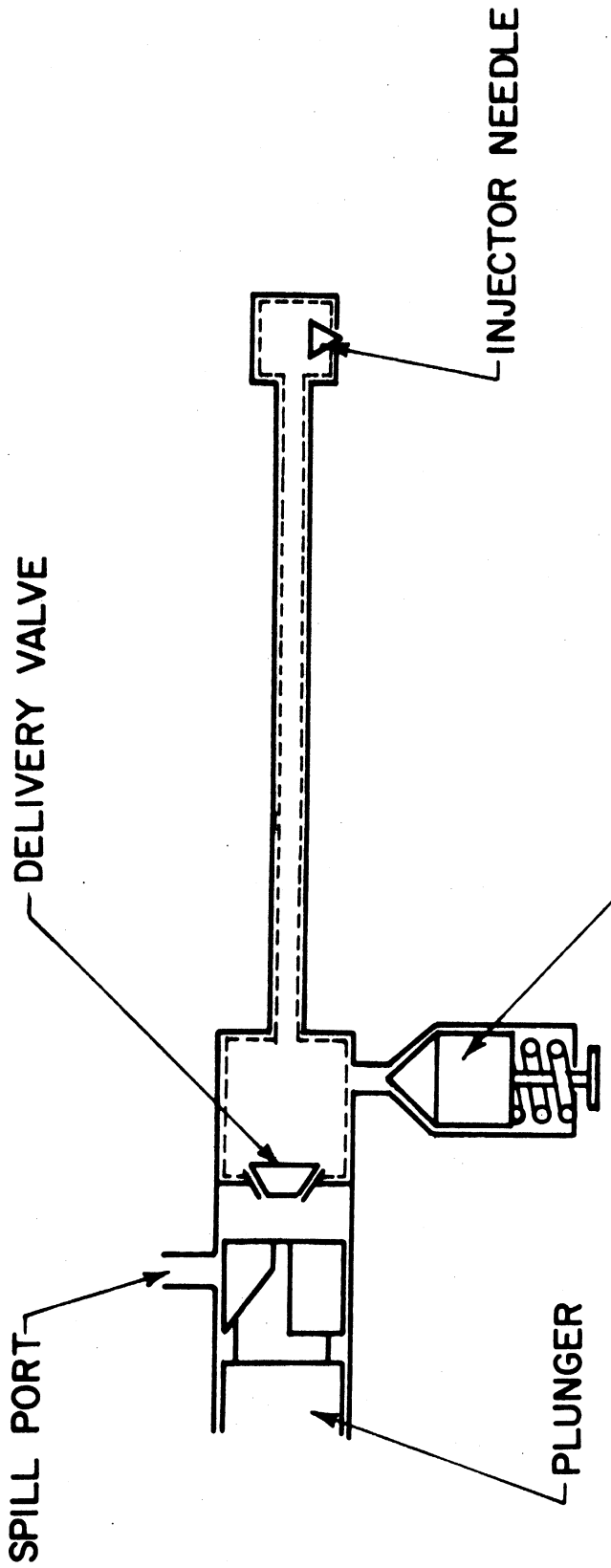

Figure 40. Schematic Representation of the Control Valve Position.

where $Q_{c.v.}$ is the flow through the control valve and is given by:

$$Q_{c.v.} = C_{dc.v.} A_{c.v.} \sqrt{\frac{2g}{\gamma} p_d} \qquad (5.24)$$

The subscript c.v. refers to the control valve and the other terms were previously defined. The calculated pressures and flows p_d and Q_{Zd} at the pump-pipe boundary during the control period are used together with a reasonable value of the valve coefficient of discharge to give the needed area of flow through the valve. A value of 0.7 was used for $C_{dc.v.}$.

The second example determines a pump spill port area from the known pump-pipe boundary conditions (p_d, Q_{Zd}). This is done by first solving the pump delivery chamber equation [Equation (3.19)] together with the delivery valve motion equations [Equations (3.24) and (3.25)]. Each of these equations can be written in a form similar to Equation (5.19). The finite difference form used in the solution takes the following form:

$$\frac{p_2 - p_1}{\Delta t} = \varphi(t_2) \qquad (5.25)$$

where the subscripts 1 and 2 refer to the beginning and end of the time period Δt. The left-hand side is the slope and the time function on the right-hand side is calculated at the end of the period. It was found that the use of average values for the right-hand side during the period results in divergence of the solution due to the

highly varying nature of the delivery valve velocity during the closing period. This is in contrast with the needle motion where the needle velocity is very stable during the needle closing period. Extreme variations in the delivery valve velocity during the closing period result from the use of light valve spring and the fact that the acting pressure force $(p_d - p_p)$ is small and is highly varying. Converging solutions were obtained by using the finite difference form given by Equation (5.25).

In the finite difference form of Equations (3.19), (3.24), (3.25), p_d and Q_{Zd} are known from previous calculations, and p_p, s_v and V_v are the unknowns to be determined. An iterative method and a convergence technique similar to that described for the injector-pipe equations given in Section 5.3.4 was used to determine these unknowns.

The calculated pressure in the pumping chamber p_p together with the calculated valve motion (s_v, V_v) are used in the finite difference from [given by Equation (5.25)] of the pumping chamber equation [Equation (3.18)] to determine the spill port area. For this equation, the feed chamber pressure p_f was assumed using previous simulation results. A value of 150 psi was used in all cases for p_f. It should be noted that the spill port area is highly insensitive to the value of p_f because p_f is much less than p_p during the major part of the spill.

5.5 Accuracy of the Design Program

The procedure presented in the previous sections utilized an assumed average elastic energy function during a control period to determine the injection system performance and to propose design changes. Some assumptions and solution techniques were used to accomplish this objective. It is important to illustrate the accuracy of the design program compared with the simulation program results.

Average elastic energy curves for Tests No. 3 through 6 (Tables III and IV) were computed using the simulation program results for the injection system pressures. These curves were given as data to the design program and the injection system performance was calculated. Results from the design program were compared to the simulation program results. In all cases, the design program results were in very good agreement with the simulation program.

A sample of these comparisons are given in Figures 41 and 42 for Test No. 6 (Table IV). In Figure 41, the upper trace is the average elastic energy calculated from the simulation results and used in the design program. Three other traces for the pressures in the pump delivery chamber, nozzle upper chamber and injection chamber are also illustrated on the same figure. Figure 42 gives comparisons of calculated results at the pump. The design program results in this figure were determined using the procedure given for the second example in Section 5.3.5. There is

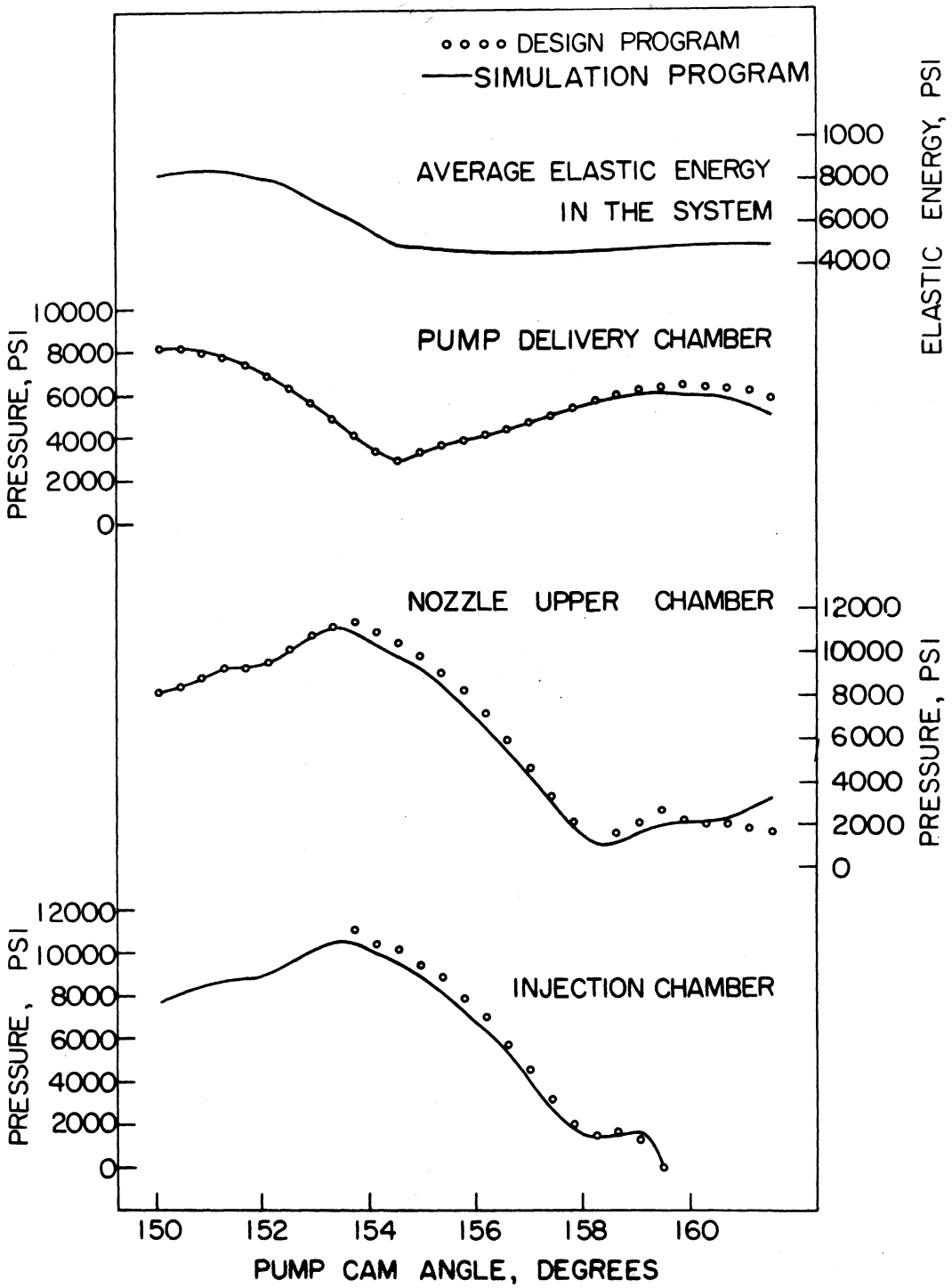

Figure 41. Simulation Check of Design Program Results of Pump Delivery Chamber and Injector Transient Pressures for Test No. 6 (Table IV).

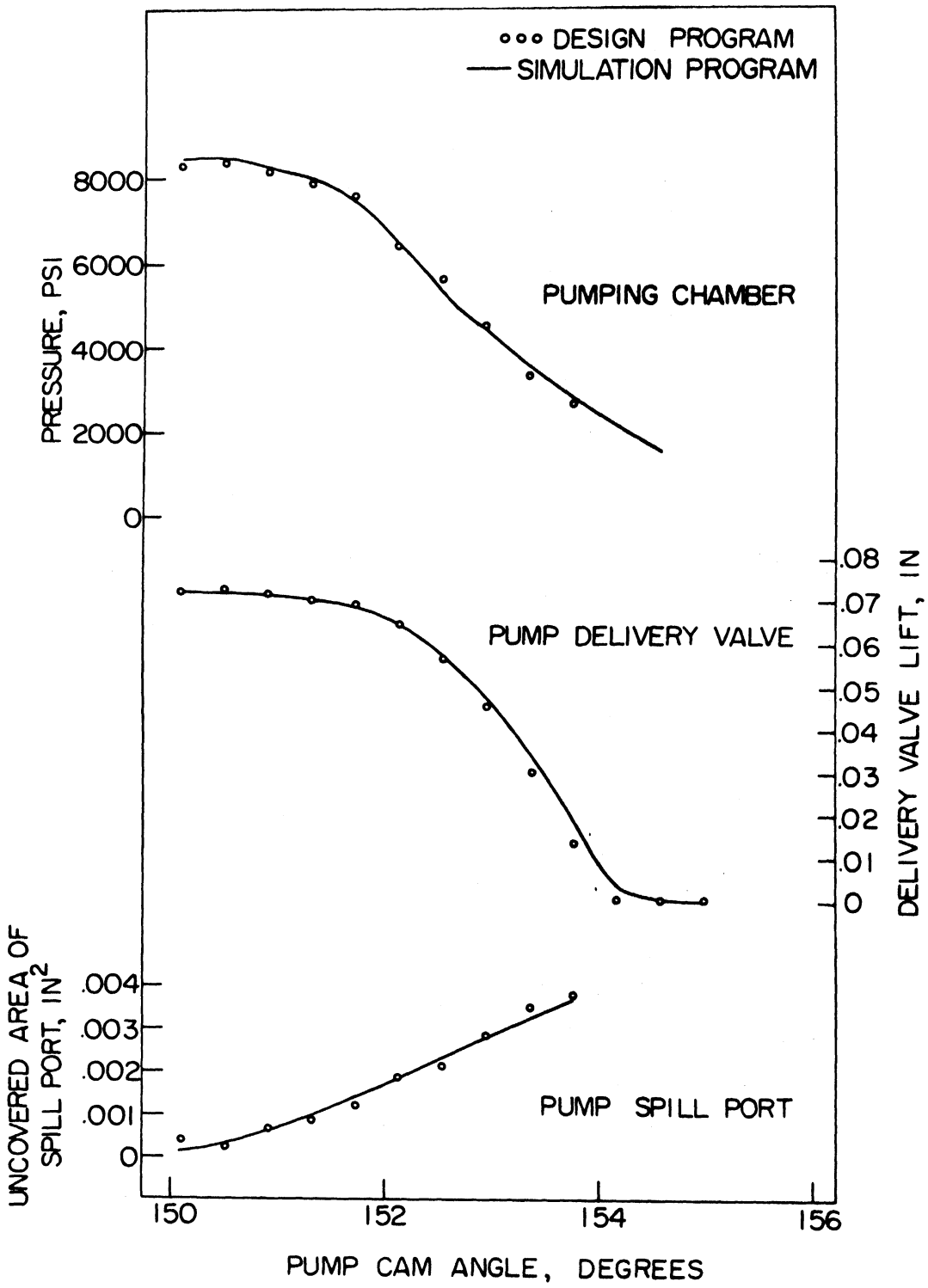

Figure 42. Simulation Check of Design Program Results at the Pump for Test No. 6 (Table IV).

essentially no difference between the simulation and design program results. The minor differences in Figures 41 and 42 result from using two different approximate solution methods.

VI. DESIGN PROGRAM RESULTS AND SIMULATION PROGRAM VERIFICATIONS OF THE RESULTS

6.1 Introduction

The previous chapter dealt with the formulation of the design program and two examples were given to illustrate its usefulness. In both examples, the system average elastic energy was used as a control parameter in the design program. This chapter considers the application of the design program to both examples. A study of the system performance as a function of the timing and the shape of the injection system average elastic energy function during the control period is given for both examples.

Certain constraints were imposed on allowable design changes made to eliminate after-injection. It was decided that the performance of the injection system during the main injection period should be maintained. This implies that the injection chamber pressure should not be seriously altered during the main injection and the system base pressure also should not be seriously altered.

6.2 Effect of the Average Elastic Energy Function on the System Transient Pressures

6.2.1 Average Elastic Energy and the Control Valve Example

As described in Section 5.3.5, the first example deals with the use of an additional control valve in the pump delivery chamber, which is used to release the system elastic energy in a controlled manner. In order to maintain the performance of the system during main injection, it was decided not to alter the original system average elastic energy function during this period. Also the

system average elastic energy must reach the system base pressure by the end of the control period. This elastic energy drop will be achieved by using the additional control valve, Figure 40. Several elastic energy alterations as applied to example No. 1 are given in Figures 43 and 44. These figures illustrate the effect of the system average elastic energy on the resulting transient pressures at the pump delivery and the injector upper chambers. All traces on these figures begin at the beginning of the control period, and the solid traces represent the system performance without alterations. The appearance of high residual energy on the solid traces and the existence of negative pressures in some of the traces are due to the fact that after-injection and cavitation were not accounted for in the design program.

Two alterations are given on Figure 43 to illustrate the dependence of pressure on the time of initiating the elastic energy drop. The results given on this figure represent Test No. 3 (Table III, Figures 30 and 37). The circles represent an elastic energy drop starting at the point of delivery valve closing, while the triangles represent an energy drop starting at the point of needle final closing. From comparisons of resulting pressures at the nozzle upper chamber, the following is clear: The first alteration (given by circles) results in added cavitation. Also, after-injection is liable to occur since the residual pressures at the injector are not damped. The second alteration (given by triangles) results in damping the residual pressures and therefore, after-injection does not occur. Also, no cavitation is detected in the second example. Thus it can be concluded that an elastic energy drop beginning at the point

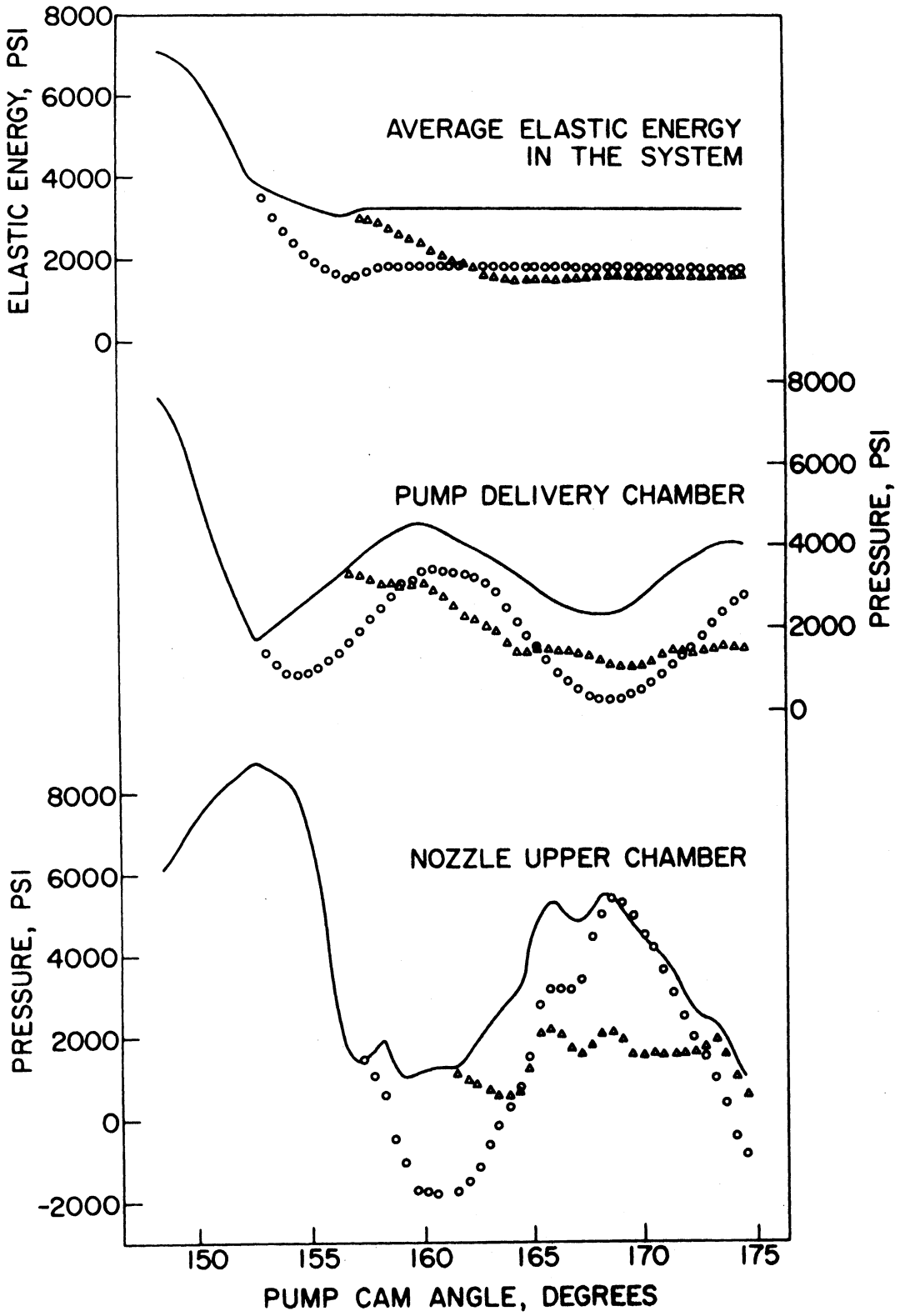

Figure 43. Injection System Variables versus Pump Cam Angle. Effect of Timing the Average Elastic Energy Drop. The Control Valve Example, Test No. 3 (Table III).

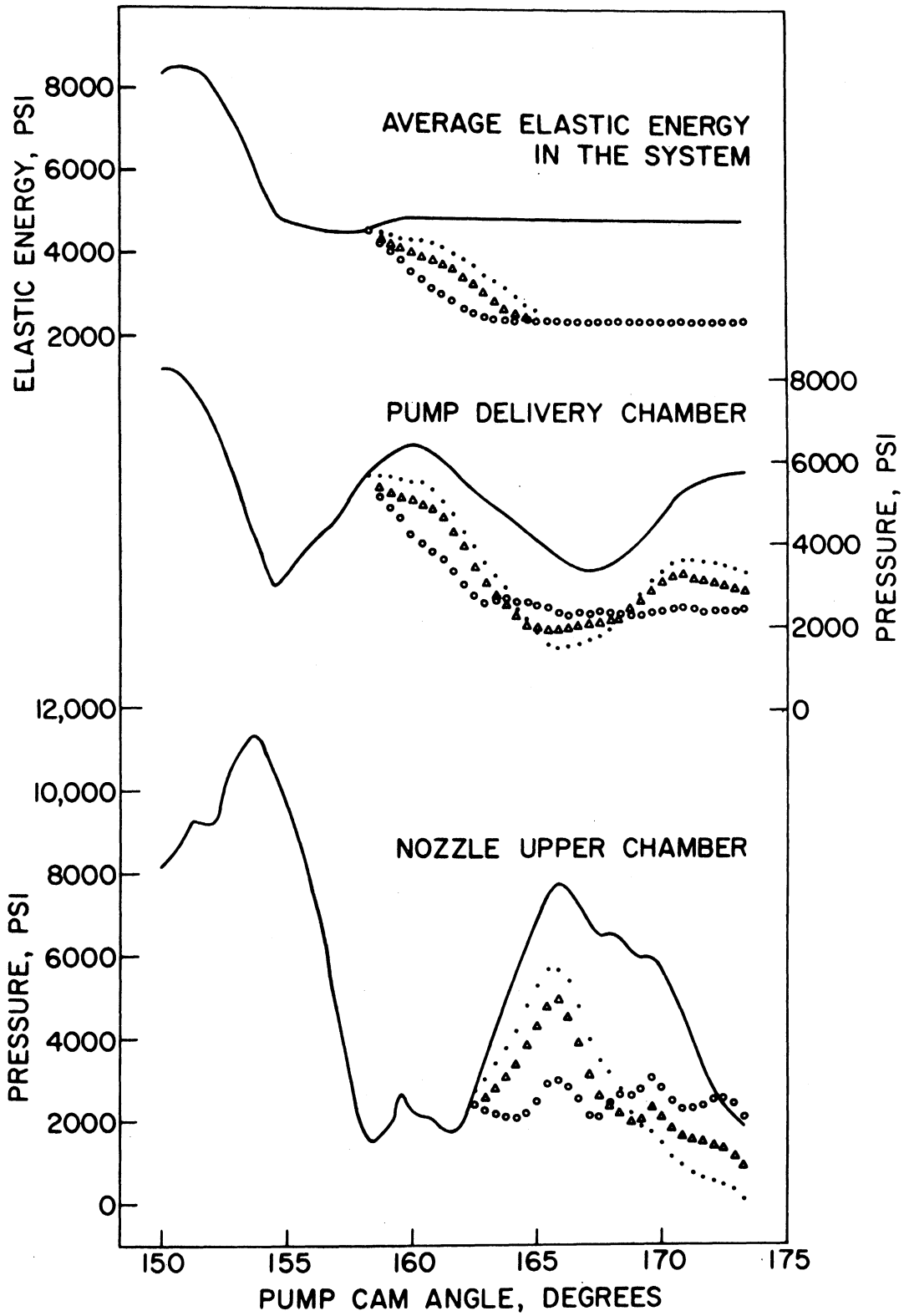

Figure 44. Injection System Variables versus Pump Cam Angle. Effect of the Shape of the Average Elastic Energy Drop. The Control Valve Example, Test No. 6 (Table IV).

of final needle closing is desirable. Several other trials have confirmed this conclusion.

Several shapes of elastic energy drop were studied and three of them are given in Figure 44. Results on this figure are for Test No. 6 (Table IV, Figure 33). In this figure, all alterations begin at the point of final needle closing. The three elastic energy alterations are represented by dots, triangles and circles. By comparing pressures at the nozzle upper chamber, it is clear that the average elastic energy function represented by the circles results in damping the residual pressures and thus eliminates the possibility of after-injection. The other two alterations reduce the magnitude of the residual pressures but do not eliminate after-injection.

6.2.2 Average Elastic Energy and the Redesigned Spill Port Example

As described in Section 5.3.5, the second example dealt with redesigning the pump spill port. The object of the new design was to release the high elastic energy in the system by controlling the fuel spilling at the port. To allow this, the pump delivery valve must be open during the control period. This can be done by using slower rates of energy release and delivery valves with high unloading volumes.

Several choices of average elastic energy functions are given in Figures 45 and 46. Results on both figures are for Test No. 6 (Table IV and Figure 33). Traces on these figures are used to illustrate the effect of the average elastic energy on the transient pressures in the system. Three of these functions are given on Figure 45 and are used to illustrate the effect of changing the rate

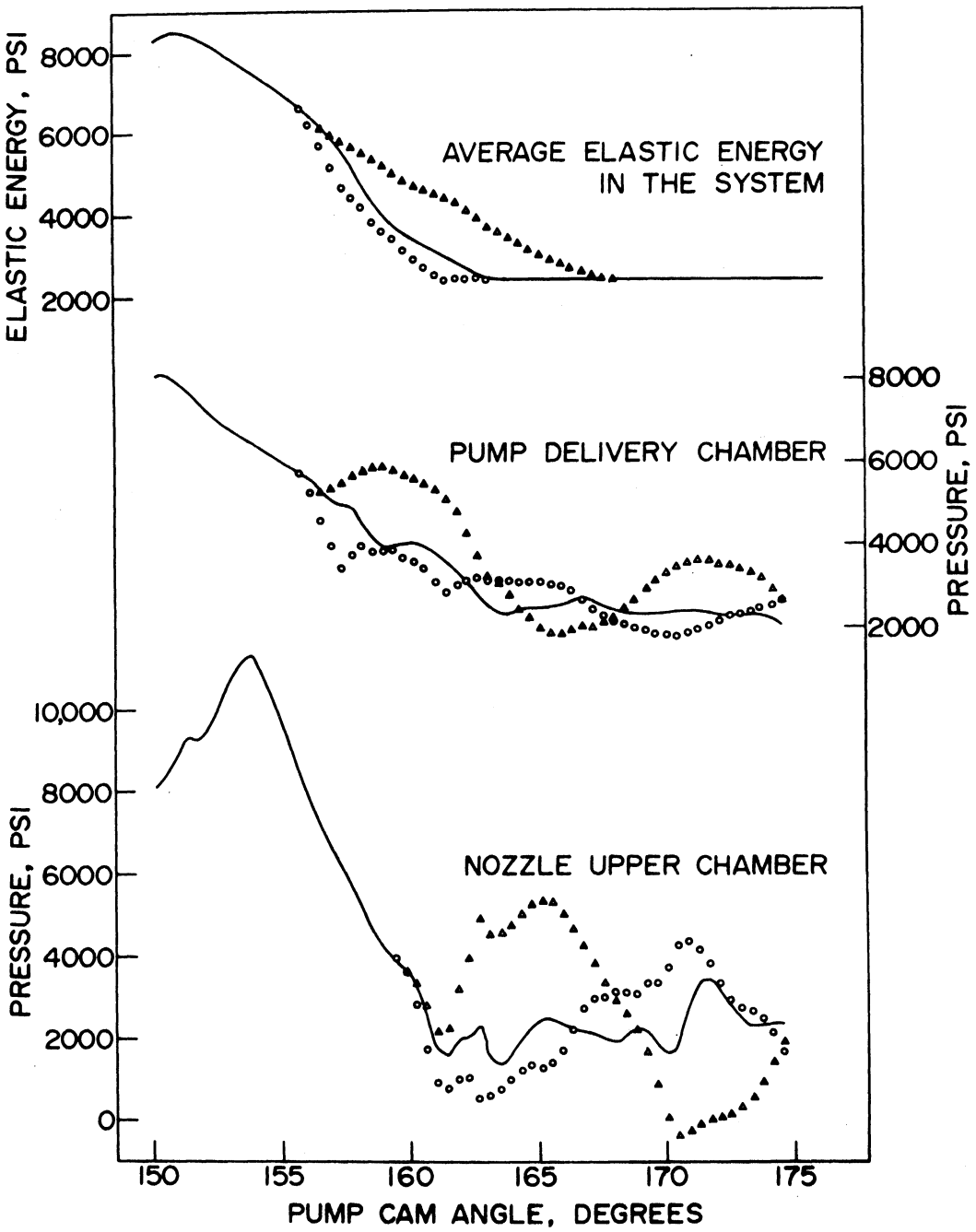

Figure 45. Injection System Variables versus Pump Cam Angle. Effect of the Rate of the Average Elastic Energy Drop. The redesigned Spill Port Example, Test No. 6 (Table IV).

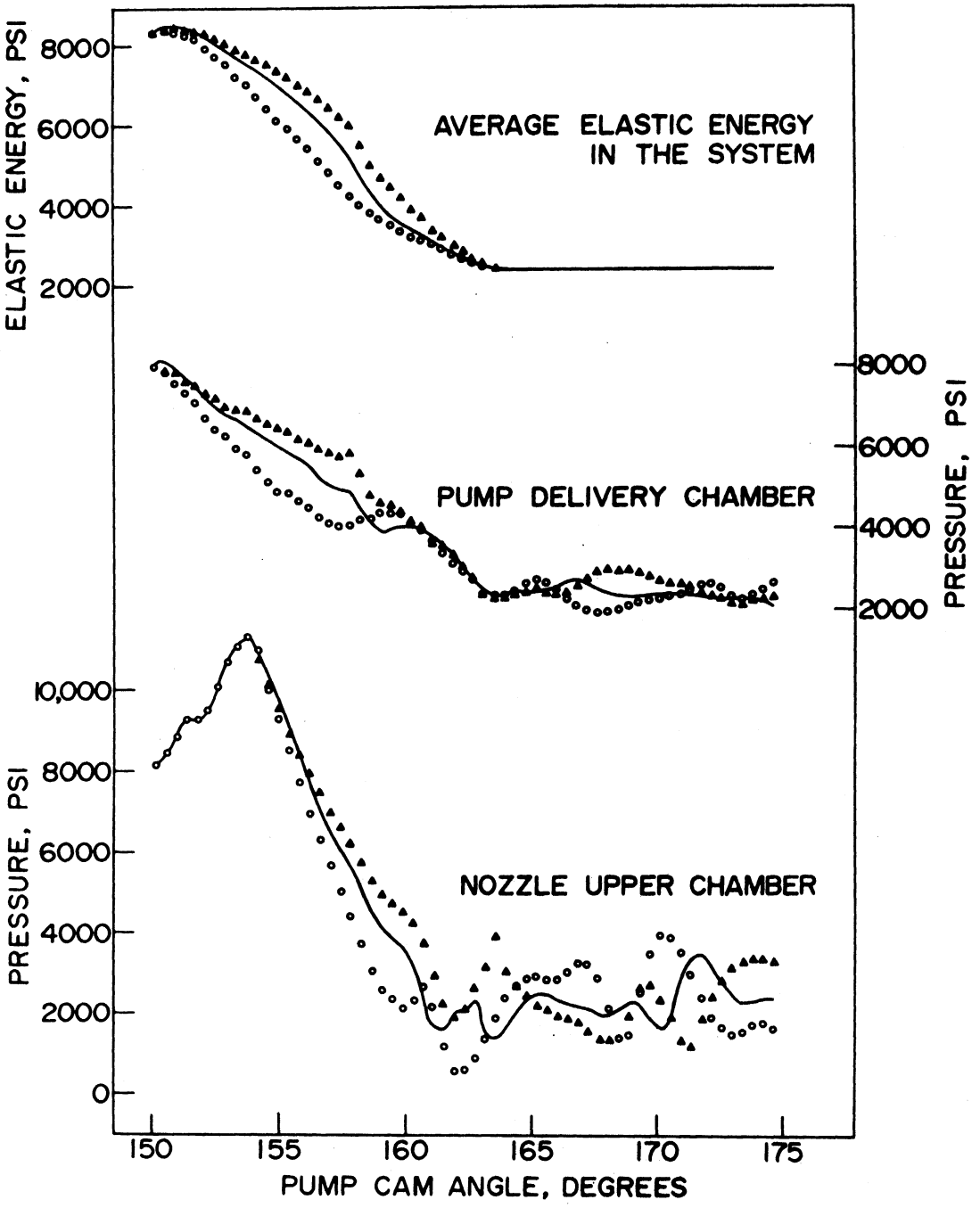

Figure 46. Injection System Variables versus Pump Cam Angle. Effect of the Shape of the Average Elastic Energy Drop. The Redesigned Spill Port Example. Test No. 6 (Table IV).

of elastic energy drop near the end of the control period on the resulting transient pressures. It is seen from this figure that the solid trace represents a desirable solution, while the opposite is true for the cases represented by circles and triangles. The triangles represent a very slow drop of the elastic energy function. The very slow drop results in high residual pressures at the nozzle upper chamber which will prolong the main injection period. The circles represent a relatively fast elastic energy drop. This change results in high nozzle upper chamber pressures which leads to after-injection. The solid trace of the elastic energy function results in damping the residual pressures and eliminating the possibility of after-injection.

Figure 46 is intended to illustrate the effect of manner of variation of average elastic energy on the resulting transient pressure. Three functions are given to demonstrate this effect. All three functions on this figure have the same beginning and end points for the average elastic energy function. The solid average elastic energy trace represents a desirable solution since it results in damping the nozzle upper chamber pressures, therefore eliminating after-injection. The other two traces (triangles and circles) have less damping effect on the transient pressures than the solid line trace.

Usually no more than four trials were needed to achieve a desirable average elastic energy trace for both examples. It should be noted that the procedures described here for the formulation and application of the design program are general and could be used with any injection system. However, the results presented here

apply only for the specific injection system described in this study.

6.3 Design Results and Verifications of the Control Valve Example

The previous section presented a study of the effect of timing and shape of the average elastic energy function on the system residual pressures. In this study, the average elastic energy curve given by circles in Figure 44 represented a desirable solution for the after-injection problem. As mentioned before, this solution is achieved by adding a control valve in the pump delivery chamber in order to release the system average elastic energy in the controlled manner. The area of flow past the control valve is calculated by the design program in the manner described in Section 5.4.4.

Design program results and simulation program verification of these results are presented in this section for Tests No. 3, 5 and 6 (Tables III and IV) and are given in Figures 47, 48 and 49, respectively. On these figures, the circles represent results obtained by the design program, while simulation program verification of these results are illustrated by solid traces. The traces include the system average elastic energy, pressures in the pump delivery chamber and injector upper chamber and the area of flow through the control valve. It should be noted that a simple valve motion was used in the simulation program. As a result, the valve area is described by a linear opening of the valve, a constant maximum opening area and a linear closing. This area was obtained by averaging the design program results for the control valve areas as shown on Figures 47 through 49.

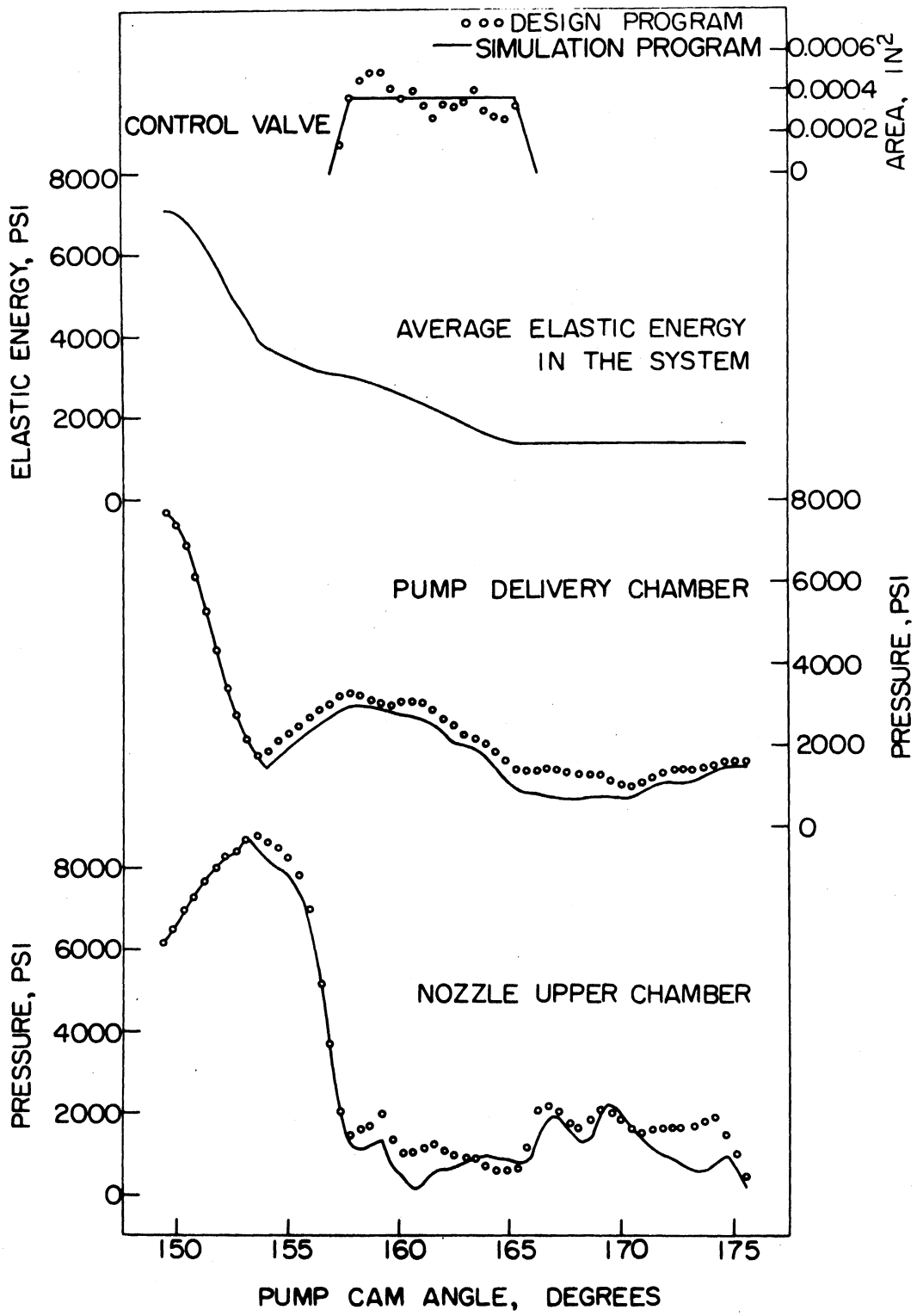

Figure 47. Design Program Results of Injection System Variables and Simulation Verification of These Results. The Control Valve Example, Test No. 3 (Table III).

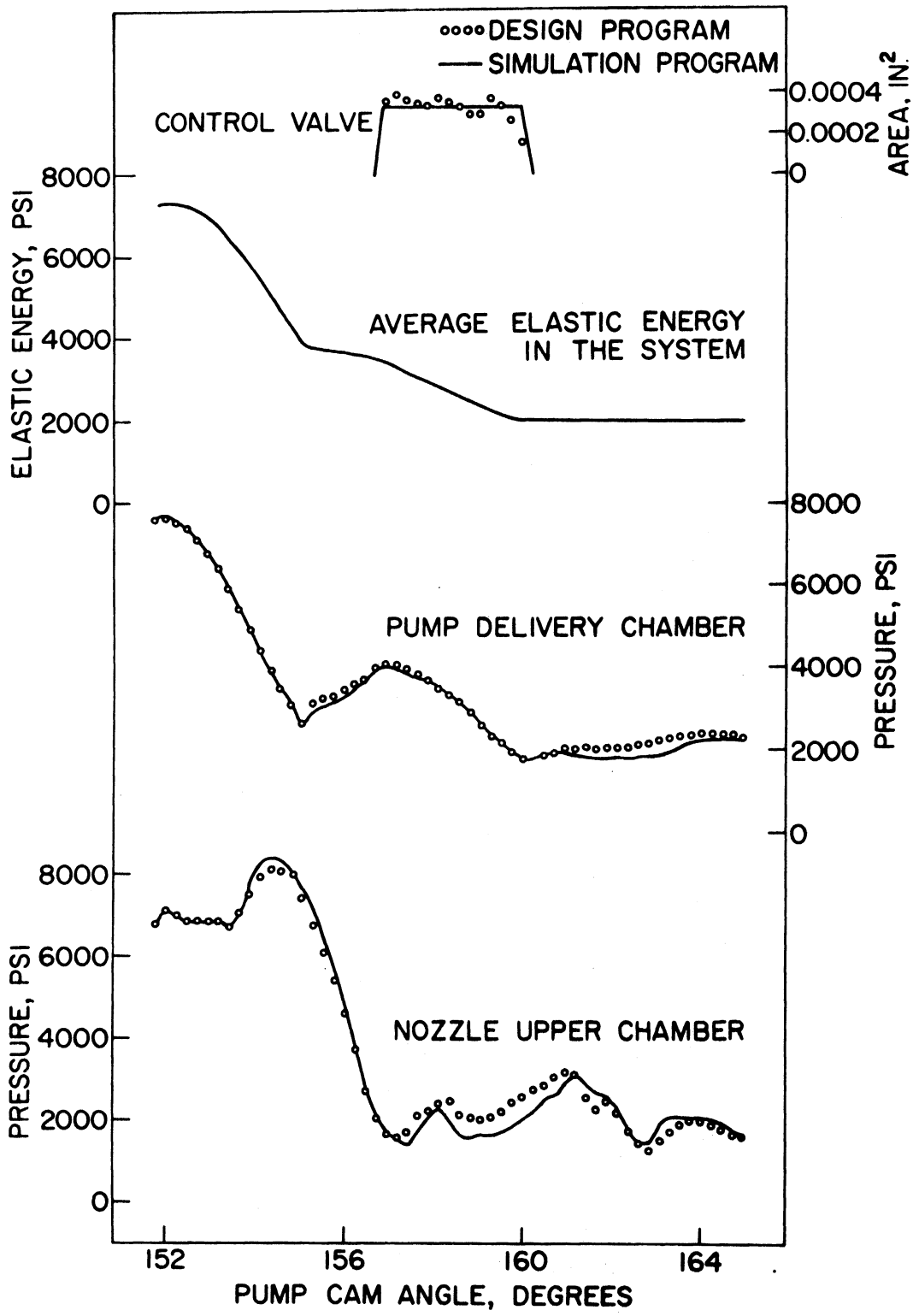

Figure 48. Design Program Results of Injection System Variables and Simulation Verficiation of These Results. The Control Valve Example, Test No. 5 (Table IV).

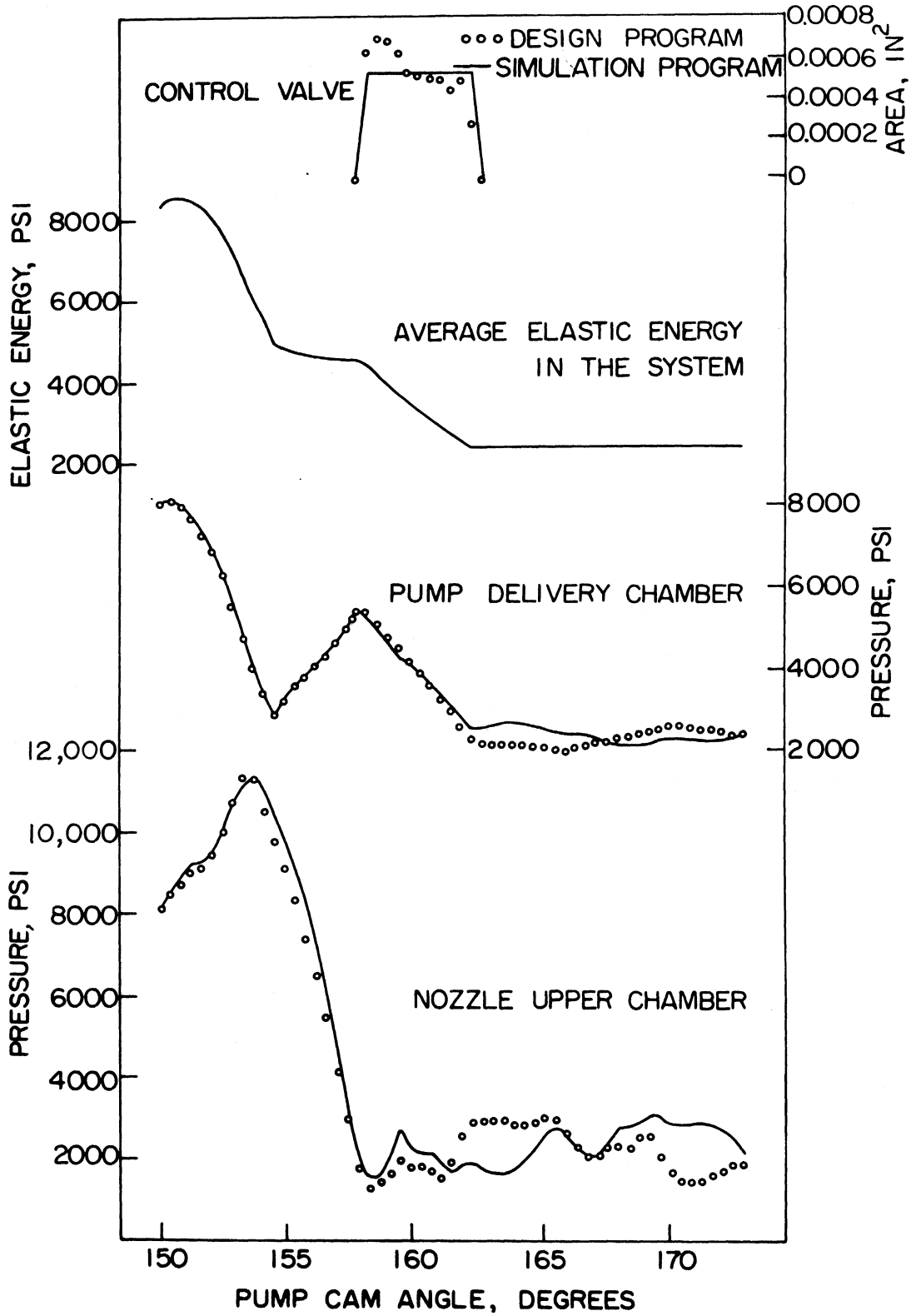

Figure 49. Design Program Results of Injection System Variables and Simulation Verification of These Results. The Control Valve Example, Test No. 6 (Table IV).

In all the cases presented, the control valve starts to open when the needle finally closes. The maximum opening area differs from one case to the other with the combined higher load and speed condtions requiring larger areas of flow through the control valve than the relatively lower speed and load conditions. The valve opening periods for Tests No. 5 and 6 (Figures 48 and 49) are both 1.2 millseconds. However, these periods are different in terms of cam angle degrees due to the speed difference between the tests. The valve opening period for Test No. 3 (Figure 47) is 2 milliseconds. This is greater than for Tests No. 5 and 6 primarily because of the relatively low base pressure associated with this test.*

The average elastic energy traces on Figures 47 through 49 result in the damping of the system residual pressures and therefore eliminating after-injection. It should be emphasized that the injection characteristics during the main injection period are not altered since the average elastic energy function during this period and the system base pressures are not changed. Simulation program results verify the design program predictions. Small differences between design and simulation results can be attributed to the use of simple valve motion in the simulation program.

6.4 Design Results and Verifications of the Redesigned Spill Port Example

The formulation and solution of the equations used with this example were presented in Section 5.4.4. Later, a study on the effect of the average elastic energy function of the system residual pressures

---

*This test uses a different nozzle area than Tests No. 5 and 6.

was presented in Section 6.2.2. In this study, the solid line average elastic energy trace on Figures 45 and 46 represented a desirable solution to the after-injection problem. This solution is achieved by redesigning the pump spill port in order to release the system elastic energy in the desired controlled manner. The new areas of flow of the pump spill port are calculated in the manner described in Section 5.4.4. Design program results together with the simulation program verifications. of these results are presented in this section for Tests No. 4 through 6 (Table IV).

The original system performance was illustrated in Figures 31 through 33. A comparison between this performance and the modified system as calculated by the design program is given in Figures 50 through 52 for Tests No. 4 through 6, repsectively. On these figures, the solid traces represent the original system performance while the circles represent the modified one. Comparisons are given for the system average elastic energy, the pump spill port areas, the pump delivery valve motion and for pressures in the pump delivery and nozzle upper chambers. As mentioned previously, the design program utilizes a controlled function for the average elastic energy to calculate the performance of the modified system. It can be seen from the above mentioned figures that the design changes result in damping the residual pressures and eliminating after-injection. Most of the elastic energy release is done at the pump by keeping the pump delivery valve oepn for longer periods compared to its original performance. This is accomplished by the relatively smaller areas of the modified spill port and by using delivery valves with higher unloading volume.

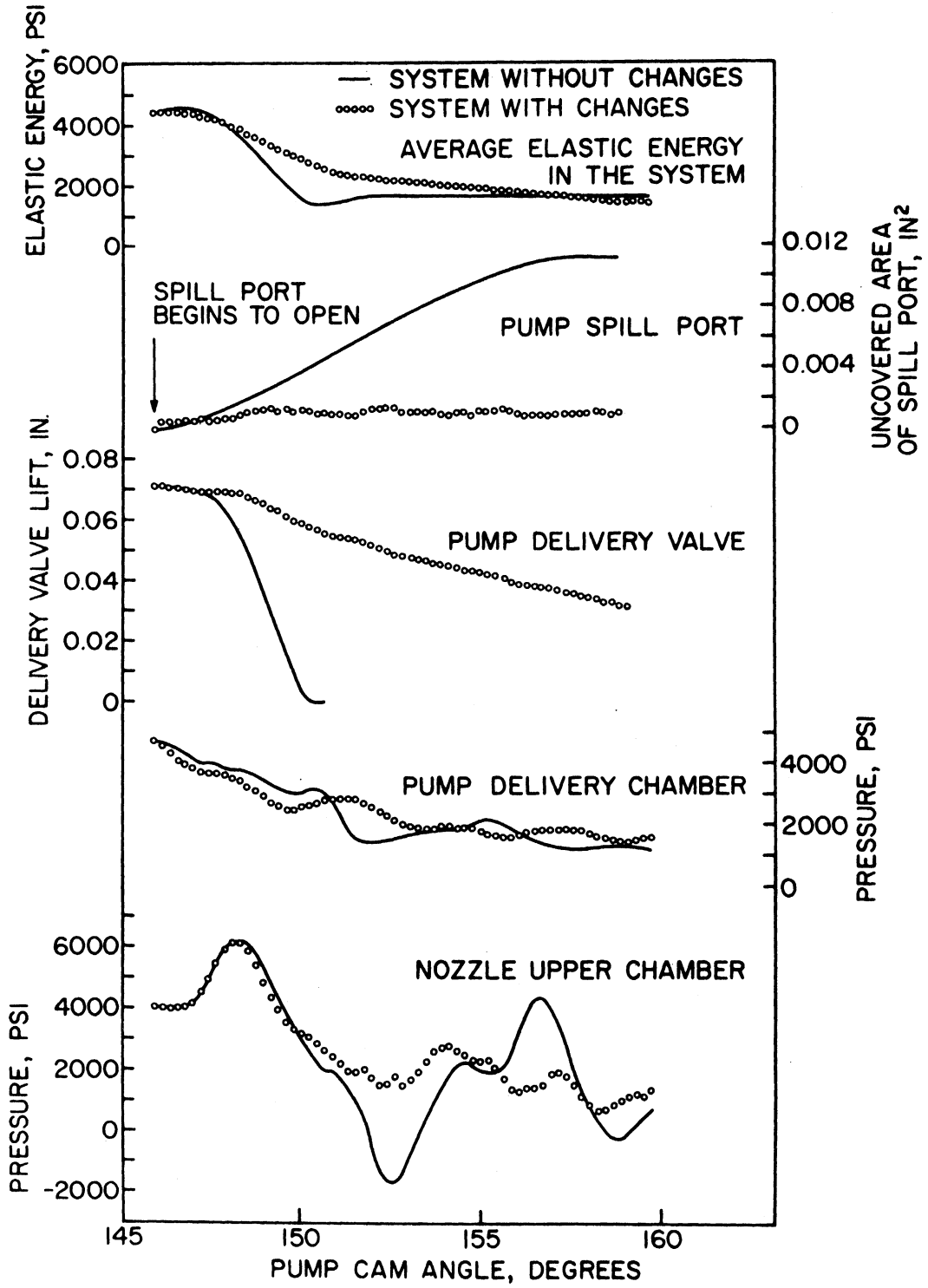

Figure 50. Comparisons of Original Injection System Performance and Design Program Results of the Modified System. The Redesigned Spill Port Example, Test No. 4 (Table IV).

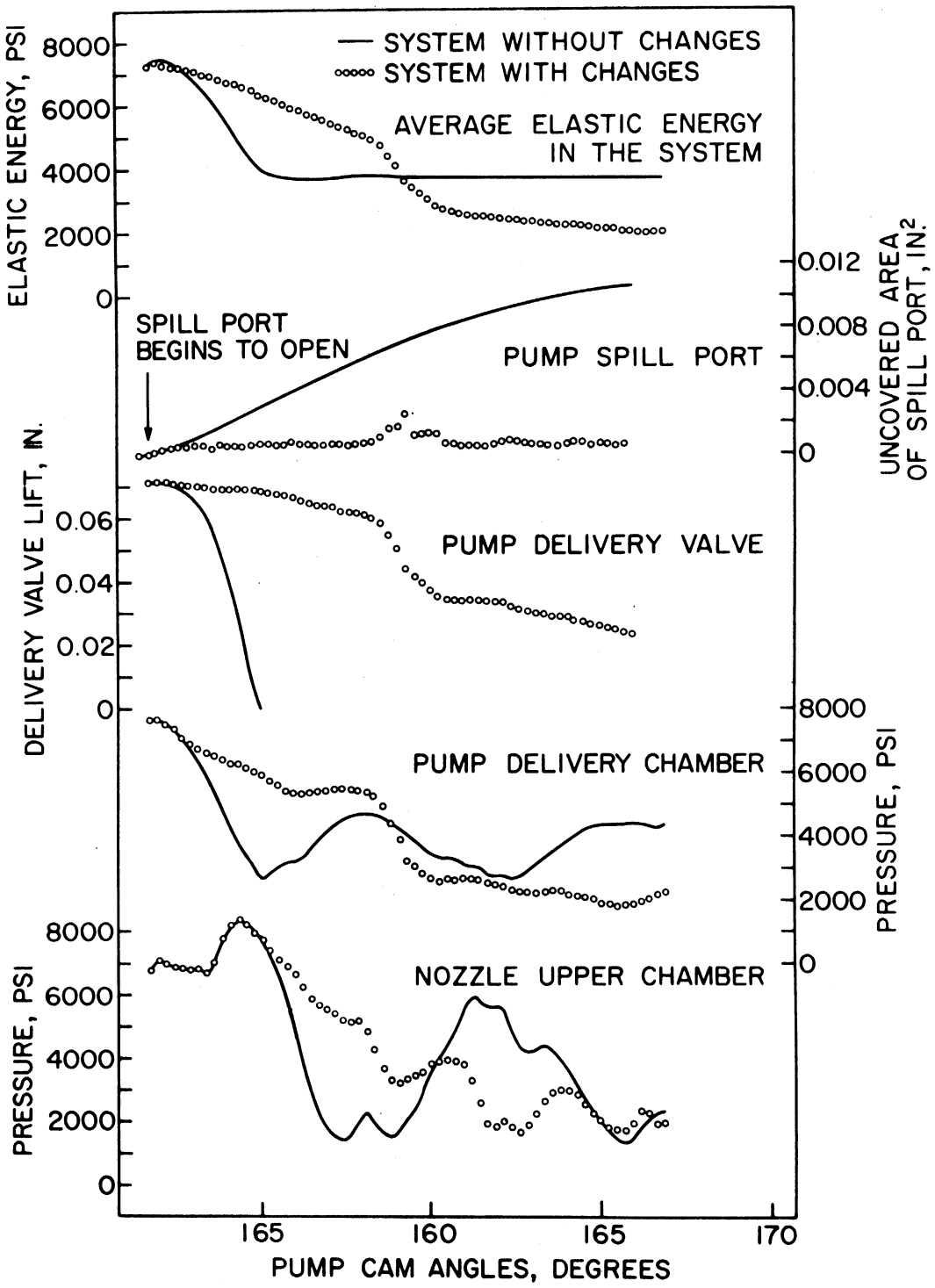

Figure 51. Comparisons of Original Injection System Performance and Design Program Results of the Modified System. The Redesigned Spill Port Example, Test No. 5 (Table IV).

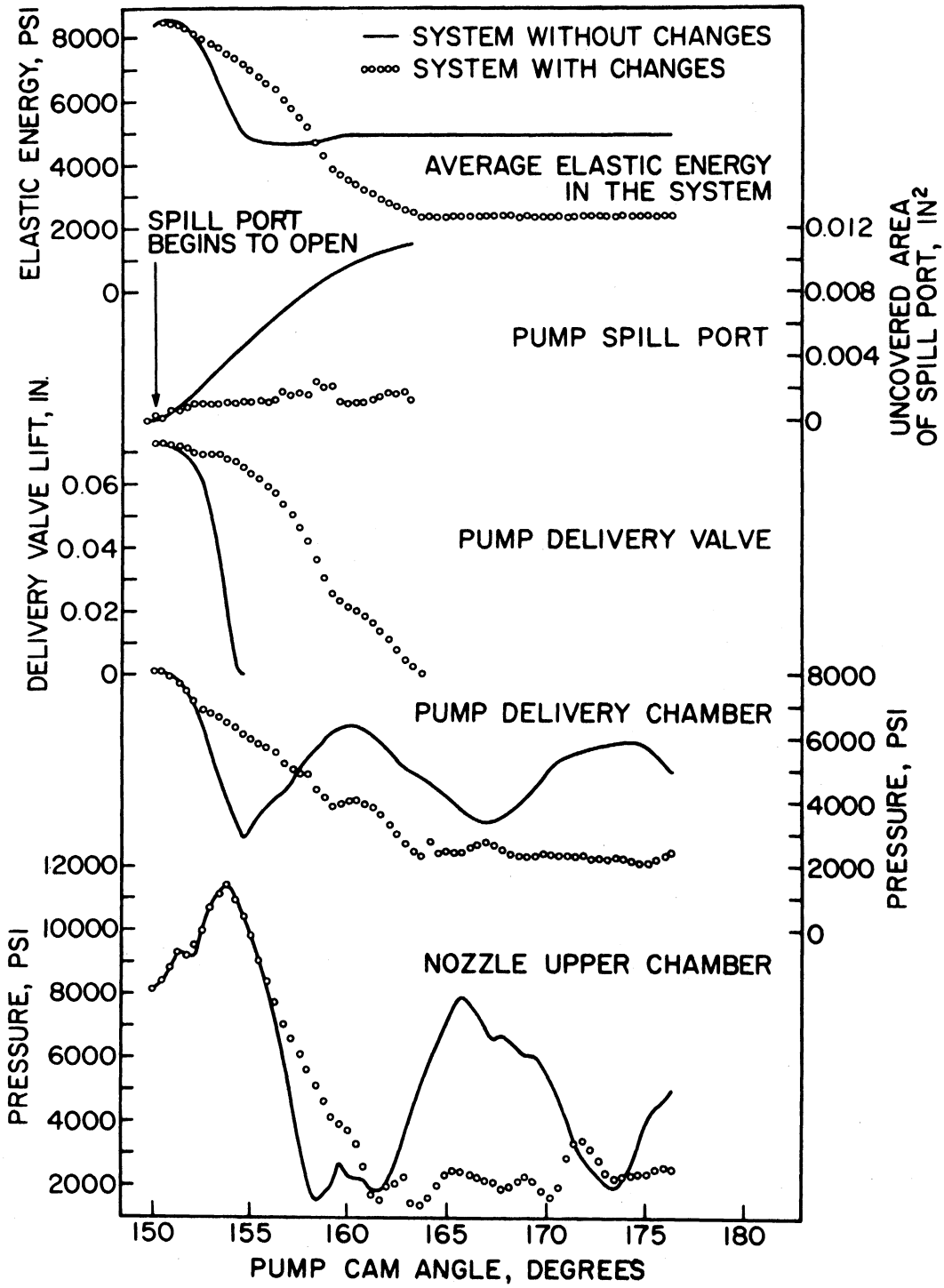

Figure 52. Comparisons of Original Injection System Performance and Design Program Results of the Modified System. The redesigned Spill Port Example, Test No. 6 (Table IV).

In all the cases, a delivery valve diameter of 0.373 inch was used instead of the original diameter of 0.236 inch. It should be noted that the resulting system base pressure for the modified system is the same as the original one, and that the resulting pressures at the injector for the modified system differ slightly from the original one.

It can be seen from Figures 50 through 52 that the resulting area of the pump spill port starts with linear opening and then reaches a constant value. In Figure 52, the spill port area begins to increase again near the end of delivery valve closing. The constant opening of the spill port is nearly the same in all cases (0.0011 inch^2). Therefore, it is possible to describe a common spill port area as a function of pump plunger lift for all the reported cases. Such a common description is not possible in terms of time or pump cam angle because of the difference in speed for each test.

A common area was used in the simulation program in order to verify the design program results. These verifications are given in Figures 53 through 58. Figures 53 through 55 illustrate the simulation program results of the injection system using the modified spill port area for Tests No. 4 through 6 (Table IV). Also, comparisons between the original and the modified systems are given in Figure 56 through 58 for the spill port areas and the injection chamber pressures. Simulation results and the comparisons which are given on Figures 53 through 58 verify the success of the proposed design changes toward eliminating after-injection. From comparing the nozzle upper chamber pressures in Figure 53 through 55 with corresponding original system pressures in Figures 31 through 33, it is clear that the proposed design changes have resulted in damping these pressures without changing the final system base pressures.

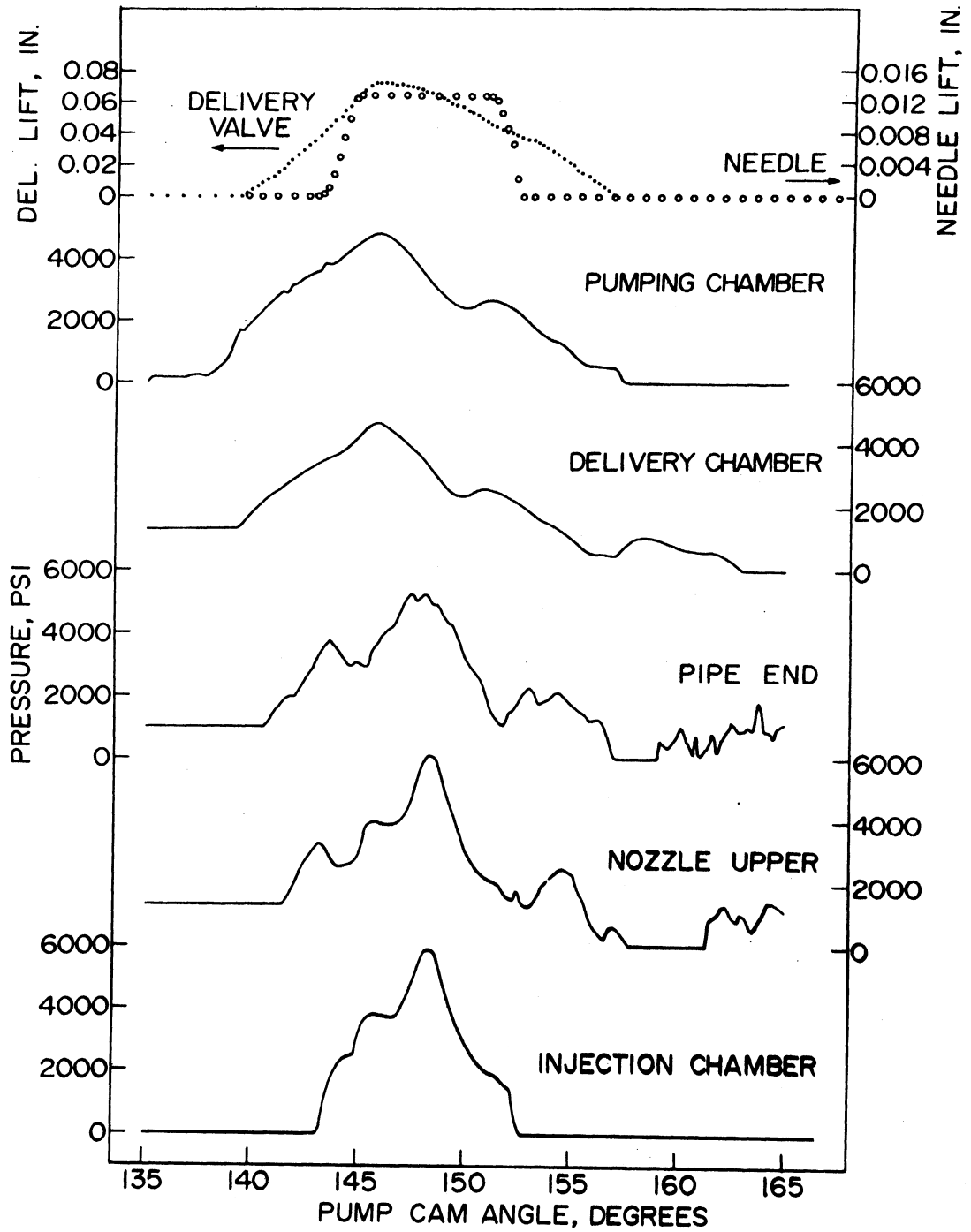

Figure 53. Simulation Program Results of the Modified Injection System. The redesigned Spill Port Example, Test No. 4 (Table IV).

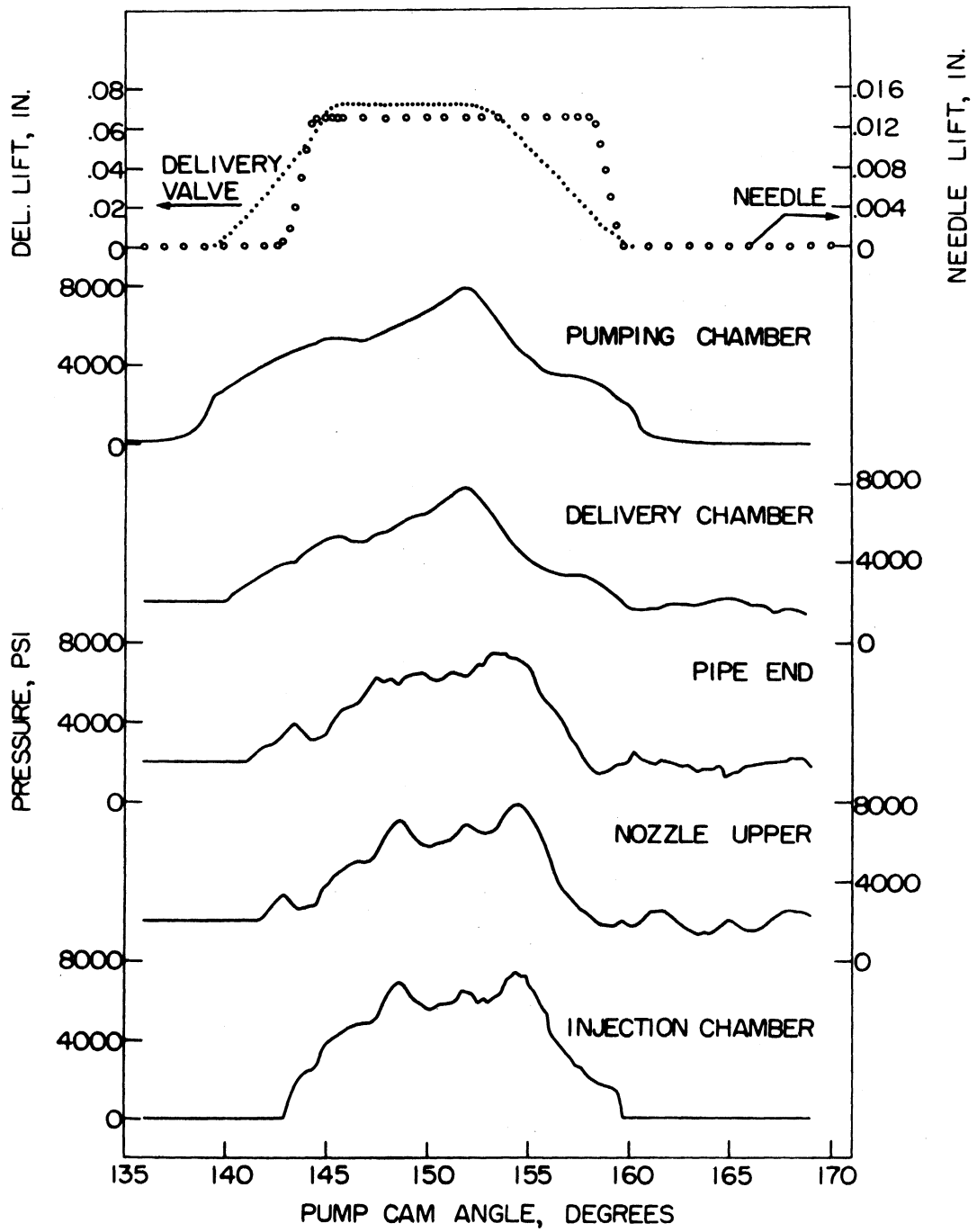

Figure 54. Simulation Program Results of the Modified Injection System. The Redesigned Spill Port Example, Test No. 5 (Table IV).

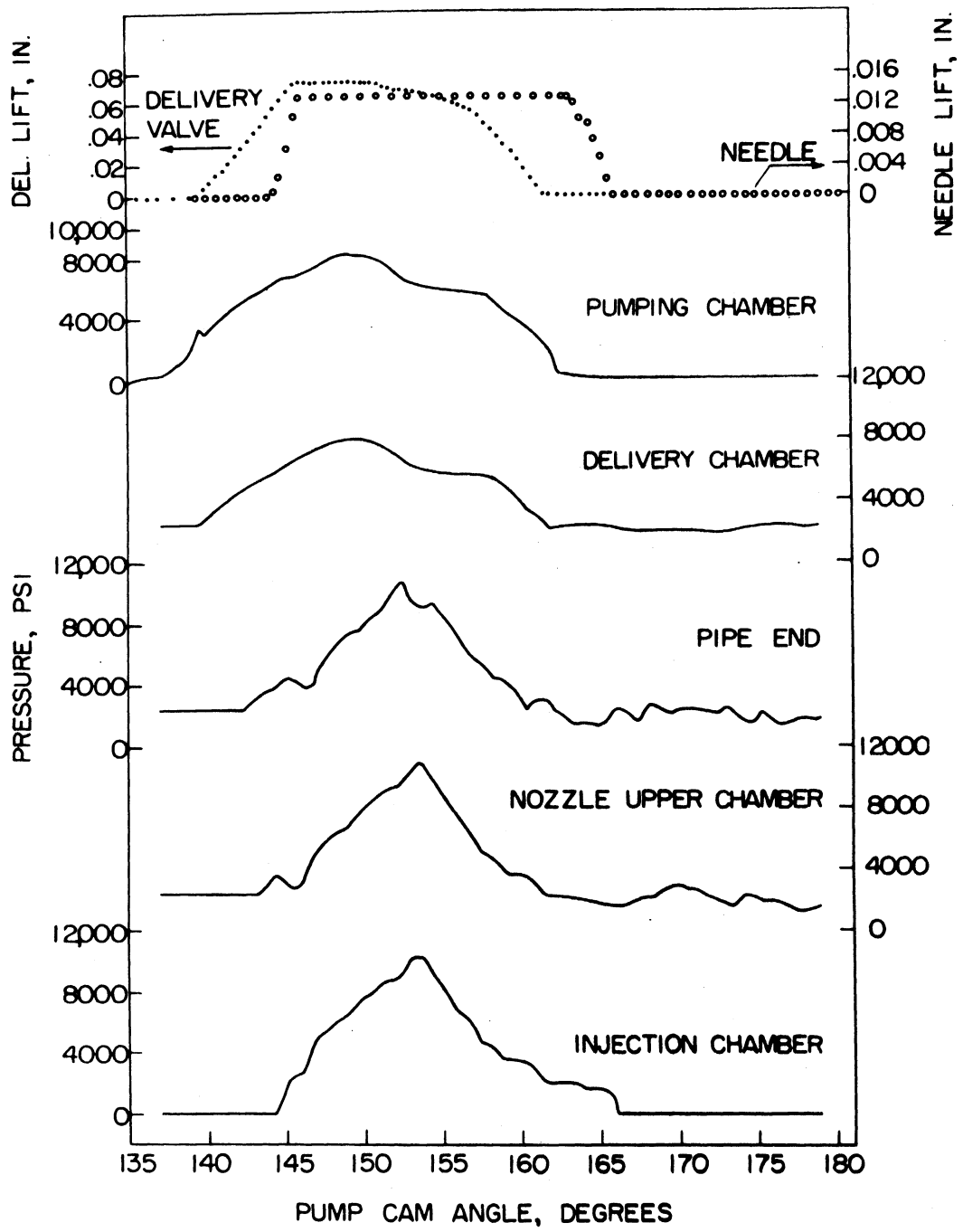

Figure 55. Simulation Program Results of the Modified Injection System. The Redesigned Spill Port Example, Test No. 6 (Table IV).

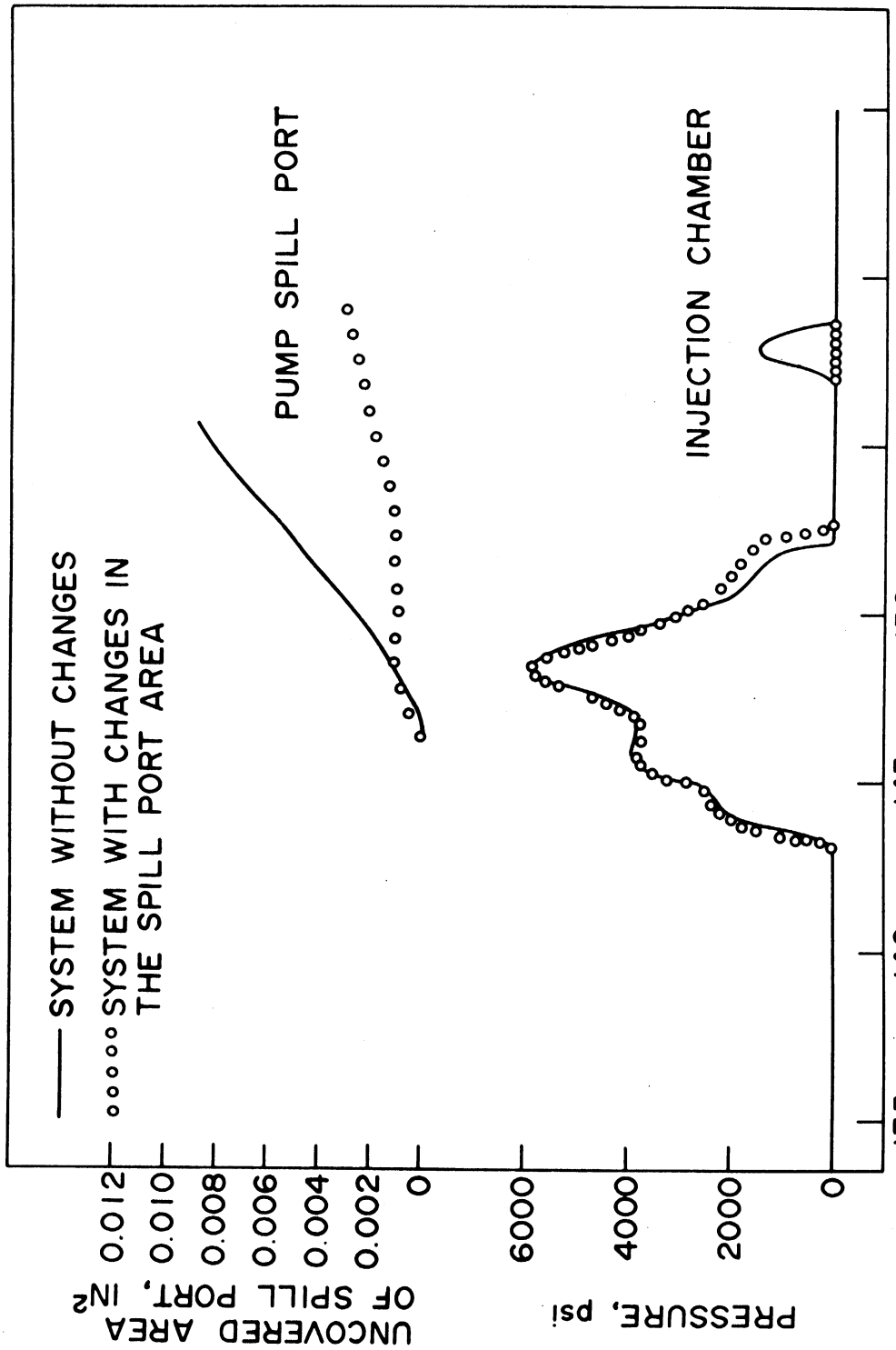

Figure 56. Comparisons of Injection Chamber Pressures of Original and Modified Systems. The Redesigned Spill Port Example, Test No. 4 (Table IV).

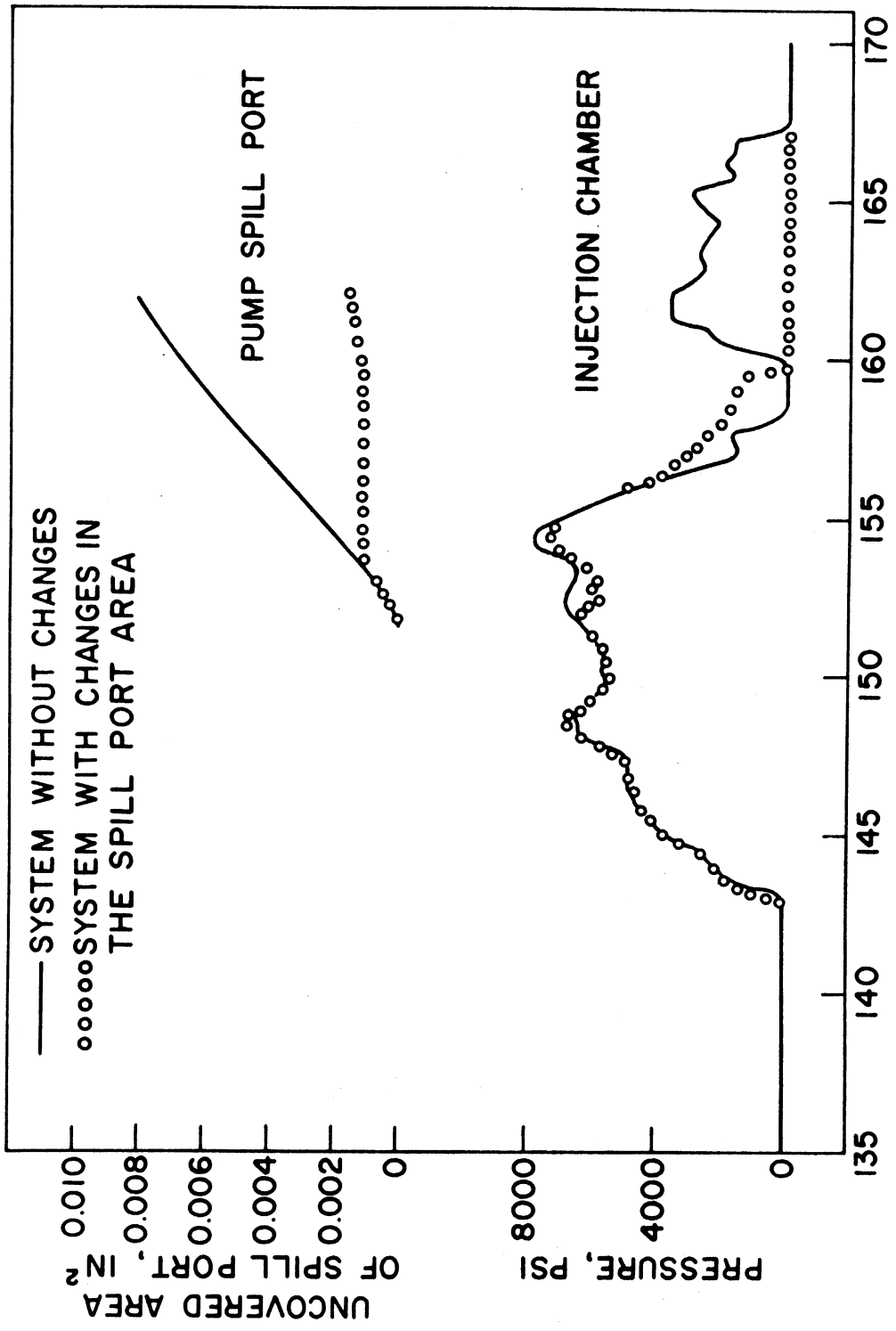

Figure 57. Comparisons of Injection Chamber Pressures of Original and Modified Systems. The Redesigned Spill Port Example, Test No. 5 (Table IV).

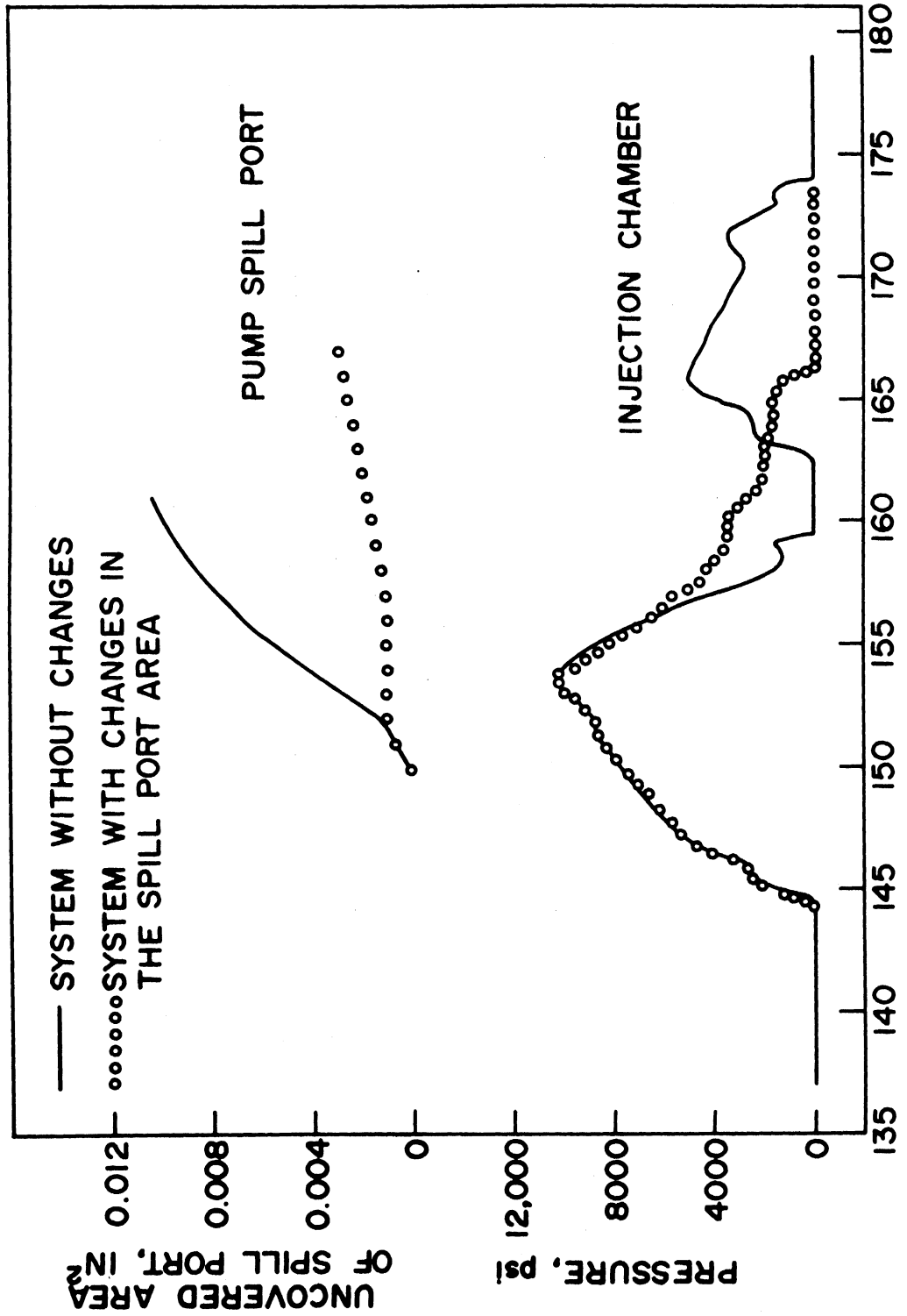

Figure 58. Comparisons of Injection Chamber Pressures of Original and Modified Systems. The Redesigned Spill Port Example, Test No. 6 (Table IV).

Modified spill port areas are drawn as function of pump cam angle and are compared with the original areas on Figures 56 through 58. As mentioned previously, these modified areas will appear the same if they are drawn as functions of pump plunger lift. On the same set of figures, comparisons between the injection pressure characteristics for the modified and original systems indicate that slight differences occur for Tests No. 4 and 5 while a relatively bigger difference was observed with Test No. 6. It should be noted that Test No. 6 has high speed and load conditions and high system base pressure (2400 psi). This relatively high base pressure is higher than the needle closing pressure (2200 psi). Therefore, it can result in prolonging the injection period as seen from Figure 58. Better results for the system injection pressures were obtained by using a different area for the spill port as seen in Figure 59. The choice of this new area was directed toward lowering the system base pressure. This was achieved by using higher uncovering rates for the spill port near the end of injection while keeping these areas the same as those on Figure 58 for the early part of the spill. The system base pressure for the results given on Figure 59 was found to be 1600 psi.

The modified spill port area associated with Test No. 6 and given on Figure 59 was used in the simulation program to investigate its effect on Tests No. 4 and 5. This area resulted in lowering the base pressures for these tests and slightly improved the injection pressure characteristics. However, extreme lowering of these base pressures at a combined low load and speed conditions (Test No. 4) results in reaching vapor pressures. It should be noted that mechanical damage due to vapor bubble collapse is less harmful at combined low speed and load conditions than at the combined high speed and load

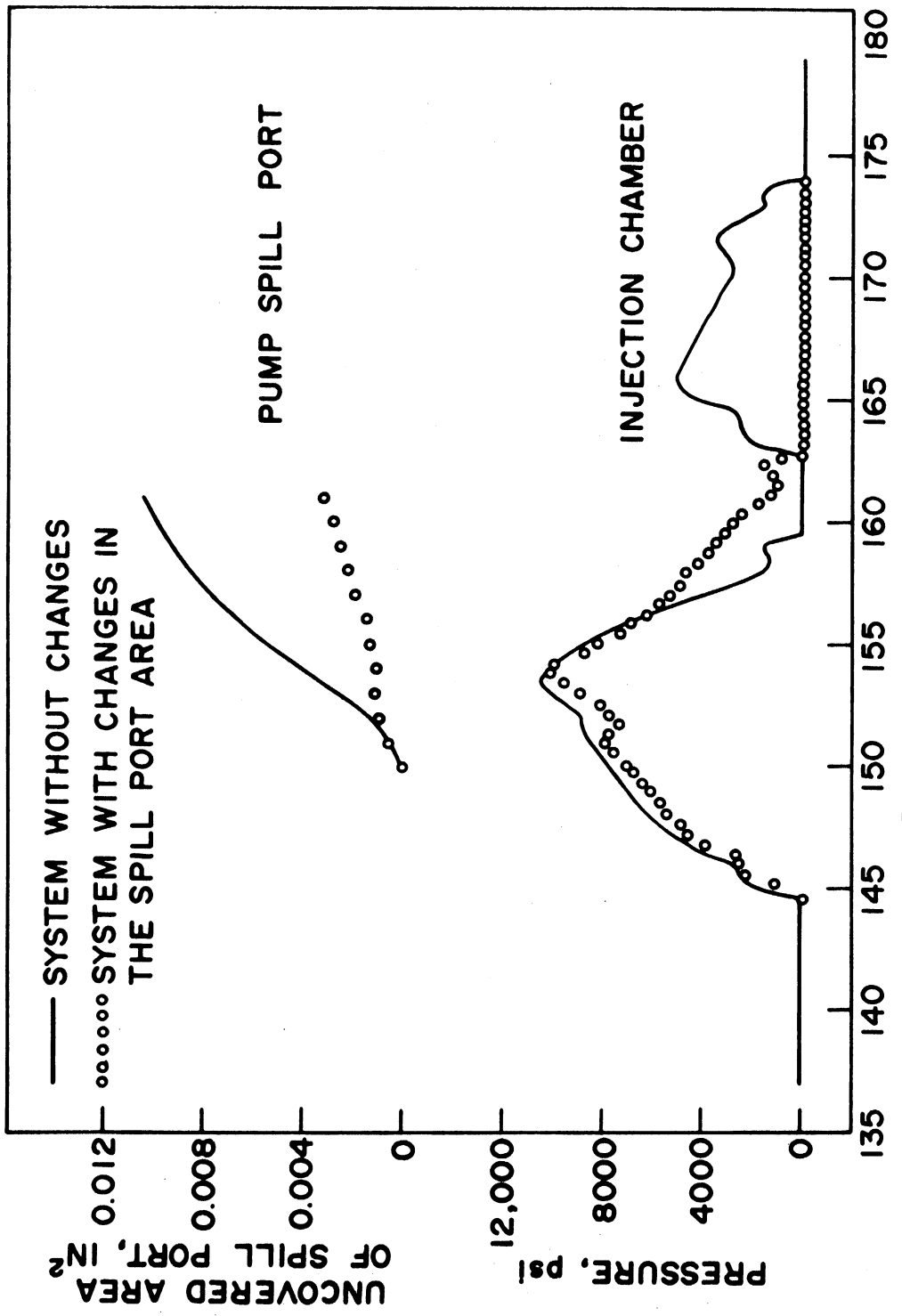

Figure 59. Comparisons of Injection Chamber Pressures of Original and Modified Systems. The Redesigned Spill Port Example, Test No. 5 (Table IV).

conditions.[23] Therefore, vapor pressures can be allowed to occur at the low load and speed conditions.

VII. SUMMARY AND CONCLUSIONS

The primary objectives of this thesis were to achieve a good understanding of the theory describing the diesel injection system and to use this understanding to develop a theoretical control method by which design changes could be determined to eliminate undesirable system characteristics (i.e. after-injection).

In this study, the after-injection phenomenon was experimentally surveyed. Then a computer simulation model was developed to predict the theoretical system performance. The results from the computer simulation were compared with experimental data taken on actual test equipment. Then, an investigation of a theoretical control parameter was carried out which led to the formulation of a design program that used the injection system average elastic energy as the control parameter. Two injection system design changes were investigated. The first was the addition of a control valve in the pump delivery chamber which is used to release the system excess elastic energy in a controlled manner and eliminate after-injection. The second change centered on re-designing the pump spill port to control the rate of fuel spill in order to eliminate after-injection. The results of both changes were determined and were verified using the simulation program.

The study included three major phases; namely, experimental survey of the after-injection phenomenon, computer simulation of the injection system, and the theoretical control of the after-injection

phenomenon. Specific conclusions related to each phase of study are given and will hopefully contribute to the development of future injection systems. These conclusions can be summarized as follows:

1. Currently used injection systems of the Bosch type are usually designed to operate at fuel deliveries and injection pressures considerably below their full capacities in order to avoid after-injection. These low injection pressures limit fuel atomization and penetration in the combustion chamber.
2. The optimum design point of injection systems is located critically close to the after-injection zone. Any accumulation of carbon or fuel impurities on the injection holes changes the system performance drastically and introduces large amounts of after-injection.
3. The computer model presented herein improves on existing injection system models by using the characteristic method to solve the exact partial differential equations representing the wave propagation phenomena in the pipe lines. It also includes the effect of variable wave speeds and uses a variable time increment solution technique (predictor-corrector method). These features improve the accuracy and efficiency of the simulation model.
4. The computer model presented here accurately simulates the injection system performance.

This is demonstrated in Tables III and IV by a mass continuity check within 4.5 percent and by a base pressure check within 300 psi. The accuracy of the system pressures is demonstrated by the good correlation between the experimental and theoretical model results as shown in Figures 28 through 34. Therefore, the analytical model can be confidently used to study the diesel injection system and the phenomena associated with its performance.

5. The injection system average elastic energy is a useful control parameter. It can be used to eliminate undesirable system characteristics. This was demonstrated in this thesis by eliminating after-injection. Further use of this concept can improve other injection system characteristics. This concept can also be applied to other similar complex systems which are characterized by high frequency internal and external boundary conditions and which cannot be controlled using existing valve stroking techniques.
6. The control method presented allows a theoretical systematic design improvement of injection systems for the first time. This has been demonstrated by two examples in which the injection system pressures after the end of the main injection were controlled in order to eliminate the after-injection

phenomenon. Such knowledge may be helpful in improving future injection systems and may lead to improved combustion and reduced exhaust emissions.

7. The pump spill port or an additional valve in the pump delivery chamber can be properly designed to eliminate after-injection. This can be done without seriously altering the injection system performance during the main injection period.

REFERENCES

1. Anders, U. W.P., "The Dynamic Delivery Rate and the Hydraulic Similarity of Injection Pumps for High-Speed Engines", ASME paper No. 71-D6P-3, April 18-22, 1971.

2. American Bosch Corp., "Fuel Injection and Controls for Internal Combustion Engines", 1963, N.Y., Simmons Boardman Publ. Corp., 1962.

3. Bassi, A., "Experimental Investigations into Diesel Injection Systems", Sulzer Research, No. 1963., 1963.

4. Becchi, P. I., "The Analytical Investigation of Phenomena Concerning the Fuel Injection in Fast Diesel Engines, Carried out at Design Stage by Means of the Electronic Computer", Tech. Bulletin, Fiat, Vol. XV, No. 2, April, 1962.

5. Becchi, G. A., "Analytical Simulation of Fuel Injection in Diesel Engines", SAE paper No. 710568, June 7-11, 1971.

6. Bosch, Wilhelm, "The Fuel Rate Indicator, A New Measuring Instrument for Display of the Characteristics of Individual Injection", SAE paper No. 660749, Oct. 17-21, 1966.

7. Bradbury, C. H., Stationary Compression Engines, London E. & F. N. Spon. Ltd., 1950.

8. Brown, G. W. and McCallion, H., "Simulation of an Injection System with Delivery Pipe Cavitation using a Digital Computer", Proc. Instn. Mech. Engrs., London, Vol. 182, 1967-68, p. 206.

9. Davis. S. J. and Giffen, E., "Injection, Ignition and Combustion in High Speed Heavy Oil Engines", Proc. Instn. of Automobile Engrs., March, 1931, p. 399.

10. De Juhasz, Kalman, J., "Graphical Analysis of Transient Phenomena in Linear Flow", Journal Franklin Inst., April, May, June, 1937, pp. 463, 643, 655.

11. Dolenc, A. and Lees, R., "Some Aspects of the Development of the OVA24 Traction Engine", Proc. Inst. Mech. Engrs., Vol. 183 (Pt 3b) (Pt 3B), p. 24, 1968-69.

12. Gelalles, A. G., "Coefficients of Discharge of Fuel Injection Nozzles for Compression-Ignition Engines", National Advisory Committee for Aeronautics, Tech. Report No. 373, 1931.

13. Giffen, E. and Rowe, A. W., "Pressure Calculations for Oil Engine Fuel-Injection System", Proc. Instn. Mech. Engrs., London, Vol. 141, 1939, p. 519.

14. Hall, G. W., "Analytic Determination of the Discharge Characteristics of Cylinderical Tube Orifices", J. of Mech. Eng. Science, Vol. 5, No. 1, 1963.

15. Henrici, P., Elements of Numerical Analysis, John Wiley & Sons, Inc., N. Y., 1964.

16. Ibrahim, A. I., "Injection Rate Diagrams, Some Methods of Obtaining These Diagrams for High Speed Diesel Engines", Automobile Engineer, March 1964.

17. Judge, Arthur, W., High Speed Diesel Engine, London, Chapman & Hall, Sixth edition, 1967.

18. Knight, B. E. (M. A.), "Fuel Injection System Calculations", Proc. Inst. Mech. Engrs. (A.D.), No. 1, 1960-61.

19. Komarof, Iwan and Kurt Melcher, "The Fuel Quantity Indicator - A New Measuring Device for Volumetric Evaluation of Individual Fuel Injection Quantities", SAE 660750, Oct. 17-21, 1966.

20. Kreith, Frank and Raymond Eisentadt, "Pressure Drop and Flow Characteristics of Short Capillary Tubes at Low Reynolds Number", ASME Trans. 56-SAE.15, 1956.

21. Lichtarowicz, A. and Duggins, R. K. and Markland, E., "Discharge Coefficients for Incompressible Non-Cavitating Flow Through Long Orifices", J. Mech. Engr. Science, Vol. 7, No. 2, 1965.

22. Lichty, Lester, C., Combustion Engine Processes, N.Y., McGraw-Hill, Sixth Edition, 1967.

23. Lustgarten, G. and Dolenc, A., "Development of Injection System for Medium-Speed Diesel Engine with Quiescent-Type Combustion Chamber", Diesel Combustion Symposium, Inst. Mech. Engrs., London, April 1970.

24. Mansfield, W. P., "A New Servo-Operated Fuel Injection System for Diesel Engines", SAE No. 650432, May 17-21, 1965.

25. Maxwell, J. B., Data Handbook on Hydrocarbons: Application to Process Engineering, D. Van Nostrand Co., Inc., N. Y., 1950.

26. Ralston, W. and Wilf, H. S., Mathematical Methods for Digital Computers, Wiley & Sons, N. Y., 1960, pp. 95-109.

27. Stone, J. A., "Discharge Coefficients and Steady-State Flow Forces for Hydraulic Poppet Valves", J. of Basic Eng., 82, 1960, 144.

28. Streeter, V. L., Fluid Mechanics, Fifth edition, McGraw Hill Co., N. Y., 1971.

29. Streeter, V. L., and Wylie, E. B., Hydraulic Transients, McGraw-Hill Book Co., N. Y., 1967.

30. Walwijk, Van E. and Van der Graaf, R., and Jansen, J.K.M., "Berekening Van brandstofinspuitsystemen Voor dieselmotoren", Werktuig-En Scheepsbouw 10/Mei 1969, W. 95.

31. Wright, W. A., "Prediction of Bulk Moduli and PVT Data for Petroleum Oils", ASLE 47AM 7B-1, May 1-4, 1967.

32. Wylie, E. B., Bolt, J. A. and El-Erian, M. F., "Diesel Fuel Injection System Simulation and Experimental Correlation", SAE paper No. 710569, June 7-11, 1971.

33. Yamaoka, K., Saito, A. and Okazaki, M., "Analysis of By-Pass Control Type Fuel Injection System for Small Diesel Engine by Digital Computer", Tech. Bulletin, Yanmar Diesel Engine Company, Ltd., May 1971.